The Ecology of Benthic Toxigenic *Anabaena* and *Phormidium* (Cyanobacteria) in the Eel River, California

By

Keith Bouma-Gregson

A dissertation submitted in partial satisfaction of the

requirements for the degree of

Doctor of Philosophy

in

Integrative Biology

in the

Graduate Division

of the

University of California, Berkeley

Committee in charge:

Professor Mary E. Power, Chair

Professor Wayne P. Sousa

Assistant Professor Laurel G. Larsen

Professor Raphael M. Kudela

Fall 2017

The Ecology of Benthic Toxigenic *Anabaena* and *Phormidium* (Cyanobacteria) in the Eel River, California

By

Keith Bouma-Gregson

Abstract

The Ecology of Benthic Toxigenic *Anabaena* and *Phormidium* (Cyanobacteria) in the Eel River, California

By

Keith Bouma-Gregson

Doctor of Philosophy in Integrative Biology

University of California, Berkeley

Professor Mary E. Power, Chair

Cyanobacteria are ubiquitous in aquatic ecosystems across the earth. In many environments they are present at low abundances, however under certain environmental conditions cyanobacteria bloom and become one of the dominant organisms in an waterbody, degrading aquatic food webs and water quality. Cyanobacteria evolved over 2 billion years ago, and cyanobacterial harmful algal blooms (cyanoHABs) have been documented for decades. Of particular concern is the production of cyanotoxins, secondary metabolites toxic to humans and other organisms, by certain strains of cyanobacteria. Most research of cyanoHABs has been of planktonic blooms in lakes or estuaries, and cyanotoxin production by benthic cyanobacteria in rivers has been more recent, but in many rivers benthic cyanobacteria are the primary source of cyanotoxins. With field surveys and monitoring, manipulative field experiments, and genome-resolved metagenomics, this dissertation investigated the ecology of benthic cyanobacteria in the Eel River, California.

Like most coastal rivers in Northern California, the Eel River is in a Mediterranean climate. During the seasonal summer drought rivers become shallow, slow flowing, and warm, excellent habitat for benthic algal production. Non-toxic benthic algae are consumed by vertebrate and invertebrate grazers and are foundational to the aquatic summer food web. However, these benthic algal assemblages can tip towards toxicity when cyanobacteria begin to dominate the assemblage. Over a dozen dogs have died in the Eel River since the year 2000 due to ingesting cyanobacteria. Neighboring watersheds have also experienced dog deaths from cyanotoxin poisoning, and benthic cyanobacterial mats are an increasing public health concern in multiple Northern California rivers. Prior to this dissertation there were few data on the distribution and ecology of benthic toxigenic cyanobacteria in California rivers.

During the summers of 2013-2015, I documented spatial and temporal patterns of cyanobacterial occurrence and cyanotoxin concentrations in the watershed, showing widespread distribution of anatoxin-a produced by benthic cyanobacteria. Solid phase adsorption toxin tracking (SPATT) samplers were deployed weekly to record dissolved microcystin and anatoxin-a levels at 10 sites throughout the watershed, and 187 cyanobacterial mat samples were collected from 31 sites to measure intracellular anatoxin-a and microcystin. Anatoxin-a levels were higher than microcystin for both SPATT and cyanobacterial mat samples. Species of benthic *Anabaena*

and *Phormidium* were frequently found to produce cyanotoxins in the Eel watershed. Of the benthic mats sampled, 50% had detectable anatoxin-a (mean μg g^{-1} DW= 1.71, max= 70.93), while 24% had detectable microcystins (mean μg g^{-1} DW= 0.067, max= 2.29). SPATT cyanotoxin levels peaked in mid-summer in warm mainstem reaches of the watershed. This is one of the first documentations of widespread anatoxin-a occurrence and anatoxin-a production by benthic cyanobacterial mats in a North American watershed.

Field experiments were used to study the buoyancy of benthic *Anabaena* spp. mats to understand implications for *Anabaena* dispersal. Experiments addressed oxygen bubble production and dissolution on the buoyancy of *Anabaena* dominated benthic mats in response to light exposure. Samples of *Anabaena* dominated mats were harvested from the South Fork Eel River and placed in settling columns to measure floating and sinking velocities, or deployed into *in situ* ambient and low light treatments to measure the effect of light on flotation. Floating and sinking occurred within minutes and were driven by oxygen bubbles produced during photosynthesis, rather than intracellular changes in carbohydrates or gas vesicles. Light experiment results showed that in a natural ambient light regime, mats remained floating for at least 4 days, while in low light mats begin to sink in <24 hours. The ability of *Anabaena* mats to maintain their buoyancy will markedly increase their downstream dispersal distances. Increased buoyancy also allows toxin-containing mats to collect along shorelines, increasing threats to human and animal public health.

Within cyanobacterial mats are a consortia of microbes interacting together to process and exchange molecules to maintain their growth. Currently, little is known about the diversity of the biosynthetic capacities of cyanobacterial species and associated microbes in freshwater benthic mats in rivers. I sampled 22 *Phormidium* mats collected across the Eel River network and used genome-resolved metagenomics to 1) investigate cyanobacterial and co-occurring microbial assemblage diversity, 2) probe their metabolic potential, and 3) evaluate their capacities for toxin production. From the genomes of seven strains from one species group I describe the first anatoxin-a operon from the genus *Phormidium*. Importantly, community composition within the mat appears to be associated with the presence of cyanobacteria capable of producing anatoxin-a. Bacteroidetes, Proteobacteria, and novel Verrucomicrobia dominated the microbial assemblages. Interestingly, some mats also contained Candidate Phylum Kapabacteria and Candidate Phyla Radiation bacteria from Absconditabacteria (SR1), Parcubacteria (OD1) and Doudnabacteria (SM2F11). Although the majority of genomes were unique to a particular sample, metabolic diversity was low across samples. In addition to oxygenic photosynthesis and carbon respiration, metabolic capacities include aerobic anoxygenic photosynthesis, sulfur compound oxidation and breakdown of urea. These results show the importance of organic carbon and nitrogen to energy flow and nutrient cycling within mats and the interactions between potential anatoxin-a production and microbial assemblage composition.

By combining watershed-scale observations, field experiments, and genomic analyses this dissertation provides novel information about the ecology of toxigenic benthic cyanobacteria in California rivers. Comprehensive knowledge of the ecology of benthic cyanobacteria is necessary to understand its impacts to public and ecosystem health and to better predict where and when blooms might occur in rivers.

Dedicated to,

Desmond Thomas Bouma-Gregson, born September 3rd, 2016.

> But, how is the coming generation to live? It is only in this way that fruitful solutions can arise, even if for the time being they are humiliating. In short it is easier by far to act on abstract principles than from concrete responsibility. The rising generation will always instinctively discern which of the two we are acting upon. For it is their future which is at stake.
>
> – Dietrich Bonhoeffer, *Letters and Papers from Prison*

Table of Contents

List of Figures

List of Tables

Acknowledgements

I would like to thank my wife, Lindsey, for all your support these last five years. Before we were even married, when you hardly knew me, you were willing to journey with me down this Ph.D. road. I am grateful for all the encouragement and support you have given over the years. Thank you for all the days you assisted in the field or in the lab. Working alongside you made the Ph.D. feel integrated into our life together, and not something that only pulled me away from you and Desmond. To my parents, Brian and Wendy, thank you for all the opportunities you gave me as a child to run around outside. There is a straight line from all those family camping trips as a kid to this dissertation. Thank you, for your encouragement and support throughout this program, especially out in the field or lab, and many rendezvous at the loading dock to transport supplies back to the field. Thanks also to Rolf and Sandy for supporting me through the Ph.D., even though it meant Lindsey and I had to move far away from you both.

Mary, thank you for being a wonderful advisor. You modeled for me how to maintain scientific rigor with humility. I am grateful for all the training you offered me, from editing proposals and manuscripts to informal conversations on the river bank. You showed me the value of the history and development of ideas, and the importance of natural history observations to inform and guide one's research. Thank you, too, for welcoming my family up to the Angelo Reserve, creating a supportive lab culture, and making science fun.

To Wayne, Laurel, and Raphe, thank you for your guidance over the years. Wayne, like Mary, you have provided fabulous ecological mentorship and helped refine my ecological thinking. Laurel, thank you for sharing your labs resources and teaching me about the hydraulics of rivers. Raphe, thank you for responding to my email back in 2012, when I proposed working with you on the Eel River. Without the support of your lab, this dissertation would not have been possible. A tremendous thank you to Kendra Hayashi, an outstanding lab manager. You have been and generous with your time in coordinating the logistics between UC Berkeley and UC Santa Cruz.

I am grateful for the caliber of other graduate students in the Power Lab and at the Angelo Reserve: Hiromi Uno, Philip Georgakakos, Gabe Rossi, and Suzanne Kelson. You all have been a pleasure to work with and made my time at Berkeley intellectually rich and very fun! I am thankful for the ease with which we all get along and for the scientific perspectives you brought to the lab. Additionally, I am grateful to all the other graduate students I have had the privilege to get to know. It has been great pondering how the world works with you all, especially: David Dralle and other students with the Eel River Critical Zone Observatory; Matt Olm, Evan Star, and the Banfield Lab; and Stephanie Carlson's lab.

Many UC Berkeley undergraduate students provided invaluable assistance with field and lab work to collect, process, and analyze data for this dissertation: Jeanine Porzio, Gina Hervey, Caroline Ribet, Arianna Nuri, Wes Cooperman, Natalie Soto, Sam Hauptman, Ryley Burton-Tauzer, Addien Wray, Victoria Uva, Garbo Gan, Candice Young, Vivian Goldfield, Nick

Lapaglia, Keana Richmond, and Hannah Hroodenrijs. It has been a pleasure working with you all over the years. The extra hands, eyes, ears, and brains you provided were essential in generating the data for this dissertation. I thank you for your patience with me during long and focused field and lab work. You all helped make the research enjoyable and with lots of laughter.

I am indebted to Patrick Higgins and volunteers with The Eel River Recovery Project. You welcomed me into the watershed and taught me much about the natural and social history of the Eel River basin. Additionally, you were essential in providing access to sampling locations and deploying SPATT samplers. In particular, Paul and Barbara Domanchuk, David Sopjes, John Filce, Bruce Hilbach-Barker, and John Evans provided valuable assistance for the SPATT monitoring program. Many other individuals in the Eel River Recovery Project have offered information, access, or encouragement, and I am incredibly grateful to have learned from you all.

Many have come before me in Mary Power's lab, and former lab members have offered advice and encouragement along the way. Sarah Kupferberg, Mike Limm, and Blake Suttle have been sources of wisdom for the natural history of the Eel River and experimental design. Jonah Pioviah-Scott was a tremendous support as a postdoc during my first year as a graduate student. Paula Furey and Rex Lowe taught me how to identify algae in the Eel. I would also like to thank Jacques Finlay and his laboratory staff for measuring dissolved nutrients. Much of this research was performed at the UC Natural Reserve System, Angelo Coast Range Reserve. I would like to especially thank the reserve manager, Peter Steel, for all the work he does to make the Angelo Reserve function smoothly.

Lastly, I would like to thank the other Christian graduate students that I have met through Christ Church, Au Sable Graduate Fellows, and The Berkeley Institute. Your friendships have helped me integrate science and spirituality and made my life feel more integrated.

This work was supported by a US Environmental Protection Agency STAR Fellowship to KBG [91767101-0]; the National Science Foundation's Eel River Critical Zone Observatory [EAR-1331940]; a UC Natural Reserve System Mathias graduate student grant to KBG; a NorCal SETAC summer graduate student research grant to KBG; and graduate student grants from the Integrative Biology Department at UC Berkeley. This work used the Vincent J. Coates Genomics Sequencing Laboratory at UC Berkeley, supported by an NIH Instrumentation Grant [S10 OD018174].

1 Widespread anatoxin-a production from benthic cyanobacteria throughout the Eel River

Abstract

Benthic algae fuel summer food webs in many sunlit rivers, and are hotspots for primary and secondary production and biogeochemical cycling. Concerningly, riverine benthic algal assemblages can become dominated by toxic cyanobacteria, threatening water quality and public health. In the Eel River in Northern California, over a dozen dog deaths have been attributed to cyanotoxin poisonings since 2000. During the summers of 2013-2015, I documented spatial and temporal patterns of cyanobacterial occurrence and cyanotoxin concentrations in the watershed, showing widespread distribution of anatoxin-a produced by benthic cyanobacteria. Solid phase adsorption toxin tracking (SPATT) samplers were deployed weekly to record dissolved microcystin and anatoxin-a levels at 10 sites throughout the watershed, and 187 cyanobacterial mat samples were collected from 31 sites to measure intracellular anatoxin-a and microcystins. Anatoxin-a levels were higher than microcystin for both SPATT and cyanobacterial mat samples. Benthic *Anabaena* and *Phormidium* were frequently found to produce cyanotoxins in the Eel watershed. Of the benthic mats sampled, 50% had detectable anatoxin-a (mean μg g^{-1} DW= 1.71, max= 70.93), while 24% had detectable microcystins (mean μg g^{-1} DW= 0.067, max= 2.29). SPATT cyanotoxin levels peaked in mid-summer in warm mainstem reaches of the watershed. This is one of the first documentations of widespread anatoxin-a occurrence and anatoxin-a production by benthic cyanobacterial mats in a North American watershed.

1.1 Introduction

Cyanobacteria are a diverse phylum of photosynthetic bacteria, and are globally distributed across aquatic environments. Often cyanobacteria are present at low biomass, but under certain environmental conditions, their accrual rates increase, resulting in a cyanobacterial bloom. Water quality can be degraded by cyanobacterial blooms, especially when they produce cyanotoxins, secondary metabolites that are harmful to humans and other organisms (Chorus and Bartram 1999, Wood 2016). Though most research has focused on planktonic blooms in lakes or estuaries, benthic cyanobacterial mats in rivers can also impair fluvial systems (Quiblier et al. 2013). Attached algae are major primary producers in many rivers (Vadeboncoeur and Power 2017), so a shift from more edible taxa (e.g. diatoms) to cyanobacterial dominance may alter nutrient cycling, energy flow, and ecological interactions. Additionally, cyanotoxins produced by mats threaten public health for those using rivers for recreation or drinking water. Knowledge of the environmental controls of freshwater benthic cyanobacterial mats lags behind our understanding of planktonic cyanobacterial ecology (Scott and Marcarelli 2012, Quiblier et al. 2013). Improved understanding of benthic cyanobacterial ecology is needed to identify and predict where and when cyanobacterial proliferations may affect aquatic ecosystems and human health.

Benthic cyanobacterial blooms have been detected in rivers worldwide (Sabater et al. 2003, Mohamed et al. 2006, Quiblier et al. 2013, Fetscher et al. 2015, McAllister et al. 2016). In New Zealand, benthic cyanotoxin blooms increased in the mid-2000s and have been documented in over 100 rivers in the country (McAllister et al. 2016). In California, a statewide survey of benthic periphyton found potentially toxigenic cyanobacterial taxa in over 300 of 1,000 samples, and microcystin in 123 of 368 samples tested across the state (Fetscher et al. 2015). The Eel River in Northern California, where over a dozen dog deaths have been linked to cyanotoxin poisonings since 2000, is one the first locations of a documented anatoxin-a dog poisoning in North America (Puschner et al. 2008, Backer et al. 2013). Anatoxin-a is a neurotoxic alkaloid that inhibits neuromuscular receptors by disrupting cellular ion channels, resulting in muscle failure and sometimes death (Devlin and Edwards 1977, Carmichael et al. 1979, Osswald et al. 2007).

Monitoring cyanotoxins and establishing water quality regulatory guidelines in rivers are challenging. Both toxigenic cyanobacterial taxa and cyanotoxin molecules are diverse. Toxin production by a given cyanobacterial taxon can be variable, and our understanding of environmental triggers for toxin production is rudimentary (Neilan et al. 2013, Omidi et al. 2017). Solid phase adsorption toxin tracking (SPATT) samplers provide a time-integrated method of detecting cyanotoxins (MacKenzie et al. 2004, MacKenzie 2010, Kudela 2017). SPATT samplers are adsorption resins placed in a water body for a given time period. Dissolved cyanotoxin molecules adsorb onto the resin, providing an estimate of dissolved cyanotoxin levels in the water column over the deployment time. By sequentially deploying and retrieving SPATT samplers at a location, it is possible to generate a time series of relative toxin levels. SPATT samplers have been successfully used to track the dynamics of microcystin in California's Monterey Bay and its associated watersheds (Miller et al. 2010, Kudela 2011, Gibble and Kudela 2014). SPATT samplers are well-suited to monitor in rivers where benthic cyanobacteria may release pulses of cyanotoxins, which are then transported rapidly downstream (Wood et al. 2011).

With multiple dog deaths reported in Northern California rivers, but minimal understanding of the benthic toxic cyanobacteria accounting for them, I conducted watershed scale surveys across the Eel River with the goals of 1) identifying common toxigenic cyanobacterial taxa in the watershed; 2) describing the spatial and temporal patterns of anatoxin-a and microcystin in the watershed; and 3) describing environmental correlates of cyanotoxin levels. I focused on two commonly occurring toxin groups, anatoxin-a and microcystins. The neurotoxin anatoxin-a was chosen due to its prior detection in the watershed (Puschner et al. 2008), while the hepatotoxin microcystin was chosen given its common detection in California watersheds (Fetscher et al. 2015).

1.2 Materials and methods

1.2.1 Study site description

The Eel River in Northern California drains 9,547 km^2 along the northern California Coast Range Mountains (Fig. 1.1). Precipitation and river discharge are highly seasonal, with winter

storms increasing river flows near the mouth to over 2,800 cubic meters per second (cms), and the summer drought decreasing summer base flows to <3 cms in September (USGS gage 11477000 Scotia, CA). During summer, as base flow drops, the river becomes warm (20-30°C), clear, and relatively shallow with only the pools being >1.5 meters deep. In sunlit reaches, these conditions facilitate the growth of benthic *Cladophora glomerata,* which is then epiphytized by diatoms. These diatoms, especially *Epithemia* spp., are highly nutritious for aquatic invertebrates and tadpoles, making the *Cladophora*/diatom assemblages foundational for the summer aquatic food web in sunlit reaches of the Eel River (Kupferberg et al., 1994; Power et al., 2010). Benthic cyanobacteria—*Anabaena* (Power et al. 2015, Bouma-Gregson et al. 2017), *Phormidium* (Bouma-Gregson personal observation) and several species of *Nostoc* (Horne and Carmiggelt 1975)—also occur in the Eel.

1.2.2 SPATT monitoring sites

Cyanotoxin dynamics in the Eel River were documented using SPATT samplers. In 2013 and 2014, SPATT deployment sites were established In the South Fork, Lower Eel, Mainstem, and Van Duzen watersheds (Fig. 1.1) at sites that were wadeable reaches where the water was flowing and well mixed. SPATT samplers were attached to a metal pipe that was hammered into the riverbed in the thalweg. The sampler was attached to the stake at approximately half of the water depth (~30-50 cm above the bed). Every 5-10 days, the samplers were removed from the river and immediately replaced with a new sampler. Upon removal, samplers were rinsed with river water, and then stored in plastic bags at -20°C until toxins were extracted. In 2015, additional sites were established in the South Fork (1), Lower Eel (1), Mainstem (3), and Middle Fork Eel River (2). All samplers in 2015 were deployed for about a month to detect the presence or absence of cyanotoxins at monitoring sites. Samplers were deployed from June to September.

1.2.3 SPATT sampler construction and cyanotoxin analysis

The construction and analysis of SPATT samplers was adapted from Lane et al. (2010) and Kudela (2011). To make SPATT samplers, 3 g of HP20 DIAION© (hereafter, HP20) resin were sandwiched between two 10 cm squares of 118 μm Nitex mesh and placed in a 6.3 cm diameter embroidery hoop ring (Westex/Caron Flex Hoop rings) (Fig. 1.2H). Immediately after construction, SPATT samplers were submerged in 100% HPLC grade methanol (MeOH; Fisher A456) for ~24 hours to activate and clean the resin. Then the methanol was rinsed off by agitating the ring for 30-60 s three times in 500 mL of Milli-Q water. After rinsing, samplers were placed in plastic bags with 20 mL of Milli-Q water and stored in the dark at 4°C until deployment in the river.

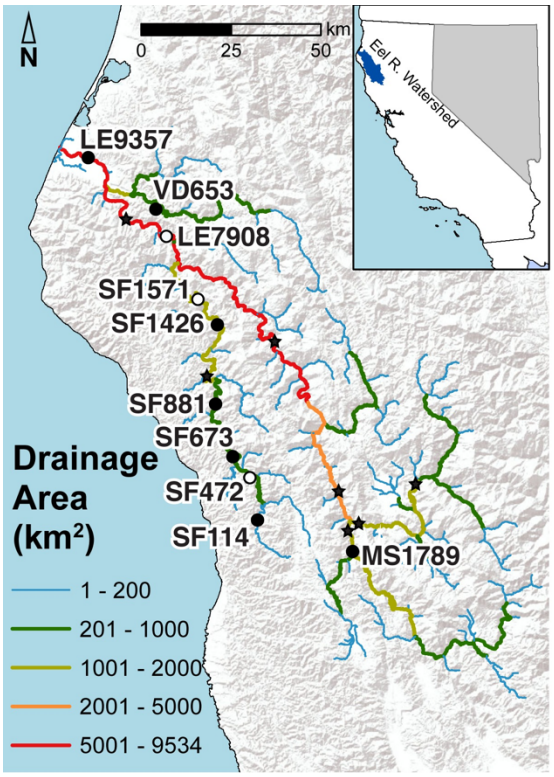

Fig. 1.1 Map of cyanotoxin monitoring locations in the Eel River**.** Site names indicate sub-watershed (letters) and drainage area in km^2 (numbers). Three sites with white circles were only monitored in 2014, all other sites were monitored in 2013 and 2014. Stars represent sites that were monitored monthly in 2015.

Toxin extraction from SPATT followed methods in Kudela (2011) and Gibble and Kudela (2014). SPATT samplers were thawed, and the resin rinsed with Milli-Q water. Then the resin was poured into a disposable liquid chromatography column and placed on a vacuum manifold. Toxins were extracted from the resin with consecutive 10, 20, 20 mL rinses of a 50% solution of MeOH (Fisher A452) and Milli-Q water.

A 1 mL subsample from each of the three extracts was analyzed separately using liquid chromatography mass spectrometry (LC-MS) with Select Ion Monitoring (SIM). Microcystin and anatoxin-a concentrations were measured on an Agilent 6130 Liquid Chromatography-Mass Spectrometry system with a Phenomenex Kinetex C18 column (microcystins) and Cogent Diamond-Hydride column (anatoxin-a) and direct-injection of 20 µL. The LC-MS measured four microcystin congeners –LR, –YR, –RR, and –LA; these values were then summed together. The concentrations from the three extracts were then summed to give nanograms of cyanotoxin per gram resin. The detection limits of the LC-MS for anatoxin-a and microcystin are 0.25 and 0.01 parts per billion (ppb), respectively. Calibration was performed using certified reference materials with a minimum of five calibration points for each batch of samples, with analytical blanks and matrix blanks included in each run. The detection limit of dissolved cyanotoxins in the river by SPATT resins and the calibration of SPATT values to dissolved cyanotoxin concentrations were not investigated. These relationships are challenging to quantify, since

SPATT adsorption is a function of environmental conditions such as hydraulics, water chemistry, temperature, light, and microbial activity. SPATT is therefore considered a semi-quantitative method (Kudela 2017).

1.2.4 SPATT adsorption/extraction characteristics

The adsorption and extraction efficiencies of HP20 resin and microcystins are described in Kudela (2011). Microcystin molecules were rapidly adsorbed to the resin in <1 hour, and ~100% of the microcystins were extracted off the resin with 10-15 sequential 10mL extractions. The extraction method with 3 sequential extractions developed in Kudela (2011) and described in section 1.2.3 above recovers ~60-100% of microcystins from the resin. Kudela (2011) only studied microcystin, and so three laboratory experiments were conducted to understand adsorption and extraction dynamics for anatoxin-a and HP20 resin. First, to understand the degradation dynamics of the anatoxin-a molecule, anatoxin-a standards were added to 0.2 µm filtered Eel River water and Milli-Q water, as a control, in constantly agitated (70 rpm) 125 mL Erlenmeyer flasks at room temperature illuminated at 125 µmol m^{-2} s^{-1}. These flasks were sampled over 48 hours to track changes in ATX concentrations due to degradation or interactions with other dissolved molecules that limited detection via LC-MS. Second, to assess the adsorption and extraction dynamics of the HP20 resin, anatoxin-a standards were added to triplicate 0.2 µm filtered Eel River and Pinto Lake water in 125 mL Erlenmeyer flasks with constant agitation. (Pinto Lake is a 44 ha lake in Santa Cruz, Co. that experiences frequent *Microcystis* blooms. It was chosen as a second environmental water source due to its proximity to laboratory facilities.) Then, 3g of HP20 resin was added to each flask and the flasks regularly sampled to measure ATX concentrations. A fourth flask with filtered Eel or Pinto water was used as a control. Third, to estimate recovery efficiency of anatoxin-a from the SPATT resin, ATX was extracted from the HP20 resin used in the second experiment with sequential volumes of 50% methanol (as described in section 1.2.3). The recovery efficiency is calculated by dividing the total ATX extracted off the SPATT by the total ATX at the beginning of the experiment, with the control (no SPATT) samples used to account for variability due to sample handling and analysis.

1.2.5 Cyanobacterial mat collections

During summers 2014-2015, 187 cyanobacterial-dominated mats were sampled with a 3.8 cm diameter PVC pipe delimiter (Table A.1). Macroscopic identifications of the dominant cyanobacteria in mats were confirmed by microscopic identification at 400x (Komarek 2013) on a Nikon Optiphot 2 microscope. For a given cyanobacterial mat, 3-5 samples were collected and combined into a single sample. In the lab, macroinvertebrates were removed from the sample and stored in ethanol. Then the mat sample was homogenized in a blender, and the volume of the homogenate recorded. A 10-15 mL subsample was collected for cyanotoxin analysis, placed in a 20 mL glass scintillation vial, and frozen at -20°C until toxin analysis.

For cyanobacterial mat toxin analysis, samples were thawed and 3 mL of sample added to a glass culture tube. Then, 3 mL of 50% MeOH was added and the tube was sonicated for 30 s using a probe sonicator at ~10W power. For anatoxin-a analysis, a 1 mL subsample was taken and 0.2 µm filtered into an LC-MS vial. Microcystin samples were cleaned using solid phase extraction

(SPE) with a Baker C18 column, and then 1 mL of eluate was added to a LC-MS vial. The cyanotoxin concentrations in the vials were measured using LC-MS as described in section 1.2.3.

1.2.6 Cyanotoxin water samples

To test for total cyanotoxins in the water column, in 2015 15 mL unfiltered water samples were collected in glass scintillation vials from ~15 cm below the water surface at sites throughout the watershed, placed in a cooler until returned to the lab, and then frozen at -20°C until analysis. Samples were thawed and a 3 mL subsample taken and combined with 3 mL of 100% HPLC grade methanol (Fisher A542), sonicated for 30 s, centrifuged at 2,500 rpm for 5 min, and then 0.2 µm filtered into a LC-MS vial. Samples were then tested for microcystins and anatoxin-a as described in section 1.2.3.

1.2.7 Temperature, nutrient, and velocity data

Attached to the bottom of each SPATT sampler pole was a DS1922L ibutton temperature logger (Maxim Integrated, San Jose, CA, USA). Ibuttons were vacuum-sealed in a plastic bag and placed inside a 1.9 x 7.6 cm PVC pipe with holes drilled into the side. Water temperature was recorded every 30 minutes.

In 2013 and 2014, during each SPATT sampler deployment, three 50 mL filtered water samples (0.7 µm Whatman GF/F) were collected for total dissolved nitrogen and phosphorus analysis. After filtration, samples were placed in a cooler and frozen at –20°C upon return to the lab. Total dissolved nitrogen (TDN) measurements were made on a Shimadzu TOC/TDN analyzer (Shimadzu, Kyoto, Japan). Total dissolved phosphorus (TDP) was measured using an acid digestion and colorimetric analysis. TDN was only measured in 2014, and TDP was measured in 2013 and 2014.

In June 2016, at 19 monitoring sites along a 2.5 km river reach in the Angelo Coast Range Reserve on the South Fork Eel, water velocity measurements surrounding *Anabaena* patches were measured with a Flowtracker (Sontek, San Diego, CA, USA) hand held acoustic Doppler velocimeter (ADV) on a top-set wading rod. *Anabaena* is frequently observed along this reach of river, and monitoring sites were established across the available range of flow velocities in light and depth environments that were conducive to *Anabaena* growth. The ADV was placed at each monitoring site and water velocities measured at 0.8 and 0.2 of the total water depth. The presence or absence of *Anabaena* growing in similar flow velocity to the monitoring site within 2 meters of the site was recorded. If *Anabaena* patches were observed within the survey reach, but not at designated monitoring sites, flow measurements were made at 0.2 and 0.8 of water column depth directly in front of or above the *Anabaena* patch.

1.2.8 Statistics

Generalized linear binomial models, linear models, or linear mixed-effect models were used to test the effects of cyanobacterial species or environmental covariates on the presence of cyanotoxins and cyanotoxin concentrations. All statistical analyses were performed with R v. 3.3.2 (R Core Team 2017). SPATT data contained many non-detects, so a zero-inflated model was used to investigate the effect of TDN, TDP, and temperature on SPATT levels. First a

generalized mixed effect logistic regression (family= binomial) was used to model the effect of these covariates on the detection of SPATT cyanotoxins with site as a random factor. Then a mixed effect model with site as a random variable was applied to the log_{10} transformed SPATT data with all non-detects excluded. Nutrient data were standardized by subtracting the overall mean and dividing by the standard deviation, and regressions constructed between standardized nutrient concentrations and transformed SPATT data. Water velocity measurements were log_{10} transformed to assume normality, and a Welch's t-test used to test for differences in water velocity where *Anabaena* patches were present or absent.

1.3 Results

1.3.1 Cyanobacterial taxa

Benthic cyanobacterial mats are macroscopically conspicuous in the Eel River and are most commonly formed by *Anabaena* and species of *Phormidium* (Figs. 1.2 and 1.3). *Cylindrospermum* can also form macroscopic patches, often on bottom of pools or on sandy and silt substrates (Bouma-Gregson, personal observation). Species of *Nostoc* and *Rivulariaceae* are also common in the Eel River, but were not sampled as part of this research. Other cyanobacterial taxa (primarily *Nodularia*, *Oscillatoria*, *Leptolyngbya*, *Tolypothrix*) also occur in periphyton, but they have never been observed as the dominant species in a macroscopic mat >5 cm^2. *Phormidium* samples have been identified as *Phormidium autumnale,* though the taxonomy of *P. autumnale* is under revision with a proposed move to the genus *Microcoleus* (Strunecký et al. 2013). *Anabaena* mats were negatively associated with water velocity ($p < 0.01$), often found when velocities are <10 cm s^{-1} (Fig. 1.4). *Anabaena* is commonly found epiphytically on non-toxic filamentous green macroalga *Cladophora glomerata* (Fig. 1.2). In contrast, *Phormidium* was found in riffles and high velocity patches of the river, and grows as epilithic orange, brown, olive, or maroon mats (Fig. 1.3).

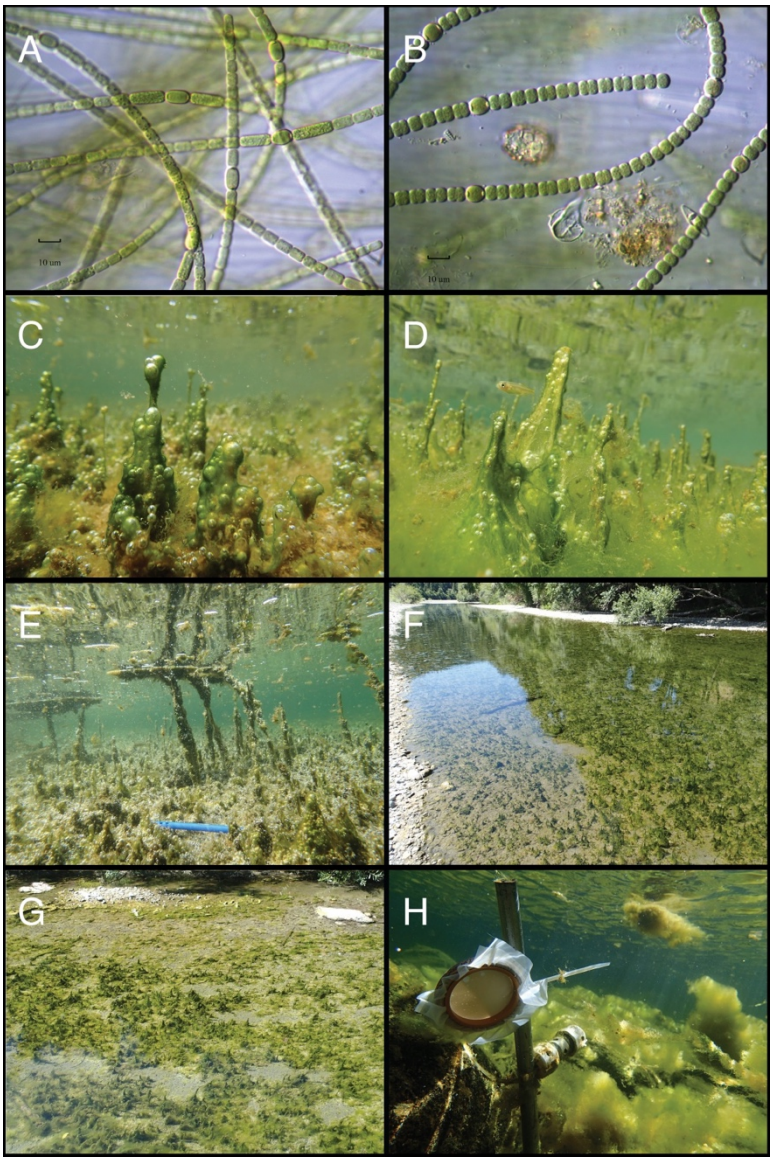

Fig. 1.2 *Anabaena* in the Eel River. A-B) Micrographs of *Anabaena* cells (400x); C-E) Dark-green *Anabaena* "spires" growing on top of senescing macro-algae *Cladophora glomerata*; F-G) *Anabaena* mats on riverbed at bottom of shallow pools; H) SPATT ring deployed in the Eel River.

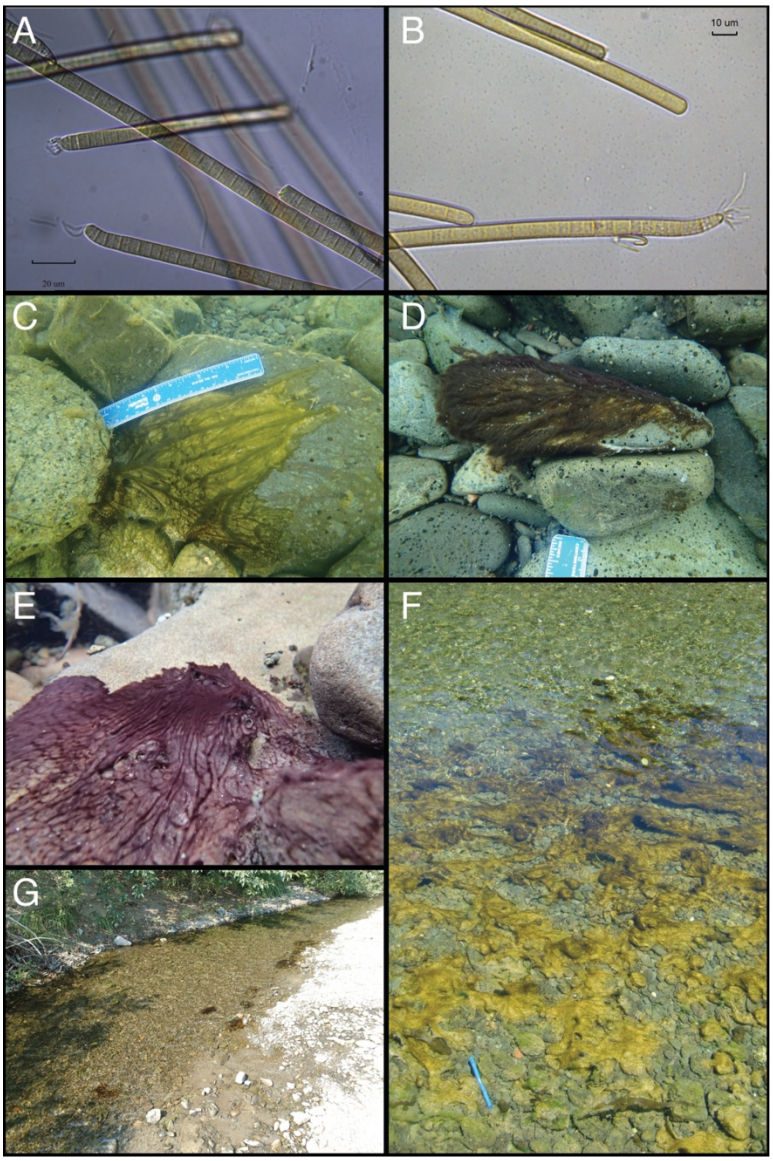

Fig. 1.3 *Phormidium* in the Eel River. A-B) Micrograph of *Phormidium* cells (400x); C-E) Underwater photographs of *Phormidium* growing on cobbles; F-G) Looking down on brown or orange patches of *Phormidium* mats (blue thermometer is 15 cm long).

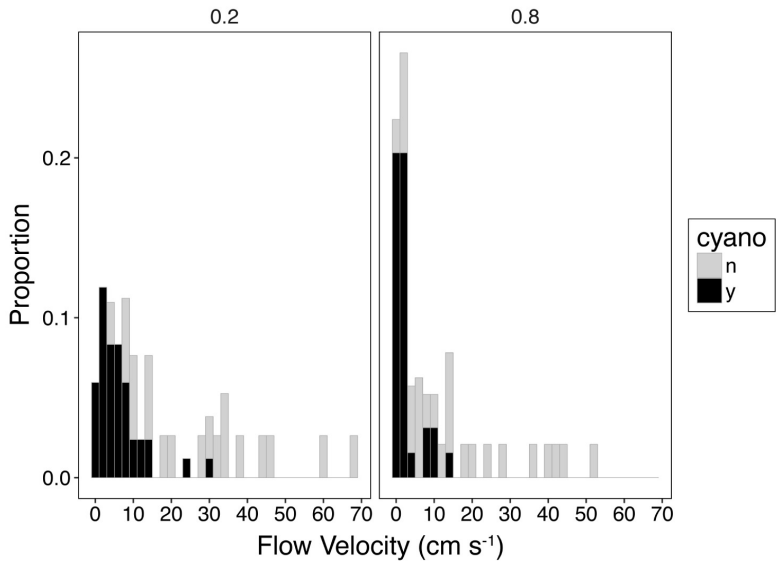

Fig. 1.4 Histogram of absence or presence of *Anabaena* at different flow velocities. Measurements taken in June 2016 at monitoring sites in the Angelo Reserve with different at 20% and 80% of total water column depth.

1.3.2 SPATT ATX adsorption and extraction results

ATX concentrations remained relatively stable over 48 hours in Milli-Q water, but decreased in filtered Eel River water (Fig. 1.5A). When SPATT resins were placed in flasks, most ATX adsorbed onto the SPATT within 12 hours, then the adsorption rate decreased (Fig. 1.5B). The ATX dynamics were similar between the Eel River and Pinto Lake water samples. The ATX concentrations in the control flasks remained stable, with minimal decreases in ATX over 72 hours. However, between 72 and 78 hours the ATX degradation rate increased for all samples. ATX recovery from SPATT resin was 58 ± 2.0% for Eel River water and 73 ± 2.4% (mean ± 1 SD) for Pinto Lake water of the total amount of ATX present at the start of the experiment.

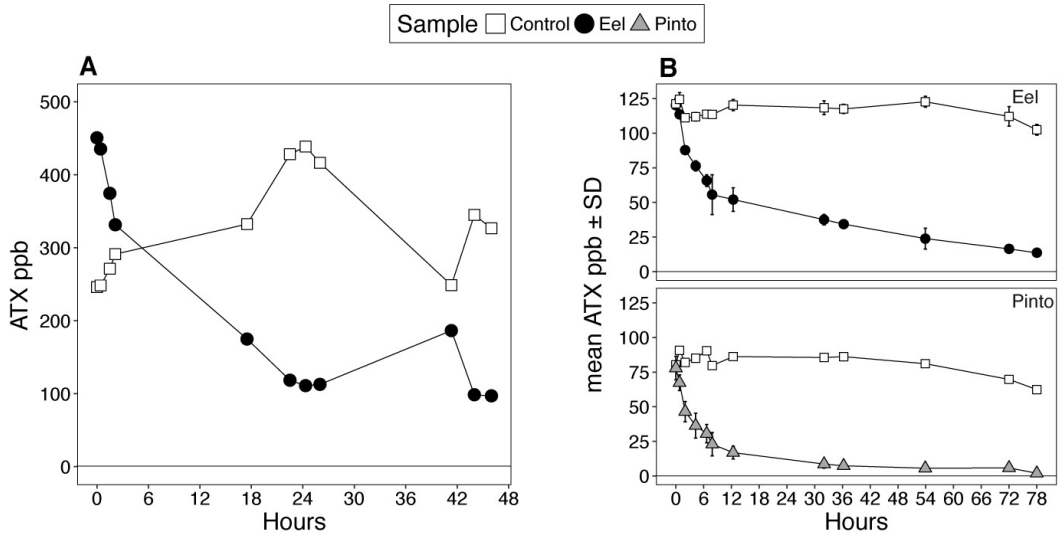

Fig. 1.5 Anatoxin-a stability and adsorption efficiency. A) Anatoxin-a (ATX) stability in Milli-Q and 0.2 µm filtered Eel River water. B) Anatoxin-a (ATX) adsorption by SPATT resin in 125 mL Erlenmeyer flasks filled with 0.2 µm filtered Eel River or Pinto Lake water. No SPATT resin was placed in control flasks.

1.3.3 SPATT monitoring results

SPATT samplers detected higher levels of anatoxin-a (mean= 34.85, max= 907.46 ng ATX g^{-1} resin) than microcystin (mean= 5.46, max= 88.78 ng MCY g^{-1} resin) at the monitoring sites in the Eel River (Fig. 1.6), but detected microcystin more frequently than anatoxin-a (Table 1.1). Most of the microcystin SPATT values were below 50 ng MCY g^{-1} resin, with only the SF114 SPATT sampler consistently detecting microcystin above 50 ng MCY g^{-1} resin (Fig. A.1). The MCY levels were driven by the –LR congener, which was consistently detected at higher levels than the other 3 congeners (Fig. A.2).

The seasonal timing of the rise and fall of SPATT-sampled cyanotoxin levels was similar in 2013 and 2014 (Figs. 1.6 and 1.7). In both years SPATT levels start to increase in late July and remain elevated into early August. However, higher SPATT levels were reached earlier in the season in 2014 than in 2013. By late August, SPATT levels at all sites were close to zero and remained low until the end of September when monitoring ceased. In both 2013 and 2014, sites from middle reaches of the South Fork Eel, SF1426, SF881, and SF673, recorded higher concentrations of anatoxin-a than upper reaches or reaches near the mouth (Fig. 1.7). SPATT samplers at both Lower Eel sites, and the site on the Mainstem at Outlet Creek, rarely detected cyanotoxins. Anatoxin-a was detected at high levels in a single, early-season SPATT sample from LE7908, but was not detected at high concentrations from subsequent samples at this location (Fig. A.1). SPATT samplers in 2015 detected microcystin and anatoxin-a in July, August, and September at almost all sites (Fig. 1.8), including the monitoring sites in the less populated eastern parts of the watershed.

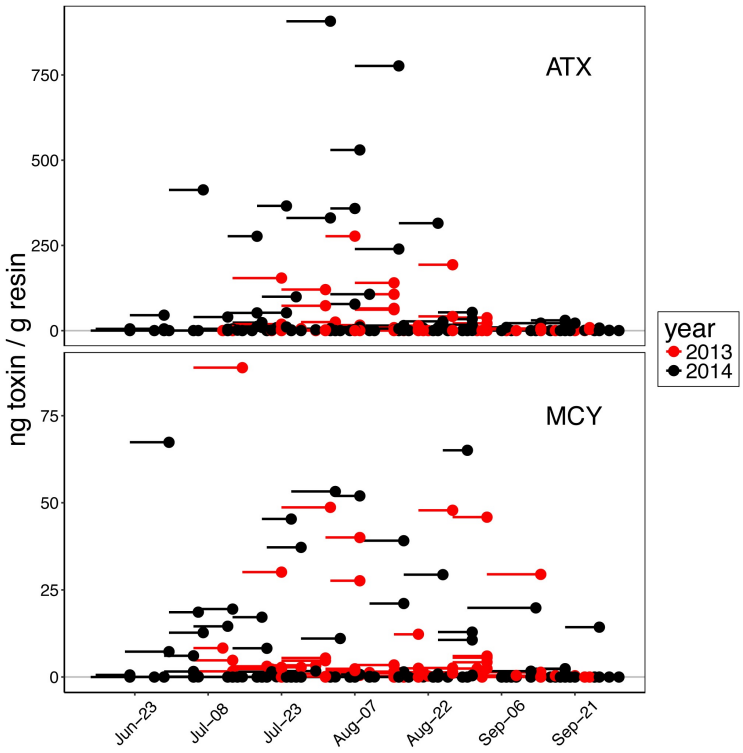

Fig. 1.6 Anatoxin-a (ATX) and microcystin (MCY) concentrations from SPATT samplers in the Eel River for 2013 and 2014. Each point represents the retrieval date of a single sampler, and the line extends back to the day the sampler was deployed. Note the different scales of the y-axis for ATX and MCY.

Table 1.1 The percentage of SPATT samplers testing positive for microcystins (MCY) or anatoxin-a (ATX).

ID*	2013 MCY	2014 MCY	2013 ATX	2014 ATX
LE9537	77% (10/13)	16% (3/19)	38% (5/13)	19% (3/16)
LE7908	NA	40% (4/10)	NA	44% (4/9)
SF1571	NA	19% (3/16)	NA	33% (5/15)
SF1426	78% (7/9)	27% (3/11)	100% (9/9)	64% (7/11)
SF881	44% (4/9)	36% (4/11)	80% (8/9)	73% (8/11)
SF653	75% (6/8)	27% (3/11)	88% (7/8)	91% (10/11)
SF472	NA	22% (2/9)	NA	50% (4/8)
SF114	100% (9/9)	100% (13/13)	33% (3/9)	62% (8/13)
VD673	73% (8/11)	55% (10/20)	45% (5/11)	57% (8/14)
MS1789	89% (8/9)	13% (1/8)	0% (0/9)	50% (4/8)

Parentheses show number of samplers testing positive over total number of samplers deployed at a given site.

* Site ID indicates sub-watershed and watershed area upstream of site in km^2. LE= Lower Eel, SF= South Fork, VD= Van Duzen, MS= Mainstem

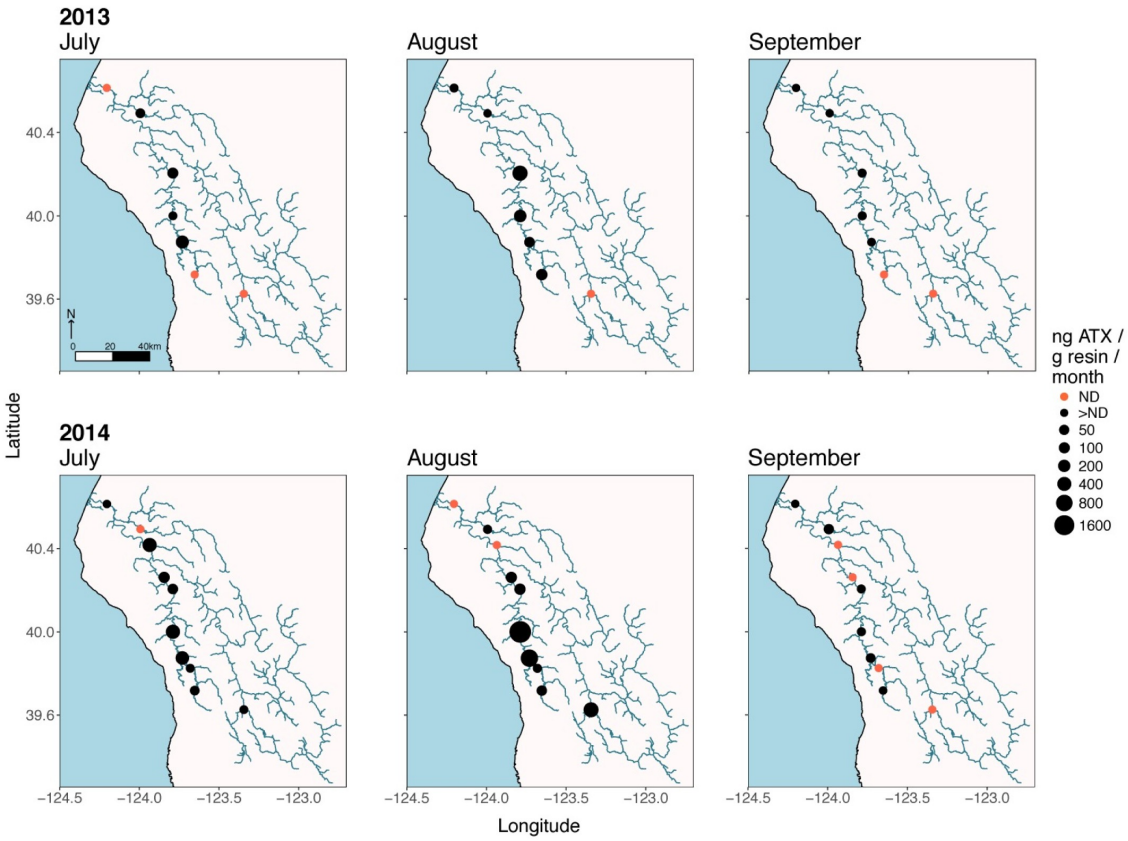

Fig. 1.7 Sum of anatoxin-a (ATX) detected each month from SPATT monitoring locations in 2013 and 2014. Red points indicate sites where cyanotoxins were not detected (ND).

1.3.4 Temperature and nutrient results

SPATT sampling locations (Fig. 1.9 and Fig. A.3) spanned a range of temperature regimes. The Lower Eel sites close to the coast were cooled by maritime influences including summer fog; the South Fork SF114 near the headwaters of the watershed was also cooler because it is heavily forested, and shaded by canyon walls. When the 7-day average temperature prior to each collection date is plotted against SPATT levels, anatoxin-a maxima cluster between 22.5 and 25°C and high microcystin levels occur at cooler sites, <22.5°C (Fig. 1.9). Mixed effect models found significant mean 7-day temperature effects on the detection and magnitude of ATX levels, but not SPATT MCY levels ($p < 0.05$). The Eel River has total dissolved nitrogen (TDN) concentrations ranging 0.031-0.304 mg L^{-1} and low total dissolved phosphorus (TDP) ranging <0.01-0.055 mg L^{-1} (Fig. 1.10). Mixed effect models found no significant relationship ($p < 0.05$) between TDN, TDP, or N:P ratios and the detection or concentration of SPATT-measured levels for ATX or MCY.

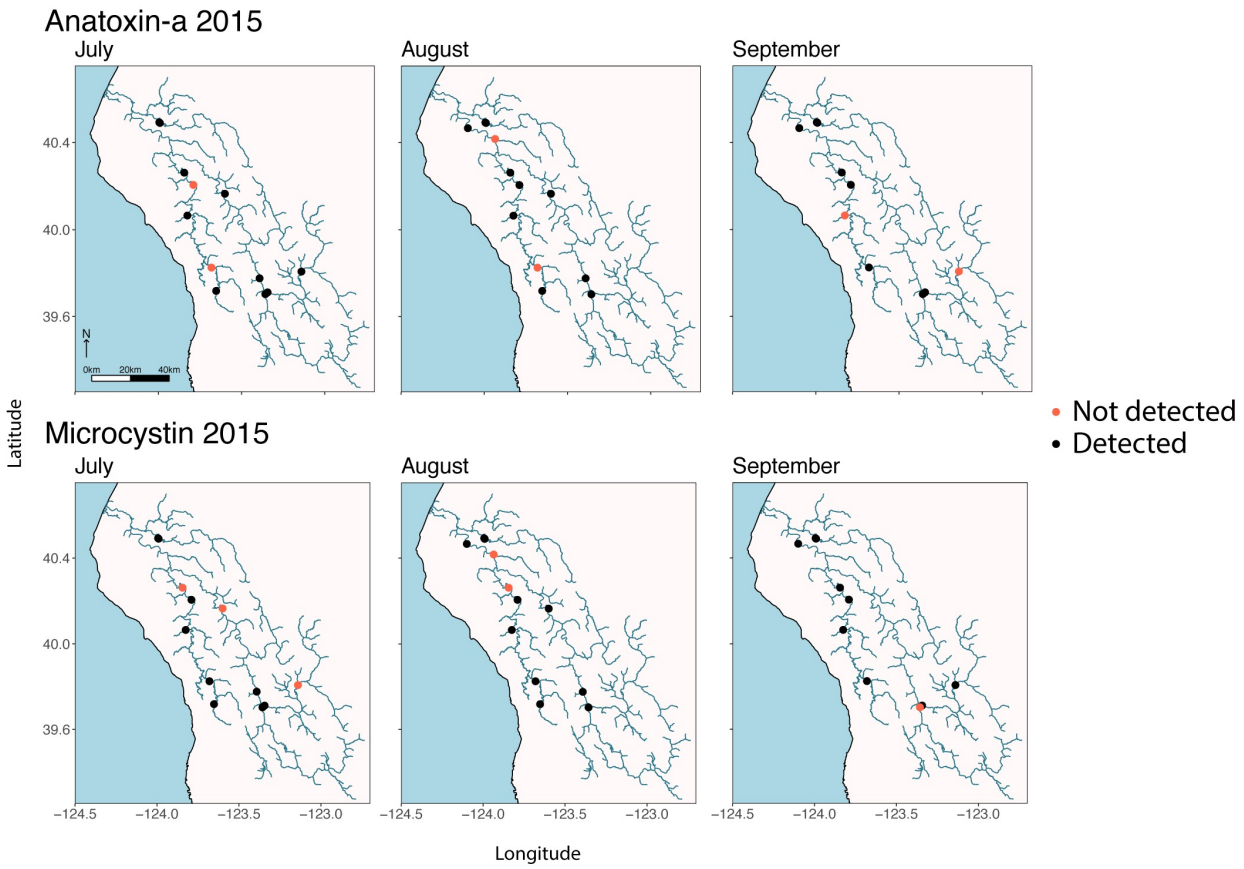

Fig. 1.8 Detection of anatoxin-a and microcystin in SPATT samplers deployed in 2015 in locations throughout the Eel River watershed.

1.3.5 Cyanobacterial mat and water sampling results

Both *Anabaena* and *Phormidium* mats sampled in 2014 and 2015 produced anatoxin-a or microcystin. Though it was rare for a single sample to contain both cyanotoxins, most *Anabaena* and *Phormidium* mat samples tested positive for either anatoxin-a or microcystins. Compared to SPATT samples, intracellular anatoxin-a was detected more frequently and at higher concentrations than microcystin in the cyanobacterial mat samples ($p < 0.01$) (Fig. 1.11 and Fig. 1.12). Anatoxin-a concentrations were higher ($p < 0.01$) in *Anabaena* samples (mean= 2.45, max= 70.93 mg ATX g^{-1} DW) compared to *Phormidium* samples (mean= 0.86, max= 24.19 mg ATX g^{-1} DW), while microcystin concentrations were higher ($p < 0.01$) in *Phormidium* samples (mean= 0.20, max= 2.23 mg MCY g^{-1} DW) compared to *Anabaena* samples (mean= 0.07, max= 0.21 mg MCY g^{-1} DW), with the microcystin congeners –YR and –LR having the highest concentrations across all samples (Fig. A.4). Toxic samples were distributed across the different sub-watersheds in the Eel River catchment and toxin production was not localized to one particular region in the catchment (Fig. A.5 and Table A.1). Both anatoxin-a and microcystin were detected in water samples from 2015, (Fig. 1.13), but at concentrations less than 0.0015 ATX and 0.00075 MCY mg L^{-1}, below state recreational warning levels of 0.02 and 0.006 mg L^{-1}, respectively.

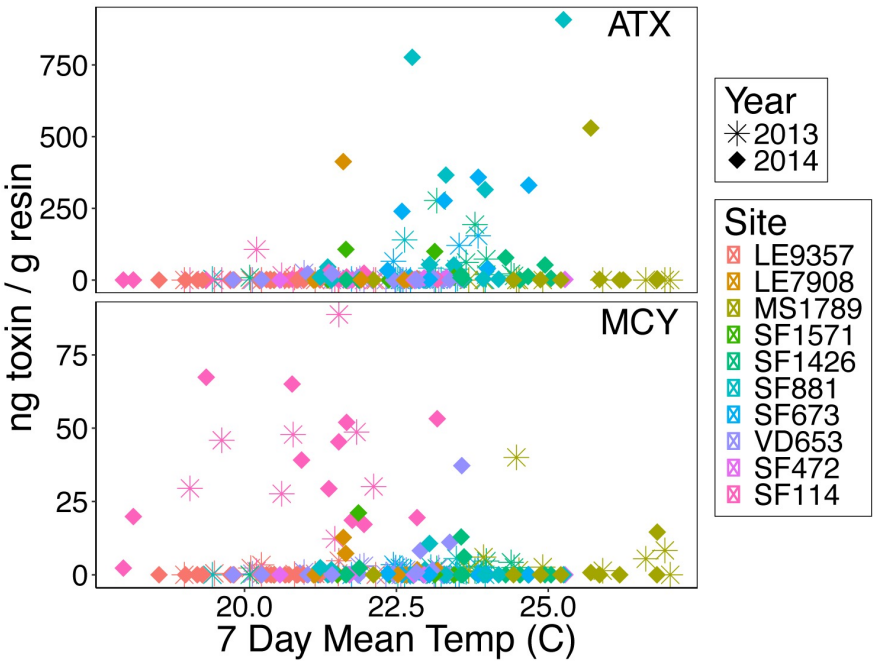

Fig. 1.9 SPATT levels of anatoxin-a (ATX) and microcystin (MCY) and average temp over the previous 7 days prior to collection of a SPATT sampler at each site.

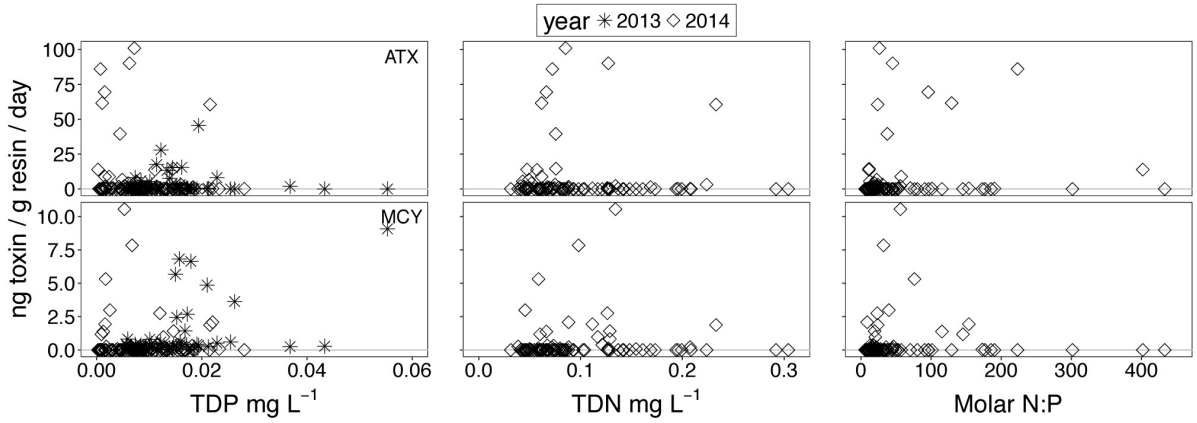

Fig. 1.10 Anatoxin-a (ATX) and microcystin (MCY) levels from SPATT samplers versus total dissolved phosphorus (TDP) and nitrogen (TDN) concentrations and molar N:P ratio of water samples collected when SPATT samplers were retrieved.

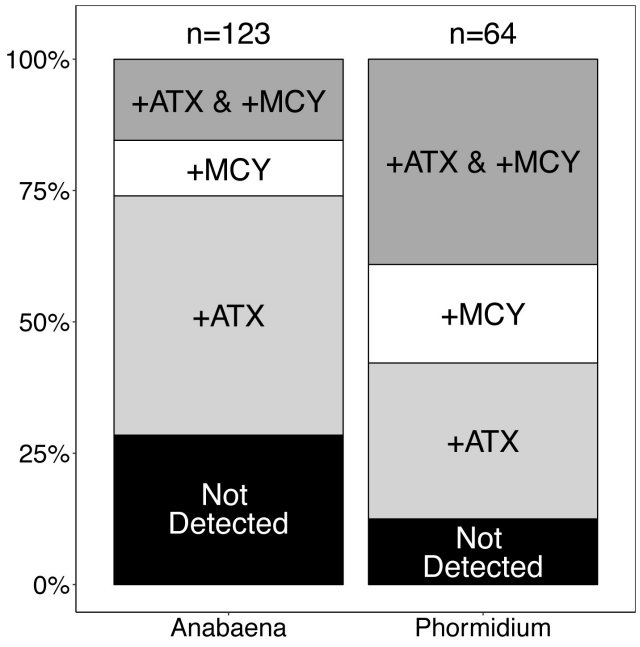

Fig. 1.11 Percentage of *Anabaena* or *Phormidium* dominated cyanobacterial mat samples with anatoxin-a (ATX) or microcystin (MCY) detected or not detected in the sample.

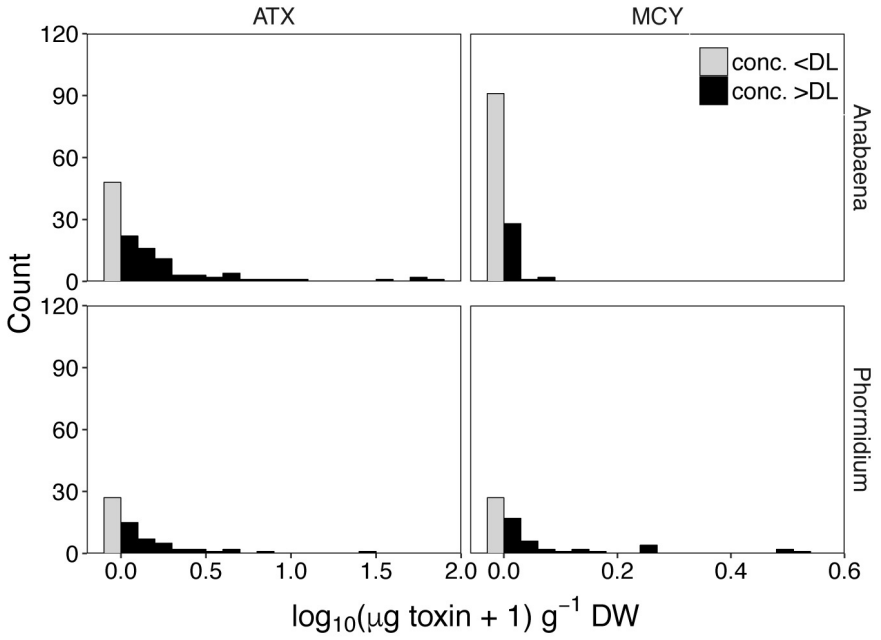

Fig. 1.12 Intracellular anatoxin-a (ATX) and microcystin (MCY) concentrations from cyanobacterial mats dominated by *Anabaena* or *Phormidium*. Samples were collected in 2014 and 2015. Counts are shaded gray if the concentration in the sample was below the detection limit (DL).

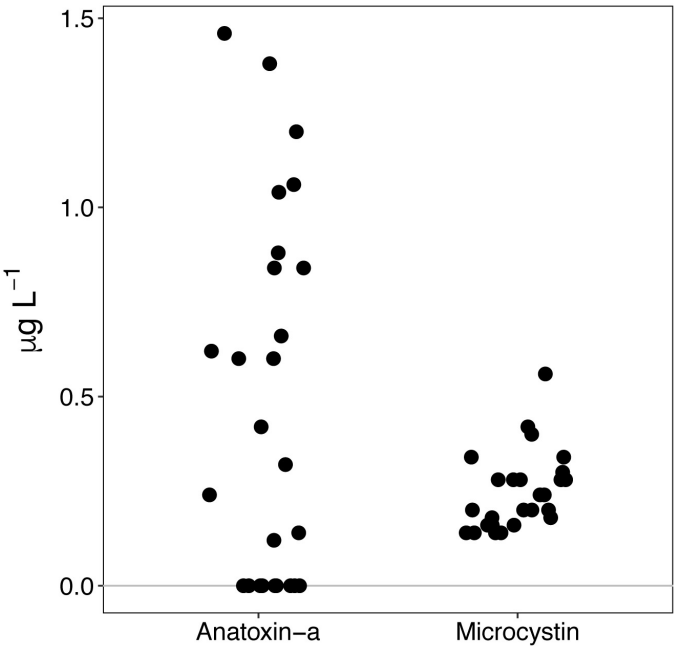

Fig. 1.13 Total anatoxin-a and microcystin concentrations (dissolved plus lysed suspended cells) in water samples collected in summer 2015.

1.4 Discussion

My results document the widespread distribution of anatoxin-a in the Eel River watershed, produced by benthic cyanobacterial taxa. Both *Anabaena*-dominated and *Phormidium*-dominated benthic cyanobacterial mats can produce anatoxin-a, but *Anabaena* mats produce higher concentrations of anatoxin-a and are more common throughout the watershed. To my knowledge, this is the first report of anatoxin-a dominance over microcystins in a North American watershed, and the first report of anatoxin-a production by benthic freshwater *Anabaena* mats (Bouma-Gregson et al. 2017).

1.4.1 Cyanobacterial taxa

Benthic *Anabaena* mats were frequently observed in the Eel River, often as epiphytes of the non-toxic green macro-alga *Cladophora glomerata*. In other regions of the world, toxic benthic cyanobacteria (e.g., *Phormidium)* are often in the order Oscillatoriales (Edwards et al. 1992, Cadel-Six et al. 2007, Quiblier et al. 2013, McAllister et al. 2016), whereas *Anabaena* is in the order Nostocales. Most data on toxic benthic *Anabaena* come from the Baltic Sea where blooms of *Anabaena* and *Nodularia* are common; however *Anabaena* in the Baltic Sea produce microcystins, and there are no reports of anatoxin-a production (Halinen et al. 2007, 2008, Karjalainen et al. 2007). Many planktonic species of *Anabaena* (now re-classified as the genus *Dolichospermum*, (Wacklin et al. 2009, Komarek 2013)) can produce anatoxin-a (Van Apeldoorn et al. 2007, Li et al. 2016a).

Phormidium-dominated mats in the Eel River also produced cyanotoxins. Higher proportions of *Phormidium* samples had cyanotoxins, especially microcystins, than did *Anabaena* samples. However, *Phormidium* samples had lower maximum concentrations of anatoxin-a than some *Anabaena* mats. While not rare, observed *Phormidium* mats were less common and smaller than *Anabaena* mats in the Eel River. *Phormidium* are also primarily confined to faster flowing riffle habitats in the watershed and not often found in sunny mainstem pools where people and dogs swim.

1.4.2 SPATT resin ATX adsorption and extractions

Anatoxin-a adsorbed more slowly and extracted less efficiently with HP-20 resin than microcystin molecules sampled and extracted by Kudela (2011). In testing different SPATT substrates for anatoxin-a detections, Wood et al. (2011) found that HP-20 adsorbed about 60% of the anatoxin-a in experimental beakers. In laboratory trials, Kudela (2011) found HP-20 adsorbed >90% of microcystin. Therefore, compared to microcystin SPATT data, anatoxin-a SPATT data are likely to underestimate *in situ* dissolved toxin concentrations. The advantage of HP-20 for monitoring programs is that multiple toxins can be extracted off of a single SPATT sampler. Understanding the different adsorption and extraction dynamics of different cyanotoxins collected from the same SPATT sampler is important for interpreting and comparing the extracted cyanotoxin concentrations (MacKenzie 2010). In high light and pH environments, extra-cellular anatoxin-a degrades within several hours (Stevens and Krieger 1991, Yang 2007, Kaminski et al. 2013). Microbes can also accelerate the degradation of anatoxin-a (Rapala et al. 1994). Control flasks in my experiment maintained stable anatoxin-a concentrations for 48 hours, suggesting increased stability under lower light and pH (Yang 2007). Presumably, the longer a SPATT sampler is in the river, the more the degradation of older anatoxin-a molecules on the resin occurs. More research into the stability of anatoxin-a molecules bound to SPATT resin in different light and pH environments could help optimize duration of SPATT sampler deployment (Kudela 2017).

1.4.3 Cyanotoxin patterns in the watershed

Anatoxin-a in the Eel River watershed was consistently detected in both SPATT samples and cyanobacterial mat samples, and both showed higher levels of anatoxin-a than microcystin. Planktonic cyanobacterial blooms have not been observed in the Eel River, and filtered water samples from the Eel River collected downstream of cyanobacterial mats in 2016 had <500 *Anabaena* cells mL^{-1} (Table A.1), suggesting that most biomass of toxigenic cyanobacteria is benthic. Due to their common occurrence and higher anatoxin-a concentrations in the samples, I hypothesize that benthic *Anabaena* are the dominant producers of anatoxin-a in the watershed.

The most upstream SPATT site (SF114) was the only site where microcystins were consistently detected, though at much lower levels than anatoxin-a. Cyanobacterial mat samples from this site did not show elevated microcystin concentrations, so it is unknown what taxa are producing these microcystin molecules. *Nostoc* spp. is common near this site and some species are known to produce microcystins. But *Nostoc* spp. are also found near downstream sites. In 2014, 10 *Nostoc* spp. samples were collected for cyanotoxin analysis, but none of the samples contained detectable

microcystins (Table A.1). More *Nostoc* samples should be collected to determine whether they are sources of microcystins near the South Fork Eel headwaters.

Cyanotoxins were rarely detected by the two most downstream SPATT samplers in the Lower Eel. Cyanobacterial mats were also less frequently found during sampling trips in these regions. It is possible that higher downstream discharge dilutes cyanotoxin concentrations resulting in lower detections from the SPATT samplers. During June – September in 2013 and 2014, river discharge between the two Lower Eel SPATT sites (USGS gage Scotia 11477000) was about 3.5x greater than along the South Fork between sites SF1426 and SF881 (USGS gage Miranda 114765000). SPATT values in the South Fork Eel were orders of magnitude higher than at Lower Eel sites, however, suggesting that reduced cyanotoxin production rather than dilution, explains the low SPATT detections in the Lower Eel. Smaller (less stable) bed sediments and lower temperatures and irradiance under the maritime coastal fog influence near the mouth might explain the decrease in cyanobacterial mats and cyanotoxins in the Lower Eel. Detection distances of upstream sources of cyanotoxins for a SPATT sampler are also unknown. The SPATT sampler sites in the South Fork Eel in 2013-2014 were tens of river kilometers apart, and I found no spatial or temporal autocorrelation among the samplers. This independence suggests that samplers were not detecting cyanotoxins produced at the same location, and could constrain the upper limits of downstream travel distance for the cyanotoxins.

Higher SPATT ATX levels were detected in warmer reaches of the South Fork Eel. However, the single Mainstem site in 2013 and 2014 (MS1789) was the hottest site, but had only 5 out of 17 SPATT anatoxin detections, of which only 1 was greater than 5 ng ATX g^{-1} resin, and cyanobacterial mats were never seen near this site. Water column nutrient concentrations did not show any spatial pattern and were not correlated with SPATT levels. However, N:P ratios increase in the Eel River as summer progresses (Finlay et al. 2011), and in New Zealand and Florida, cyanobacteria proliferate at low phosphorus concentrations (Rejmánková and Komárková 2005, McAllister et al. 2016). Lower P concentrations in summer might be driving the increase in cyanobacterial biomass, but decreasing P is also correlated with increasing temperatures and decreasing river flow over time, so experiments will be needed to tease apart the independent and interactive effects of these variables on benthic cyanobacterial growth. The relationship of dissolved nutrients to benthic algal productivity is often obscure, because benthic proliferations can rapidly deplete and store nutrients from the water column, and continue to derive nutrients from local recycling or the substrate (Wood et al. 2015, Vadeboncoeur and Power 2017).

Cyanobacterial mat samples collected *in situ* from the river were mixed microbial assemblages dominated by cyanobacteria, and samples may have contained multiple strains or taxa producing cyanotoxins. Cell counts confirmed, however, that while other taxa (*Nodularia*, *Cylindrospermum*, *Leptolyngbya*, or *Oscillatoria* trichomes), were present in mats dominated by *Anabaena* or *Phormidium*, they were uncommon (Table A.3) and usually dominated by Leptolyngbya which has a low bio-volume per cell. Different species or strains of both *Phormidium* (Aboal et al. 2005, Wood et al. 2012, Quiblier et al. 2013) and *Anabaena* (Quiblier et al. 2013, Li et al. 2016a) produce either microcystins or anatoxin-a. Toxin concentrations in mats can even vary at the

centimeter scale (Wood et al. 2012). Therefore, the isolation of *Anabaena* and *Phormidium* strains from the Eel River will be necessary to determine which produce anatoxin-a.

All data were collected during years of drought in California, with 2015 being one of the driest years in recorded California history. Drought conditions favor cyanobacterial growth in the river by elevating water temperatures (Paerl and Otten 2013) reducing flow velocity, and increasing residence times of water held in sunlit mainstem pools. *Anabaena* are found in slow-flowing sections of the river, which develop earlier in the summer during drought. Future climate projections in California predict more extreme summer droughts (Cayan et al. 2008), which could increase the spatial and temporal occurrence of cyanobacteria in coastal California rivers.

1.4.4 Conclusion

To my knowledge, this is the first report of widespread anatoxin-a production by benthic *Anabaena* in a river. My data corroborate the study linking dog deaths in the watershed to anatoxin-a (Puschner et al. 2008). In Mediterranean climates, benthic algal production and biomass supports aquatic and riparian food webs (Power et al. 2008, 2013), and consequences of increasing cyanobacterial biomass for these food webs are unknown. Water quality and public health are also threatened by benthic cyanobacteria in rivers. Monitoring methods and regulatory guidelines established in lakes and estuaries are not easy to apply in rivers, where cyanobacteria are attached and aggregated into mats. Additionally, river flow transports cyanotoxins and any detached cells or mats downstream (Bouma-Gregson et al. 2017). Passive cyanotoxin sampling can be used in rivers to detect cyanotoxin patterns across a watershed, and can be coupled with additional sampling methods to monitor riverine cyanobacterial dynamics. As human population growth and land use put increasing stress on water resources and aquatic food webs, understanding the biology and ecology of cyanobacteria is necessary to maintain water quality and protect the beneficial uses of aquatic ecosystems.

2 Rise and fall of toxic benthic freshwater cyanobacteria (*Anabaena* spp.) in the Eel river: buoyancy and dispersal

Abstract

Benthic cyanobacteria in rivers produce cyanotoxins and affect aquatic food webs, but knowledge of their ecology lags behind planktonic cyanobacteria. The buoyancy of benthic *Anabaena* spp. mats was studied to understand implications for *Anabaena* dispersal in the Eel River, California. Field experiments were used to investigate the effects of oxygen bubble production and dissolution on the buoyancy of *Anabaena* dominated benthic mats in response to light exposure. Samples of *Anabaena* dominated mats were harvested from the South Fork Eel River and placed in settling columns to measure floating and sinking velocities, or deployed into *in situ* ambient and low light treatments to measure the effect of light on flotation. Floating and sinking occurred within minutes and were driven by oxygen bubbles produced during photosynthesis, rather than intracellular changes in carbohydrates or gas vesicles. Light experiment results showed that in a natural ambient light regime, mats remained floating for at least 4 days, while in low light mats begin to sink in <24 hours. Floating *Anabaena* samples were collected from five sites in the watershed and found to contain the cyanotoxins anatoxin-a and microcystin, with higher concentrations of anatoxin-a (median 560, max 30,693 ng / g DW) than microcystin (median 30, max 37 ng / g DW). The ability of *Anabaena* mats to maintain their buoyancy will markedly increase their downstream dispersal distances. Increased buoyancy also allows toxin-containing mats to collect along shorelines, increasing threats to human and animal public health.

2.1 Introduction

Cyanobacterial harmful algal blooms (cyanoHABs) have become increasingly common phenomena in many freshwater systems (Paerl and Huisman, 2009; Carey et al., 2012; Taranu et al., 2015). Most of these are nuisance blooms of planktonic species and occur in lakes, estuaries, or regulated lowland rivers, but benthic cyanobacteria can also produce cyanotoxins (Quiblier et al. 2013). Benthic cyanobacterial species are generally different from planktonic species, forming dense mucilaginous mats on bottom substrates. Benthic cyanoHABs are caused by species of *Anabaena* (Mohamed et al. 2006), *Phormidium* (McAllister et al. 2016), *Oscillatoria* (Edwards et al. 1992), *Lyngbya* (Cowell and Botts 1994), and *Nodularia* (Lyra et al. 2005). Toxic benthic cyanobacteria in rivers have been documented in many countries including Egypt, Spain, France, California, and New Zealand (Mohamed et al., 2006; Sabater et al., 2003; Cadel-Six et al., 2007; Fetscher et al., 2015; McAllister et al., 2016; for review Quiblier et al., 2013).

Different hydraulic and physicochemical environments between benthic and planktonic cyanobacteria have led to different ecological interactions and strategies for cyanobacteria growing in each habitat (Scott and Marcarelli 2012). In benthic cyanobacterial mats, light

attenuates rapidly through the mat (Jorgensen et al. 1987), strong geochemical gradients develop (Wood et al. 2015), and nutrients are acquired from within the mat, from overlying water and sometimes from substrates (Stevenson et al. 1996, Aristi et al. 2017). Planktonic cyanobacteria, on the other hand, often experience a spatial separation between light and nutrients availability in stratified waters, with high light and low nutrients near the water surface, and high nutrients and low light in deeper waters. To access these essential resources, many planktonic cyanobacteria migrate between surface and bottom waters by regulating their buoyancy with the formation of gas vesicles to increase buoyancy (Reynolds 1972, Walsby 1975) and the formation of dense carbohydrate granules to decrease buoyancy (Kromkamp and Mur 1984, Reynolds et al. 1987). Colonial species, like *Microcystis,* and filamentous species, like *Dolichospermum,* (formerly *Anabaena*, (Wacklin et al. 2009, Komárek 2010)), use these mechanisms to move up and down through the water column (Visser et al. 1997, Bormans et al. 1999). While dispersal mechanisms have been well-studied in river phytoplankton (Bormans and Condie 1997, Maier et al. 2001), much less is known about dispersal by benthic cyanobacteria (or other benthic algae) in rivers. Studies on benthic species dispersal have been on detached and floating green algae (Power 1990, Mendoza-Lera et al. 2016) or diatoms (Stevenson and Peterson 1989, 1991), and more recently on the cyanobacterium *Phormidium*, which also poses a public health risk (McAllister et al. 2016). To better understand benthic algal dispersal, this paper reports observations on the buoyancy of *Anabaena* spp. in the Eel River of northwestern California, where it grows epiphytically on the green macroalga, *Cladophora glomerata* (Power et al. 2015).

Benthic *Anabaena* produce no gas vesicles (Komarek 2013, Li et al. 2016b), and are not able to regulate their density via intracellular mechanisms used by planktonic cyanobacteria. There are, however, other potential mechanisms for dispersal of benthic *Anabaena*: 1) trichome motility via gliding (Hoiczyk 2000); 2) vegetative overgrowth of host algae; 3) detachment of individual trichomes from the mat (Otten et al. 2015); 4) akinete formation and dispersal, followed by germination (Cirés et al. 2013); and 5) detachment of macroscopic floating clumps advected downstream by the river flow (Cadel-Six et al. 2007, McAllister et al. 2016).

This paper focuses on downstream dispersal of floating detached clumps (mechanism 5), which likely accounts for long-range dispersal from the original mat location. Benthic cyanobacteria are known to produce oxygen bubbles from photosynthesis (Wilson 1965, Bosak et al. 2010). These bubbles become trapped in the intercellular mucus of the mats, lifting the top of the mat to form a vertical, spire-like shape, which is a common morphology for benthic cyanobacterial mats (Figure 2A-B, Figure 3C; Bosak et al., 2010; McGregor and Rasmussen, 2008). In the Eel River, California, *Anabaena* mats are delicate, and easily detached by flows of >5 cm s^{-1} or by gentle water agitation (Bouma-Gregson, personal observation). When these mats disintegrate, the bubbles in the mucus cause the majority of an *Anabaena* mat to float to the water surface as many small clumps (1-5 cm diameter). During summer, floating clumps of *Anabaena* are frequently observed in the river, moving hundreds of meters, primarily in a downstream direction unless wind-driven over slow pools. Floating clumps often concentrate at channel margins and recreational swimming areas, and dogs have died in the Eel River due to anatoxin-a poisoning after ingesting cyanobacterial mats (Puschner et al. 2008), making toxic benthic cyanobacteria a public health concern each summer.

Given the consequence for water quality and animal and public health from cyanotoxin exposure, more knowledge is needed about how filaments, clumps, or mats of benthic cyanobacteria disperse in rivers during summer low flow periods. Combined with the river flow velocity, the time scales of floating and sinking will control the distance scales of dispersal of floating clumps and mats in the river. To understand these time-scales and the processes responsible for buoyancy, field experiments were used to 1) study the effects of light on macroscopic oxygen bubble production, and 2) the effect of bubbles on the buoyancy of benthic *Anabaena* dominated mats.

2.2 Materials and methods

2.2.1 Study system and site description

The Eel River, draining 9,546 km^2, is located in the coastal mountains of Northern California (Fig. 2.1). Forestry has been the principal land-use since European settlement, with dairy and small-scale agriculture near the estuary. A history of logging and dense networks of unpaved roads along with two large floods (1955 and 1964) have loaded massive amounts of fine sediments into channels, rendering them wider, shallower, and easier to warm or de-water at low flow (Lisle 1990). The Eel is in a Mediterranean climate with rainy winters and seasonal summer droughts. Daily average river temperatures in the summer range from 20-25°C, and daily maximum temperatures can exceed 30°C along shallow channel margins. Experiments took place at the Angelo Coast Range Reserve (angelo.berkeley.edu), a 3,100 ha reserve on the South Fork (SF) Eel River where the channel drains 150 km^2 (Fig. 2.1).

Anabaena spp. appear in June-August in sunny, slow-flowing (<10 cm s^{-1}) river reaches, first as small, blue-green epiphytic tufts near the top of fresh or senescent, diatom-covered *Cladophora* proliferation*s* (Power et al. 2015). Over the following weeks or months, if flows remain slow (<10 cm s^{-1}) and relatively warm (20-25°C at midday), *Anabaena* mats can spread, turning several square meters of *Cladophora*/diatom assemblages a blue-green color (Fig. 2.2). There are at least three common species of mat forming *Anabaena* in the Eel River: *Anabaena oscillarioides*, *A. cylindrica*, and *A. sphaerica* (Komarek 2013). These species are difficult to differentiate based on macroscopic mat morphology and all grow in similar habitats.

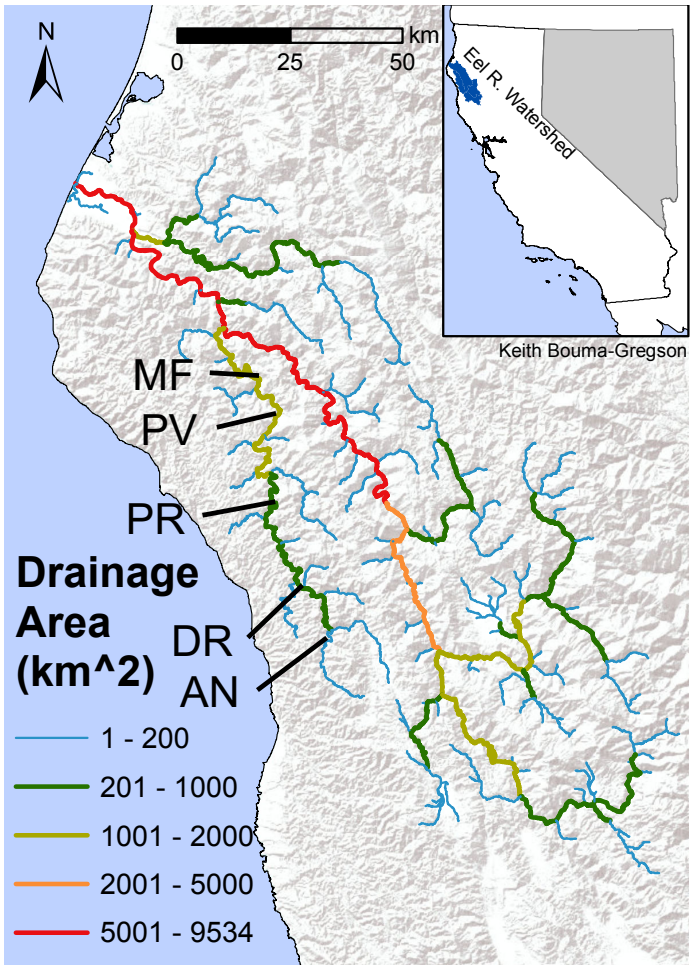

Fig. 2.1 Map of the Eel River watershed showing sites along the South Fork Eel River where floating *Anabaena* spp. clumps were collected in 2014. Field experiments were conducted at the AN site in 2016.

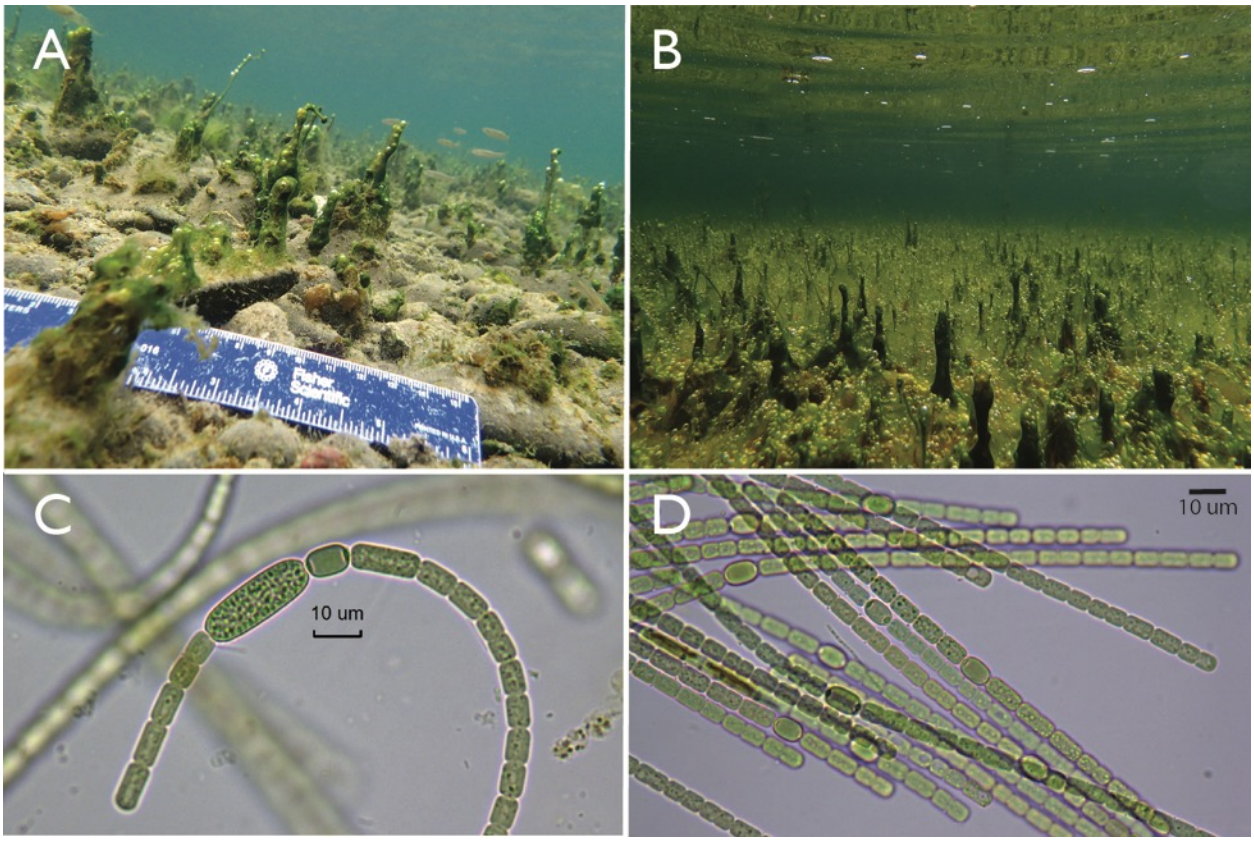

Fig. 2.2 A-B) Underwater photographs of *Anabaena* spp. spires. The dark green patches are *Anabaena* spp. growing on top of *Cladophora glomerata* filaments. Note the trapped bubbles in the *Anabaena* mucus. C-D) *Anabaena cylindrica* trichomes at 400×, panel C shows a developing akinete.

2.2.2 Light Experiment

To investigate the effect of light on flotation and bubble production, an *in situ* field experiment was conducted during June 20-24, 2016. Vertically-placed PVC pipes (25 cm diameter and 1 meter length, 10 pipes total) were set into the SF Eel River, with the top 2-6 cm of the pipe above the river surface (Fig. 2.3). Mesh windows (0.3 × 0.3 mm, dia. 9 cm) on the sides of each pipe allowed enough water exchange to keep inside temperatures at ambient levels. Five replicate pipes each were used for Ambient-Light and Low-light treatments. Low-light treatment pipes were wrapped in black polyurethane plastic to decrease light intensity inside the pipe. A spoon was used to harvest benthic *Anabaena* from nearby naturally occurring mats without disturbing bubbles, and three *Anabaena* clumps (3-48 × 7-80 mm) were placed in each pipe (Fig. 2.3). All clumps were floating when placed in the pipes. Then an aluminum foil covering was placed over the Low-light treatment pipes. Clumps were placed on the afternoon of day 0. Beginning on day 1, every morning (~06:00, before direct sunlight hit any pipes) and afternoon (14-16:00, at the hottest time of the day) clumps were observed to see if they were still afloat or had sunk. The number of bubbles in each clump was also counted and measured to the nearest millimeter. The experiment concluded after the morning measurement on day 4. In some pipes, two clumps

merged together to form a single clump, therefore the proportion of clumps floating at each measurement was used as the response variable.

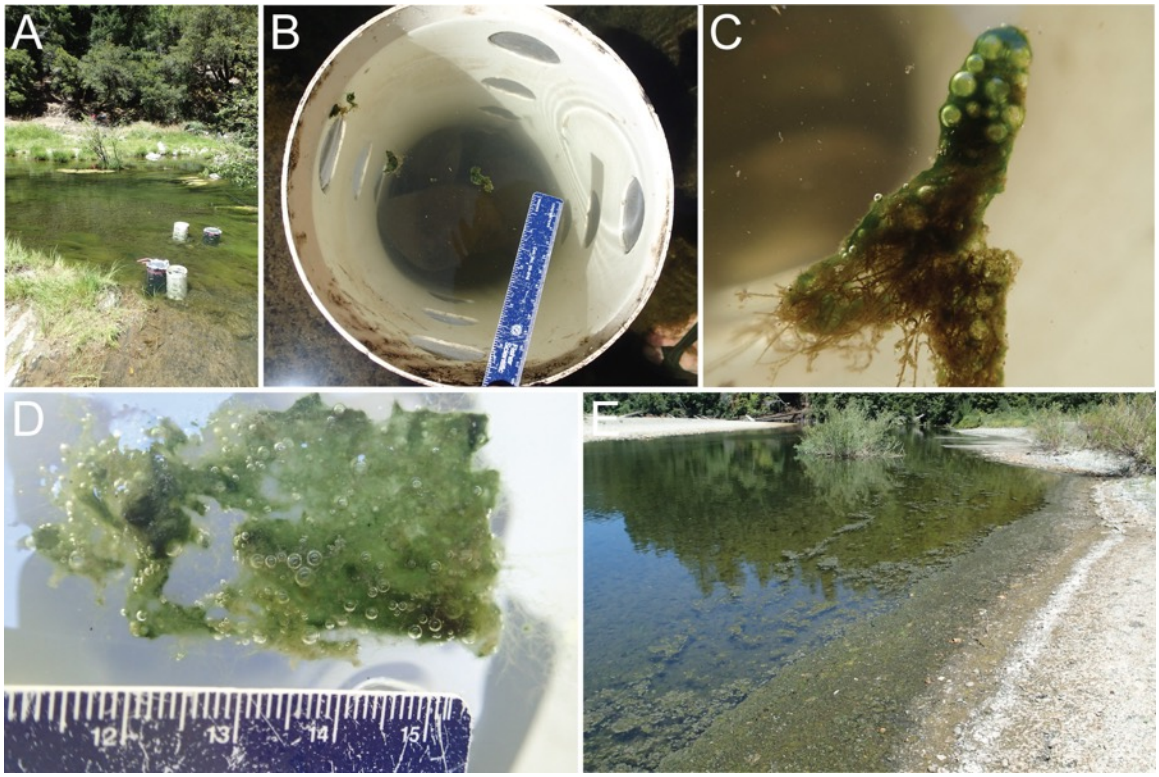

Fig. 2.3 A) Two of the replicate Low-light and Ambient-light treatment pipes. B) Floating *Anabaena* spp. clumps in a flow through pipe. C-D) Floating *Anabaena* spp. clumps showing the accumulation of bubbles within extracellular mucus. E) Accumulation of floating *Anabaena* spp. clumps along the river margin in July 2016.

To determine the light reduction in the Low-light treatment pipes, Hobo Pendant temperature and light sensors (UA-002-08; Onset, Bourne, Massachusetts, USA) were deployed on day 4 after the *Anabaena* clumps were removed from the pipes. In each of the five Low-light and Ambient-light pipes, two sensors were deployed for 24h at the water's surface, one with the light sensor pointing upwards to the sky, and the other with the sensor pointing downwards into the water. After positioning the sensors, Low-light pipes were again covered with aluminum foil.

At deployment and on day 4, samples from each clump were collected and stained with SYTOX green (Sigma-Aldrich, S7020) to test for cell wall integrity. If flotation was stressful for the cyanobacteria, an increase in cell wall degradation might be expected at the end of the experiment. An *Anabaena* clump sub-sample was placed in a 2mL microfuge tube filled with ~1 mL of river water. Then, 20 µL of 5 µM SYTOX green was added and the total volume brought to 2mL for a final SYTOX concentration of 0.5 µM. The SYTOX solution was briefly vortexed and incubated for 10 minutes in the dark at room temperature. Stained cells, indicating degraded cell walls, were counted at 200× with epi-fluorescent microscopy (Nikon Optiphot 2, 490/520nm

ex/em λ). The species identification and cell condition for all samples were determined by microscopy on fresh material using the same Nikon Optiphot 2.

2.2.3 Buoyancy Experiments

To determine floating and sinking velocities of *Anabaena* clumps from different algal assemblages, subsamples of algal mats from different origins were collected: floating *Cladophora glomerata* mats detached from bottom substrates, floating *Cladophora* mats still attached to bottom substrates, and *Anabaena* spires attached to bottom substrates. Sub-samples from the *Cladophora* mats were divided into two categories: clumps from *Cladophora* mats dominated by *Cladophora*, and clumps from *Cladophora* mats dominated (>50%) by epiphytic *Anabaena* growing on the *Cladophora*. Experiments were performed on June 22 and July 20-21, 2016. Glass Pyrex graduated cylinders (1,000 mL) filled with river water and exposed to natural sunlight were used as settling columns to measure velocities. Floating and sinking of clumps was recorded with a video camera, using time elapsed and the graduated scale on the cylinder to quantify upwards and downwards velocities. The temperature of the river water was also measured. Bubbles were removed from floating clumps by either manual pinching or by shaking the cylinders. Subsamples of mats collected *in situ* were either directly exposed to natural sunlight or first placed in the dark for 12 hours to remove bubbles and ensure that clumps sank. Once clumps had sunk, the graduated cylinder was placed in the light until bubbles formed and the clumps floated to the surface.

2.2.4 Cyanotoxin analyses

To determine if floating *Anabaena* clumps contained cyanotoxins, twenty samples of floating *Anabaena* spp. were collected in late June through mid-September, 2014 from five different locations on the SF Eel River (Fig. 2.1) and analyzed for anatoxin-a (ATX) and microcystins (MC) using liquid chromatography and mass spectrometry (LC-MS). Fifteen of these samples came from weekly sampling events at the monitoring site PV. The remaining five samples, were collected on different days in July 2014 at four additional sites MF, PR, DR, and AN. Floating samples were collected with a bulb syringe or skimmed off the surface with an 80 μm plankton net, transferred into glass sample jars, placed in a cooler, and within 6 hours returned to the laboratory for overnight storage in the dark at 4°C. The next day samples were homogenized and sub-samples frozen at -20°C for dry weight and cyanotoxin analysis. To measure the dry weight, samples were dried at 55°C for 24 hours and then weighed to the nearest 0.1 mg. A subsample was also collected for microscopic analysis to identify the dominant species of cyanobacteria in the sample.

For cyanotoxin analysis, samples were thawed, then sonicated for 30 s (Fisher Sonic Dismembrator 100) in 6 mL of 50% methanol (Fisher A452), then centrifuged (Model IEC Centra CL2; Thermo Fisher Scientific, Massachusetts, USA) for 5 min at 1,083 rcf, and the supernatant sampled. For ATX analysis, a 1 mL subsample was filtered (0.2 μm) into a LC-MS vial. Samples for MC analysis were cleaned using a Baker C18 solid phase extraction column, and 1 mL of cleaned sample was transferred to an LC-MS vial.

MC and ATX were analyzed separately by liquid chromatography coupled with a mass spectrometer on a Single Quadrupole Agilent 6130 LC-MS (Agilent Technologies). ATX analysis followed Cogent method 141 (MicroSolv Technology Corporation, Leland, NC, USA; http://kb.mtc-usa.com/getAttach/1114/AA-00807/No+141+Anatoxin-a+ATX-A.pdf). Briefly, a Cogent diamond hydride column (100A, 4um, 100x2.1mm) was used with a gradient elution of 50% MeOH with 0.1% formic acid, and 100% acetonitrile with 0.1% formic acid with the MS in Select Ion Mode (SIM) for MW 166.1 and 149.1. Quantification was based on standard curves (run daily) with a CRM-ATX standard from National Resource Council Canada (http://www.nrc-cnrc.gc.ca/eng/solutions/advisory/crm/list_product.html#B-CT). MC analyses followed the method in Gibble and Kudela (2014), which was adapted from Mekebri et al. (2009). Briefly, a gradient-elution method was used as the mobile phase, with HPLC water (solvent A) and LC-MS acetonitrile (solvent B), both acidified with 0.1% formic acid. The gradient starts with 95:5 of solvent A:B and ends with 25:75 at 19 min, is held for 1 min, then followed by a 5 min equilibration at initial conditions prior to injection of the next sample. Standard curves (for each batch of samples) using pure standards (Fluka 33578 and Sigma–Aldrich M4194) were used to calibrate samples. For sample runs lasting more than 8 hours, standards were run again at the end of the run. The LC-MS measured four microcystin congeners (–LR, –YR, –RR, and –LA), and their values were summed to give total microcystin (MC). The limit of detection for ATX and MC are 0.25 and 0.01 ppb, respectively.

2.2.5 Statistics

For the light experiment, generalized linear mixed models (glmms), with replicate pipe as a random effect, were used to model the effect of light treatment, day, and time of measurement (AM/PM) on the flotation of clumps (binomial distribution) and the number of bubbles (Poisson distribution). For the buoyancy experiment, one-way ANOVA was used to test the effect of algal assemblage on sinking and floating velocities. Likelihood ratio or F ratio tests between full and reduced models were used to estimate the statistical significance of model parameters (alpha= 0.05). All statistics were performed in the R environment, version 3.3.2 (R Core Team 2017), with the lme4 package (Bates et al. 2015) used for glmms.

2.3 Results

2.3.1 Anabaena cell condition

Samples for light and buoyancy experiments were dominated by *Anabaena* cylindrica, with <1% of trichomes being A. oscillarioides (Fig. 2). At the time of collection, all *Anabaena* trichomes were fully pigmented, had heterocytes, and <1 akinete per trichome, as well as containing many dividing cells, indicating a relatively healthy physiological status. SYTOX green staining from light experiment samples indicated <<1 cell per trichome had a cell wall permeable to SYTOX green on samples from Day 0 and Day 4, a further indication of healthy cells.

2.3.2 Light experiment

Light intensity data showed that Low-light treatment had values <0.01% of the Ambient-light treatment with the mean maximum intensity from the upward facing sensor for the Ambient-light and Low-light treatments being 235,877 ± 12,567 and 58 ± 31 lumens / m^2, respectively.

The diel range in river surface temperatures was 16.5-23.5°C, with Low-light treatments being 0.5-1°C warmer than Ambient-light treatments in the afternoon and having the same temperatures in the morning.

All clumps were floating at the onset of the light experiment. Clumps began sinking within 24 hours in the Low-light treatments (Fig. 2.4). By day four, all the clumps in four of the five Low-light treatment replicates had sunk. In the Ambient-light treatment, by day 4 only one individual clump had sunk. Any clump that sunk in the Low-light treatment never re-floated, whereas the clump in the Ambient-light treatment that sunk after the Day 1: PM measurement, refloated on day two due to bubble production (Fig. 2.4). This clump then remained floating for two more days until sinking on day four. The binomial glmm found a significant positive effect of light treatment ($p < 0.005$), a significant negative effect of day ($p < 0.001$), and a positive, but non-significant, treatment*day interaction effect ($p = 0.092$) on flotation.

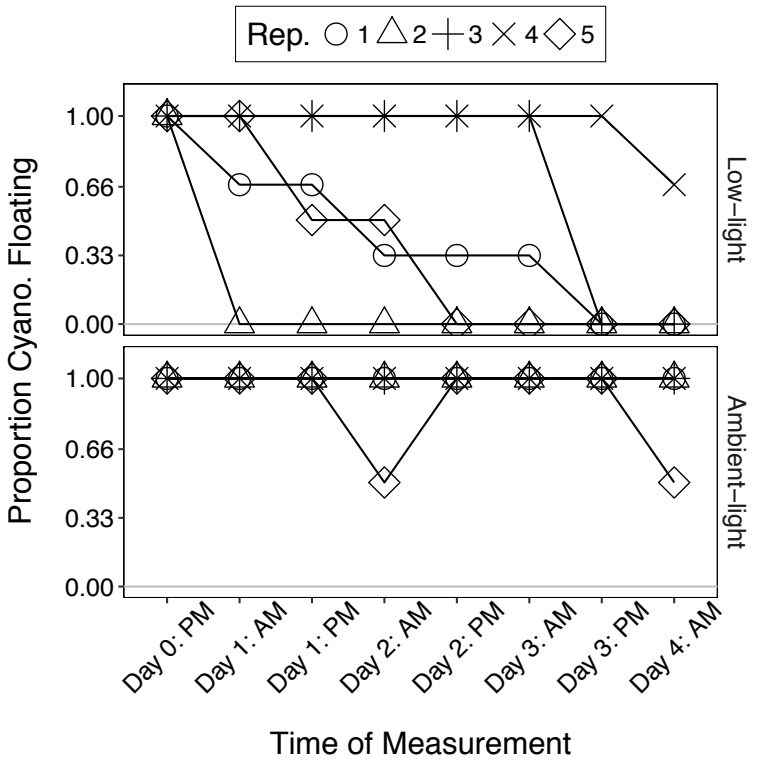

Fig. 2.4 Proportion of floating *Anabaena* spp. clumps in each of the five replicates of the Low-light and Ambient-light treatments at each morning (AM) and afternoon (PM) measurement over the 4 days of the experiment.

The number of bubbles in the clumps were similar at deployment on Day 0 (Fig. 2.5). Bubble numbers subsequently decreased in the Low-light treatments, but remained relatively constant in Ambient-light treatments. The glmm model showed a significant treatment effect ($p < 0.005$) and day*treatment interaction effect ($p < 0.005$) on the sum of bubbles in each replicate pipe

during the experiment, with the Ambient-light treatment having more bubbles than the Low-light treatment. There was also a significant positive interaction effect between the time of day (AM/PM) and light treatment ($p < 0.005$) indicating more bubbles at each of the afternoon (PM) measurements in the light treatment compared to the previous morning's (AM) measurement (Fig. 2.5), while in the Low-light treatment there was no difference in bubbles between morning and afternoon.

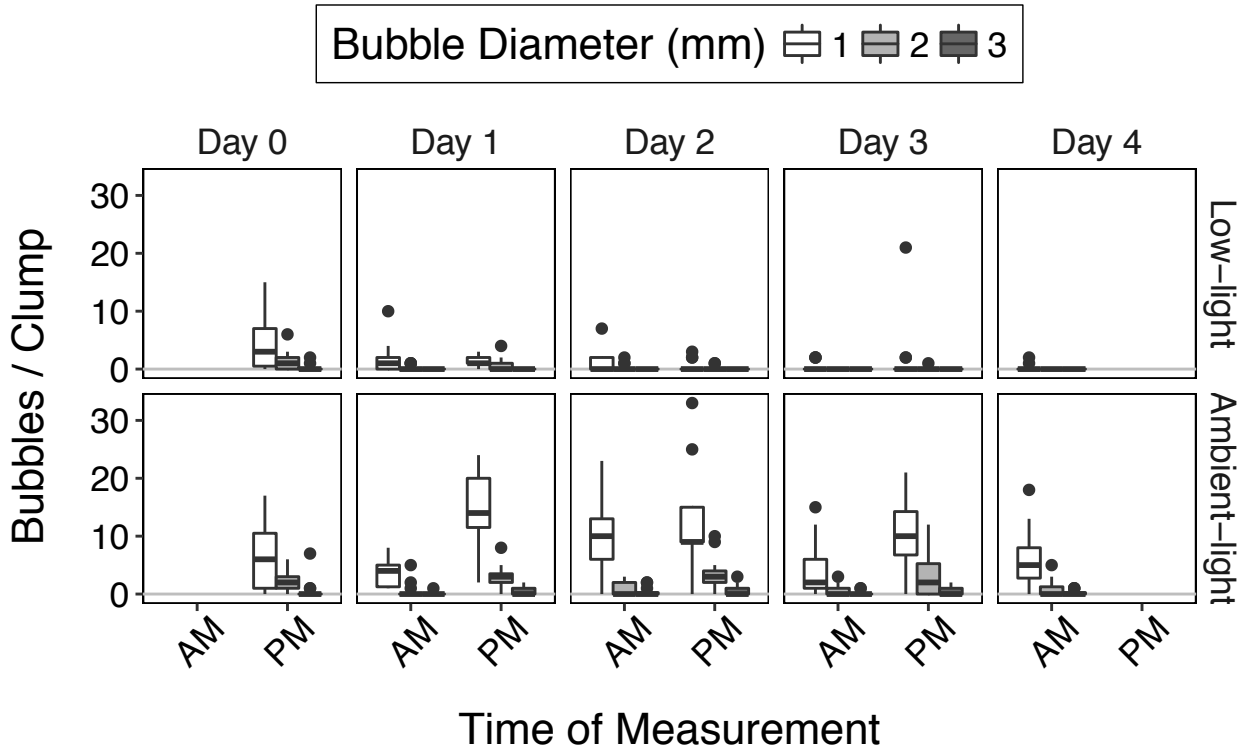

Fig. 2.5 Boxplots of number of bubbles in *Anabaena* spp. clumps in the Low-light and Ambient-light treatments at each measurement time. Bubble diameter was measured to the nearest millimeter.

2.3.3 Buoyancy experiment

All small *Anabaena* clumps (1 to 3 cm^3) collected from bottom *Anabaena* spires in situ in mid-afternoon on June 22, 2016 floated at the surface of the glass cylinder placed in sunlight (water temp. 18.5°C). Oxygen bubbles were observed in all clumps, some on the outside of the clumps, but mostly within the mucus of the mat. The bubbles were manually removed by pinching to assess the role of oxygen on the buoyancy of the clumps. Following the removal of oxygen bubbles, all clumps began to sink within 60 seconds, with mean velocities of 0.7 cm s^{-1} (Fig. 2.6). After around 30 minutes in full sun, they began to rise again with mean velocities of 0.9 cm s^{-1} (Fig. 2.6). Slightly different floating velocities were observed depending on the morphology, smaller clumps (~1 cm^3) floating faster than larger ones (~3 cm^3).

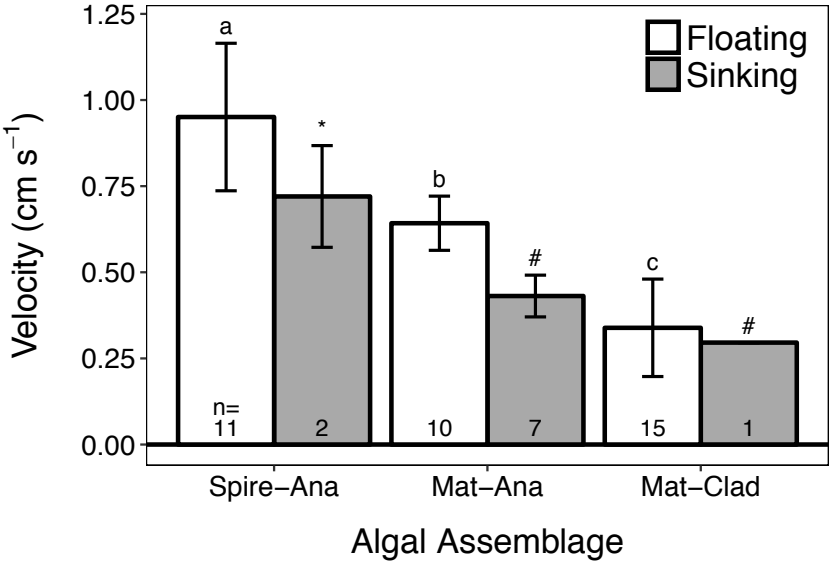

Fig. 2.6 Combined results from the buoyancy experiments showing the mean ± SD floating and sinking velocities of clumps from different algal assemblages. Spire-Ana: clumps sampled directly from *Anabaena* spp. spires that were almost exclusively *Anabaena* spp.; Mat-Ana: clumps from *Cladophora glomerata* mats overgrown by epiphytic *Anabaena* spp. overgrowth; and Mat-Clad: clumps from *Cladophora* mats dominated by *Cladophora,* with less than 50% *Anabaena*. Number of replicates (n) indicated at the bottom of each bar. Different letter superscripts indicate statistically significant differences in mean floating velocities and different symbol superscripts indicate statistically significant differences in mean sinking velocities between algal assemblages based on one-way ANOVA and Tukey-Kramer *post hoc* tests (alpha= 0.05).

Subsamples collected in situ in late afternoon on July 20, 2016 from detached floating *Cladophora* mats epiphytized by *Anabaena* stayed at the surface of the glass cylinders placed in sunlight (water temp 19.5˚C). All of them displayed visible oxygen bubbles. The water was gently mixed in the cylinder by manual shaking for a few seconds and this disrupted the mat, which disintegrated into small sinking clumps. Within minutes after sinking to the bottom of the cylinder, these *Cladophora-Anabaena* clumps started to float and to re-aggregate. *Cladophora* clumps heavily overgrown by *Anabaena* floated more rapidly than *Cladophora* clumps with sparser (<50%) epiphytic *Anabaena* cover (ANOVA $F_{(2, 33)} = 49.67$, $p < 0.01$; Tukey-Kramer post hoc test $p < 0.05$) (Fig. 2.6). Oxygen bubbles were observed during the rise of the mats, with larger bubbles associated with the *Anabaena* and smaller bubbles with *Cladophora*.

After being in the dark for 12 hours at 19˚C, all samples from the three different source mats sank to the bottom of cylinders, and no obvious oxygen bubbles were observed initially. Once placed in the sunlight, bubbles formed after 30 to 40 minutes, and the mats began to float. Again, clumps dominated by *Anabaena* rose faster than clumps dominated by *Cladophora* (ANOVA $F_{(2, 7)} = 13.23$, $p < 0.01$; Tukey-Kramer post hoc test $p < 0.05$) (Fig. 2.6). After gentle mixing of the cylinders by shaking them manually for a few seconds, the mats disintegrated into small clumps that settled to the bottom of the cylinder. The *Anabaena* broke apart more easily than the *Cladophora*, formed much smaller clumps and sank faster. The *Cladophora* did not

disintegrate and sank more slowly than *Anabaena* (Fig. 2.6). Regardless of the habitat and algal taxa within the mat assemblages, floating velocities were consistently higher than sinking velocities. However, the observed range between 0.25 and 1 cm s^{-1} suggested that clumps would rise and fall in a 50 cm deep still river pool, representative of much of the South Fork Eel habitat during the low flow summer season, within less than five minutes.

2.3.4 Cyanotoxins

Both ATX and MC were detected in the floating *Anabaena* samples collected in the SF Eel watershed (Table 2.1). Fourteen of the 20 samples contained ATX (median and mean concentrations of 560 and 3,184 ng ATX / g DW, respectively). In contrast, only 3 samples tested positive for MC and all had much lower MC concentrations (< 50 ng MC / g DW). All three positive MC samples also contained ATX. Toxin concentrations varied weekly at the Phillipsville (PV) site, though due to the movement of floating clumps the same mat was not sampled each week. ATX concentrations also varied spatially, the difference in ATX concentrations between duplicate samples collected on the same date from the PV site ranged from 0 to 10,424 ng ATX / g DW.

2.4 Discussion

2.4.1 Processes responsible for regulating buoyancy

Unlike planktonic cyanobacteria, in which buoyancy is regulated via intracellular processes including formation of gas vesicles (Walsby et al. 1991) and carbohydrates (Visser et al. 1997), in benthic *Anabaena* mats, the results of this study indicate that buoyancy is regulated by photosynthetic oxygen production and respiration. Oxygen bubble production by photosynthesis has been suggested as responsible for algal lift in rivers (Mendoza-Lera et al. 2016), for laboratory-generated bloom formation in planktonic cyanobacteria Microcystis after gas vesicle collapse (Dervaux et al. 2015), and for persistent buoyancy of Microcystis colonies leading to cyanobacterial scums on lakes (Medrano et al. 2016). For benthic *Anabaena* bubbles cause floating and sinking to occur within minutes and flotation to be maintained for days.

Table 2.1 Concentration of cyanotoxins anatoxin-a (ATX) and microcystin (MC) in floating *Anabaena* spp. clumps collected from the South Fork Eel River. Microcystin congeners –LR, –YR, –RR, and –LA were summed together to calculate the MC value.

Date Collected	Site	Collection Method	ATX (ng / g DW)	MC (ng / g DW)
07-Jul-14	AN	bulb syringe	NA[1]	NA[1]
18-Jul-14	DR	bulb syringe	2,744	0
12-Jul-14	MF	bulb syringe	172	0
18-Jul-14	PR	bulb syringe	30,693	0
24-Jul-14	PR	bulb syringe	0	0
29-Jun-14	PV	plankton net	0	0
12-Jul-14	PV	plankton net	647	0
18-Jul-14	PV	plankton net	3,184	0
18-Jul-14	PV	bulb syringe	3,703	0
24-Jul-14	PV	plankton net	0	0
02-Aug-14	PV	bulb syringe	15	0
02-Aug-14	PV	plankton net	4,985	0
07-Aug-14	PV	bulb syringe	0	0
07-Aug-14	PV	plankton net	0	0
16-Aug-14	PV	bulb syringe	560	0
16-Aug-14	PV	plankton net	416	30
24-Aug-14	PV	bulb syringe	11,203	9
24-Aug-14	PV	plankton net	780	37
31-Aug-14	PV	bulb syringe	6,465	0
19-Sep-14	PV	bulb syringe	3,108	0

[1] Dry weight was not measured for this sample. However, the LC-MS detected MC, but no ATX, in the sample.

Light experiment results show that in low light, the number of macroscopic bubbles decreased, but under ambient diel summer light regimes, bubble numbers initially increased on day 1, and then numbers remained relatively constant for the duration of the experiment. Indeed, Bosak et al. (2010) showed bubbles could be stable for weeks in cyanobacterial mats. The buoyancy experiments demonstrated the direct flotation of clumps collected in mid-afternoon on a sunny summer day, as well as the flotation within minutes upon exposure to natural sunlight of negatively buoyant clumps held for 12h in darkness. Intracellular buoyancy mechanisms cannot explain the *Anabaena* flotation observed in these experiments, which were dominated by *Anabaena* cylindrica. Indeed, benthic *Anabaena* cylindrica and *Anabaena* oscillarioides do not form gas vesicles (Komarek 2013, Li et al. 2016b), and no intracellular gas vesicles in *Anabaena* trichomes were observed under microscopic examination. Over the short time scale of minutes when flotation was observed to occur, there would not be time for either lipids nor carbohydrates

to be produced, as both types of molecules fluctuate at longer, daily, time scales (Ibelings et al. 1991, Chu et al. 2007).

In the graduated cylinders, the artificial manual removal of bubbles led to a sinking rate of clumps between 0.3 to 0.9 cm s^{-1} (Fig. 2.6). This suggests that without the macroscopic oxygen bubbles, *Anabaena* clumps will sink at speeds of the order of 1 cm s^{-1}. As with flotation, intracellular processes cannot account for the rapid shift from floating to sinking. As *Anabaena* clumps float downstream, bubbles are most likely removed through physical disturbance, rather than cellular respiration or gas diffusion through the extracellular mucus. It is therefore likely that bubble removal primarily occurs through hydraulic turbulence, such as when clumps flow through a riffle. Though respiration consumes oxygen in the bubbles and decreases buoyancy, the light experiment results show that under a natural summer light regime, oxygen consumption from respiration is not sufficient to induce sinking. Only under several days of low light, when photosynthesis is suppressed, do respiration and diffusion affect buoyancy enough to cause sinking (Fig. 2.4). However, the positive day by treatment interaction effect from the glmm model was not statistically significant ($p= 0.092$), suggesting no difference in flotation between light treatments. This statistical result was likely due to low replication and less power inherent to binomial models. Considering that the direction of all parameter estimates matched my hypotheses and that there was minimal variation in the floating or sinking response of clumps in the treatments, with more replicates or a longer experiment it is expected that the interaction would be statistically significant.

Although these data were not sufficiently precise to test the size dependence of the clumps on the floating and sinking rates, qualitative observations indicated that smaller clumps of equivalent algal composition sank faster than larger ones. If they are spherical, larger clumps of similar density sink faster than smaller ones, therefore this result suggests that the elongated shape of the clumps, which acts as resistance to floating and sinking, is more important than the actual size of the clumps in accordance with the modified Stoke's law (Jaworski et al. 1988, Padisak et al. 2003, Walsby and Holland 2006, Fraisse et al. 2015).

Attached *Anabaena* mats in situ consistently have a spire-like morphology with visible bubbles in the spires (Fig. 2.2). The processes that initiate flotation remain unknown. One likely explanation is that as growth rates increase, photosynthetic oxygen production creates enough bubbles that the buoyancy force exceeds the tensile strength of part of the *Anabaena* clump or entangled attachments of host *Cladophora*, detaching it from the substrate. *Anabaena* spires are fragile and easily detached by hydraulic turbulence or other physical disturbance. For example, walking slowly through a large proliferation will generate pressure waves that detach many spires, even meters away.

2.4.2 Cyanotoxin productions

Results from this study provide further evidence for the presence of microcystin and anatoxin-a in the Eel River watershed. Freshwater benthic *Anabaena* have been documented to produced microcystins (Mohamed et al. 2006), but the authors are not aware of published studies of benthic freshwater *Anabaena* producing anatoxin-a. The floating samples analyzed for cyanotoxins were not pure cultures of *Anabaena*, and so it is possible that other taxa could be

producing anatoxin-a. Though the occasional Oscillatoria, Cylindrospermum, or Nodularia may occur, based on microscopic observations *Anabaena* was >100x more abundant than other cyanobacterial taxa in the samples. Given the high concentrations of anatoxin-a in the samples, it is unlikely that they would originate from other cyanobacterial taxa than *Anabaena*. Creating pure cultures of *Anabaena* spp. from the Eel River and testing them for cyanotoxins will be necessary to definitively conclude that *Anabaena* are producing anatoxin-a. Additionally, with the presence of anatoxin-a in the watershed confirmed, future sampling could investigate the presence of the homologue homoanatoxin-a and the anatoxin-a degradation product dihydroanatoxin-a in the watershed (Osswald et al. 2007). The results from these samples supports previous data, which identified anatoxin-a poisoning as the cause of dog deaths in the Eel River watershed (Puschner et al. 2008), though the cyanobacterial species producing anatoxin-a were not identified in that study.

2.4.3 Consequence for dispersal

Since entrapped oxygen bubbles prevent *Anabaena* from sinking, *Anabaena* will likely travel further downstream than less buoyant algae. The light experiment showed that after four days of floating, *Anabaena* trichomes appeared healthy. If growth rates in floating *Anabaena* mats remain high, then instead of *Anabaena* being isolated in discrete benthic mats throughout the watershed, the release of floating clumps from mats results in a semi-continuous presence at the water's surface at the kilometer scale. Therefore, when floating clumps do eventually sink after travelling through riffles which have been observed to dislodge bubbles, they could grow and form a new benthic *Anabaena* mat at that location. This phenomenon of new colonization could contribute to the widespread distribution of *Anabaena* mats in the SF Eel watershed in summer. Additionally, the downstream fate of floating *Anabaena* clumps will likely be controlled by hydraulics and winds. Clumps advected by currents and blown by winds will tend to accumulate along channel margins and in backwater eddies. Once trapped, cells could become stressed although accumulations of floating *Anabaena* have been observed to last several weeks. Considering that floating *Anabaena* clumps contain anatoxin-a (Table 2.1), flotation also poses public health concerns, since clumps accumulate in slow flowing pools, including popular recreational swimming locations, and channel margins. Freshwater cyanotoxins can also affect nearshore marine ecosystems (Miller et al. 2010, Gibble and Kudela 2014) and flotation increases the probability of cyanobacteria being transported from rivers to oceans. Future research on downstream dispersal could use 2-dimensional hydraulic models of river profiles to estimate the number of riffles/km or backwater pools, and produce flow-specific estimates of the effect of riffles on removing bubbles and effects of backwater pools on entraining floating mats over specific mapped reaches. Understanding how buoyancy and dispersal mechanisms differ between benthic and planktonic cyanobacteria is needed to manage for public health and water quality in freshwater environments where toxic benthic cyanobacteria occur.

3 Microbial diversity and metabolic potential in cyanotoxin producing *Phormidium* spp. mats in the Eel River

Abstract

Microbial mats formed by Cyanobacteria of the genus *Phormidium* spp. produce the neurotoxin anatoxin-a that has been linked to animal deaths. Blooms of planktonic Cyanobacteria have long been of concern in lakes, but recognition of potential harmful impacts of riverine benthic cyanobacterial mats is more recent. Consequently little is known about the diversity of the biosynthetic capacities of cyanobacterial species and associated microbes in mats throughout river networks. Here I acquired genomic information for 22 *Phormidium* mats collected across the Eel River network in Northern California to investigate cyanobacterial and co-occurring microbial assemblage diversity, probe their metabolic potential and evaluate their capacities for toxin production. I genomically defined four Cyanobacterial species clusters that occur throughout the river network, three of which have not been described previously. From the genomes of seven strains from one species group I describe the first anatoxin-a operon from the genus *Phormidium*. Importantly, community composition within the mat appears to be associated with the presence of cyanobacteria capable of producing anatoxin-a. Bacteroidetes, Proteobacteria, and novel Verrucomicrobia dominated the microbial assemblages. Interestingly, some mats also contained Candidate Phylum Kapabacteria and Candidate Phyla Radiation bacteria from Absconditabacteria (SR1), Parcubacteria (OD1) and Doudnabacteria (SM2F11). Although the majority of genomes were unique to a particular sample, metabolic diversity was low across samples. In addition to oxygenic photosynthesis and carbon respiration, metabolic capacities include aerobic anoxygenic photosynthesis, sulfur compound oxidation and breakdown of urea. These results show the importance of organic carbon and nitrogen to energy flow and nutrient cycling within mats and the interactions between potential anatoxin-a production and microbial assemblage composition.

3.1 Introduction

When Cyanobacteria proliferate in freshwater environments, the production of toxins can threaten water quality and public health (Paerl and Otten, 2013). Harmful cyanobacterial blooms in lakes have been described for decades (Francis 1878). In rivers, however, research on toxigenic benthic cyanobacterial mats is relatively recent (Quiblier *et al.*, 2013). Nevertheless, nuisance benthic cyanobacterial mats in rivers have already been documented across the globe, including New Zealand (Heath et al. 2011, McAllister et al. 2016), California (Fetscher et al. 2015, Bouma-Gregson et al. 2017), France (Gugger et al. 2005, Cadel-Six et al. 2007), and Spain (Sabater et al. 2003, Cantoral Uriza et al. 2017). Benthic mats are often formed by filamentous genera such as *Anabaena*, *Phormidium*, *Nodularia*, *Lyngbya*, or *Oscillatoria*, and are able to produce cyanotoxins such as anatoxin-a, microcystins, lyngbyatoxin (Quiblier et al. 2013). Given

predictions of increasing cyanobacterial blooms in lakes and estuaries due to eutrophication and warming (Paerl and Huisman 2009, Rigosi et al. 2014), we need better understanding of riverine benthic cyanobacterial mats to anticipate environmental and ecological factors that may stimulate toxigenic benthic cyanobacterial blooms in rivers.

Heterotrophic bacteria often grow attached to or in close proximity to cyanobacterial filaments in benthic mats, exchanging nutrients and carbon (Paerl 1996, Xie et al. 2016). Cyanobacterial growth rates and other physiological process are often enhanced in the presence of co-occurring microbes (Allen 1952), and few antagonisms between cyanobacteria and other bacteria have been reported (Paerl 1996, Berg et al. 2009). The microbial assemblage of lakes shifts when cyanobacteria bloom (Woodhouse et al. 2016, Tromas et al. 2017), and the assemblage composition differs depending on the cyanobacterial species causing the bloom (Bagatini et al. 2014, Louati et al. 2015). With most interactions among Cyanobacteria and co-occurring bacteria facilitating cyanobacterial growth, identifying the diversity and metabolisms of the whole microbial assemblage within toxigenic cyanobacterial mats is central to understanding the ecological processes that drive the proliferation of toxigenic mats in rivers.

Little is known about the microbial assemblage associated with freshwater toxigenic cyanobacterial mats in rivers. I know of only one published study on this topic, which documented shifts over time in the microbial assemblages of *Phormidium* mats (Oscillatoriales) in New Zealand rivers (Brasell et al. 2015). Proteobacteria were abundant in these assemblages, including taxa known to produce alkaline phosphatase, which may be important for mat growth in phosphorus-limited New Zealand rivers (Wood et al. 2015, 2017, McAllister et al. 2016). The New Zealand mats were profiled using 16S rRNA gene amplicons, and therefore could not provide specific information about metabolic functions or metabolites from the microbial assemblages.

Cyanobacterial mats occur each summer in the Eel River in Northern California (Fig. 3.1). Mats are dominated by filamentous Cyanobacterial taxa such as *Phormidium* (Oscillatoriales) and *Anabaena* (Nostocales) and produce cyanotoxins, especially anatoxin-a (Puschner et al. 2008, Bouma-Gregson et al. 2017). Anatoxin-a is a neurotoxic alkaloid that inhibits neuromuscular receptors by disrupting cellular ion channels, which causes muscle failure and can lead to death (Devlin and Edwards 1977, Carmichael et al. 1979, Osswald et al. 2007). Anatoxin-a synthesis starts from proline, a cyclic amino acid, which is transformed by an eight-gene (anaA-H) polyketide synthase (PKS) operon (Cadel-Six et al. 2009, Méjean et al. 2010, 2014). Not all strains within anatoxin-a producing species contain the anatoxin-a gene operon, and concentrations of anatoxin-a can be driven by changes in the abundance of toxin-producing genotypes within a mat, rather than differential toxin production per cell (Wood and Puddick 2017). Variation between toxin and non-toxin producing strains occurs over small spatial scales (<1 cm) (Wood et al. 2012, Wood and Puddick 2017).

In spite of their important ecological and public health impacts, few toxin-producing cyanobacterial genomes have been sequenced (Shih et al. 2013, Brown et al. 2016, Pancrace et al. 2017). Currently, there have been no culture-independent genome-resolved metagenomic investigations of toxigenic freshwater cyanobacterial mats, which, compared to primer-based

amplicon analyses, can provide more information about taxonomic diversity and provide direct insight into the metabolic potential of microbes. Using genome-resolved metagenomics, I studied *Phormidium*-dominated mats across the Eel River watershed to 1) identify the diversity of toxin-producing *Phormidium*, 2) document the diversity of non-cyanobacterial taxa associated with the *Phormidium* mats, 3) describe the anatoxin-a gene operon of *Phormidium* within the watershed, and 4) identify different metabolic potentials present in mats.

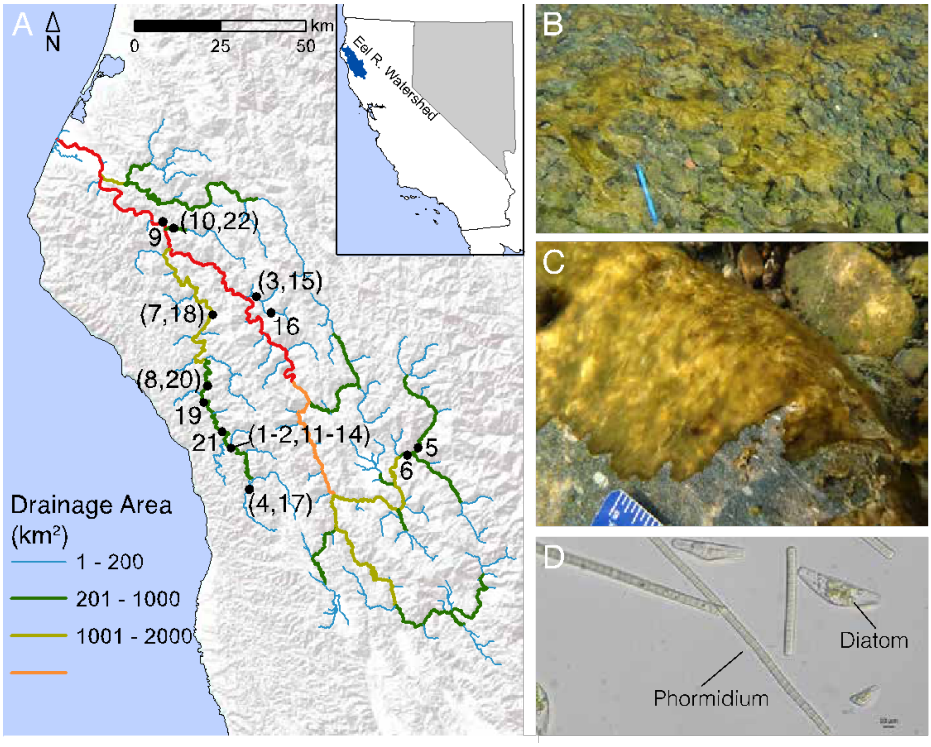

Fig. 3.1 A) Map of Eel River watershed showing location of 22 samples collected in the Eel River watershed in August 2015. B) *Phormidium* mats in the Eel River. C) Underwater photograph showing *Phormidium* mat on a cobble. D) Micrograph of *Phormidium* trichomes and eukaryotic diatoms (400x).

3.2 Materials and methods

3.2.1 Sample collection

Samples were collected from *Phormidium* (Oscillatoriales) mats over 3 weeks in August 2015 in the Eel River watershed in California (Fig. 3.1). The upstream drainage areas at sites ranged from 17 km^2 to 7908 km^2. *Phormidium* mats were identified macroscopically by their brown, orange-olive, or maroon coloration and epilithic growth. *Phormidium* mats are usually found in riffles, and all samples were collected from water 5-70 cm deep with surface flows of 5-100 cm s^{-1}. Previous microscopic identification and 16S rRNA gene sequencing confirmed that these mats are dominated by *Phormidium* (Bouma-Gregson, unpublished). At each site, a cobble covered by a *Phormidium* mat was lifted from the river and placed in a tray that had been cleaned using a

70% ethanol solution. Using sterile forceps, ~0.5 g of biomass was sampled from the mat and placed in a sterile cryotube. Samples were immediately flash-frozen by filling a Styrofoam cooler with 2 L of ethanol and then adding ~250 mL of dry ice to rapidly lower the temperature. Cryotubes were immediately placed in a plastic bag and submerged in the ethanol for 2 minutes. Then cryotubes were stored on dry ice until placed at -80°C upon returning to the laboratory. When enough *Phormidium* biomass could be located at a site, an upstream and downstream sample was collected about 30-50 meters apart from each other. In total, 22 samples were analyzed from 13 sites (Fig. 3.1).

To measure the environmental conditions at each site, filtered water samples (0.7 μm) were collected and measured for total dissolved nitrogen (Shimadzu TOC-VCPH TC/TN analyzer), total dissolved phosphorus using persulfate acid digestion and molybdate colorimetry analysis, nitrate (Lachat QuikChem 8000 Flow Injection Analyzer), and ammonium (OPA method; Holmes *et al.*, 1999). At each site, I also measured depth, surface flow velocity, canopy cover (with a spherical densiometer), conductivity, temperature, dissolved oxygen (ProPlus, YSI Inc., Yellow Springs, OH), alkalinity (Alkalinity Test Kit AL-DT, Hach Company, Loveland, CO) and pH (HI991001, Hanna Inst., Woonsocket RI). The watershed area upstream of each sampling site was calculated using ArcGIS 10.2 (Esri, Redlands, CA, USA). The relationship of samples based on environmental variables was analyzed with principal components analysis using the vegan package (Oksanen et al. 2017) in R v. 3.4.2 (R Core Team 2017).

3.2.2 DNA extraction and sequencing

DNA was extracted from samples using a MoBio (Carlsbad, CA, USA) DNeasy PowerBiofilm kit. Frozen cyanobacterial mat samples were thawed at room temperature for 1 h, and approximately 0.15 g of mat removed for DNA extraction. The DNA extraction followed manufacturer's protocol, except the cell lysis step in the protocol was modified to 5 minutes of bead beating and submersion for 30 minutes in a 65°C water bath. DNA was eluted into double distilled H_2O, and sequenced on an Illumina (San Diego, CA, USA) Hi-Seq 4000 with 150 bp paired-end reads at the QB3 Genomics Sequencing Laboratory (http://qb3.berkeley.edu/gsl/, Berkeley, CA, USA).

3.2.3 Metagenome assemblies and binning

Reads were filtered to remove Illumina adapters and contaminants with BBtools then trimmed with SICKLE (Joshi and Fass 2011) using default parameters. Assembly and scaffolding was performed by IDBA_UD (Peng et al. 2012). For assembled scaffolds longer than 1 kbp, protein-coding genes were predicted with Prodigal in the meta-Prodigal mode (Hyatt et al. 2010). Predicted genes were then annotated against KEGG (Kanehisa et al. 2014), UniRef100 (Suzek et al. 2007), and UniProt using USEARCH (Edgar 2010) with a bitscore cutoff of 6.0. Genomes were binned manually using coverage, GC content, single copy genes, and phylogenetic profile with ggKbase (ggkbase.berkeley.edu), as described in Raveh-Sadka *et al.* (2015).

3.2.4 Microbial assemblage diversity

The taxonomic composition of the microbial assemblage in the samples was investigated using the ribosomal protein S3 (rpS3) gene. The amino acid sequences of all assembled scaffolds >1kb were searched for the rpS3 gene using custom Hidden Markov Models (HMMs) (https://github.com/AJProbst/rpS3_trckr). The rpS3 amino acid sequences were then clustered at 99% sequence identity to approximate the same species and create unique rpS3 clusters for each organism bin. The longest scaffold from each rpS3 cluster was identified, and reads from each sample were mapped onto that set using bowtie-2 (Langmead and Salzberg 2012) allowing ≤ 3 mismatches per read. An organism was considered present in a sample if the rpS3 sequence was found on an assembled scaffold, or if reads from a sample mapped to the rpS3 sequence with a breadth >95%. The coverage values from read mapping for all rpS3 bins in a sample were then normalized by the number of sequenced gigabase pairs (gbp) that went into the assembly. Preliminary taxonomic identifications for each rpS3 cluster were derived by BLASTing the amino acid sequence against a combined database from previous publications (Hug et al. 2016, Anantharaman et al. 2016) and selecting the best match. Refinements to the taxonomic annotation were made using the maximum likelihood tree described below.

A phylogenetic tree was built to investigate the taxonomic diversity of rpS3 sequences. Reference rpS3 amino acid sequences were downloaded from NCBI and aligned with sample sequences using MUSCLE (Edgar 2004) and amino acid sites with >95% gaps after the alignment were stripped from the analysis in Geneious v8.1.8 (Kearse et al. 2012). After stripping the alignment, duplicate sequences were removed. A maximum likelihood phylogenetic tree was constructed from the remaining 363 reference and sample sequences using RAxML (Stamatakis 2014) with the PROTGAMMALG amino acid evolution model and the number of bootstraps automatically determined (autoMRE). Once the tree was built, eukaryotic rpS3 clusters were excluded for further analyses. Beta diversity, species overlap among samples, was calculated with the R package, vegan (Oksanen et al. 2017) based on the presence or absence of rpS3 bins using the β_{sim} metric, which minimizes the influence of high species richness differences between samples on the beta diversity metric (Lennon et al. 2001, Koleff et al. 2003). Minimum β_{sim} values of zero indicate identical species lists between samples, and maximum values of one indicate no shared species between samples. All clustering of data used Ward's method (Ward 1963) in the R package, vegan (Oksanen et al. 2017).

Average nucleotide identity (ANI) was used to investigate the diversity of the dominant cyanobacterial taxa in the mat. The quality of the 35 assembled genome bins in the order Oscillatoriales was assessed using CheckM (Parks et al. 2015). Genomes <75% complete or with >10% contamination were excluded from further analysis. ANI was calculated on the remaining 28 genomes with the ANIm method (Richter and Rossello-Mora 2009) implemented using the Python module PYANI (https://github.com/widdowquinn/pyani) (Pritchard et al. 2016). Genomes with ANI less than 96% were considered different species (Richter and Rossello-Mora 2009, Kim et al. 2014).

3.2.5 Metabolic potential and phosphorus acquisition

The metabolic potential and phosphorus acquisition of genome bins (>70% complete and <10% contamination according to CheckM) were investigated. Scaffolds from the genomes were compared to TIGRFAM (Haft et al. 2003) and custom HMMs for metabolic pathways involving arsenic, C1 compounds, carbon, carbon monoxide, halogenated compounds, hydrogen, nitriles, nitrogen, oxygen, sulfur, and urea (Anantharaman et al. 2016). Cut off values for HMM scores derived by Anantharaman et al. (2016) were used (Table B.1). The number of proteins with HMM scores above the cutoff were recorded for each metabolic pathway in each genome.

Phosphorus acquisition and transport were investigated by searching genomes for genes involved in phosphorus transport, solubilization, mineralization, and regulation using Pfam or TIGRfam HMMs (Table B.2) (Bergkemper et al. 2016). Cutoff values were derived by downloading 21 annotated isolate genomes and searching them using the HMMs. Search results were verified with blastp against the NCBI RefSeq database (June 2017) by looking for enzyme name keywords from Table B.2 indicating gene functions and cutoff values established.

3.2.6 Anatoxin-a gene operon

Some, but not all, genes in the anatoxin-a operon were correctly annotated via the procedures described above. Additional genes were identified by investigating genes surrounding correctly annotated genes. To search for additional scaffolds with anatoxin-a operons, HMMs were built with hmmbuild (hmmer.org) for each gene in the anatoxin-a operon using reference sequences from NCBI. Scaffolds that had multiple genes with HMM e-value less than 10^{-50} were further investigated for the presence of anatoxin-a genes, using the same methods described above. Lastly, raw reads were mapped with Bowtie-2 to anatoxin-a reference sequences and genes identified through the methods above. Once all anatoxin-a genes were identified, the protein domains of the samples were compared to reference sequences using hmmscan (https://www.ebi.ac.uk/Tools/hmmer/search/hmmscan), and genes were mapped to a reference anatoxin-a operon using Geneious v8.1.2 (Kearse et al. 2012) to analyze gene synteny and sequence identity among sample and reference gene sequences. The relationship between the presence of the anatoxin-a operon and the microbial assemblage was investigated with non-metric multidimensional scaling of Bray-Curtis dissimilarities using the R package vegan (Oksanen et al. 2017).

3.2.7 Anatoxin-a measurements

Anatoxin-a concentrations in *Phormidium* mats were measured using liquid chromatography mass spectrometry (LC-MS) with Select Ion Monitoring (SIM). After a mat sample was collected for DNA extraction, ~1 g of mat remaining on the cobble was placed in a 250 mL glass jar and placed in a cooler on ice, brought to the laboratory, and stored at 4°C overnight. The next day the sample was homogenized with a blender, and a 15 mL subsample transferred to a glass vial and frozen at -20°C. For anatoxin-a extraction, samples were thawed, and 3 mL sub-sample added to a glass culture tube with 3 mL of 100% MeOH (Fisher A452), then the tube was sonicated for 30 s using a probe sonicator (Sonic Dismembrator 100; Thermo Fisher Scientific, Massachusetts, USA) at ~10W power. After sonication, the tube was centrifuged (Model IEC Centra CL2; Thermo Fisher Scientific) for 5 min at 1083 rcf, and 1 mL of the

supernatant was 0.2 µm filtered into an LC-MS vial. The anatoxin-a concentration in the extract was measured on an Agilent 6130 Liquid Chromatography-Mass Spectrometry system with a Cogent Diamond-Hydride column and direct-injection of 20 µL. Detection limits were 0.7 parts per billion for anatoxin-a. Calibration was performed using certified reference materials with a minimum of five calibration points for each batch of samples, and analytical blanks and matrix blanks included in each run. After centrifuging, the cyanobacterial mat in the culture tube was transferred to a weighing tin and dry weight measured after 48 hours in a drying oven at 50°C. Anatoxin-a concentrations were then calculated as ng anatoxin-a per gram dry weight.

3.3 Results

3.3.1 Environmental conditions

At the collections sites, temperatures ranged 17-26°C and maximum dissolved nitrogen and phosphorus concentrations were <100 and <30 µg L^{-1}, respectively (Table B.3). From the PC on the environmental variables, the first two axes explain 60.7% of the environmental variation among the sites. Canopy cover and temperature were negatively correlated and explain much of the variation in environmental conditions at each site along PCA axis 1 (Fig. 3.2). The second PCA axis describes variation in nitrogen, pH, and dissolved oxygen.

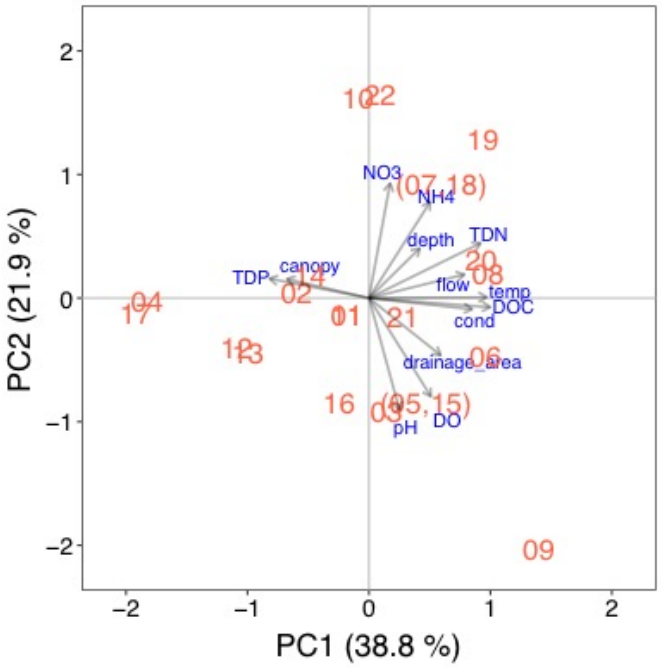

Fig. 3.2 First two principal components analysis axes of the environmental conditions at each of the sampling sites (red) and the percentage variation explained by each axis. Names of samples from upstream and downstream sites that share the same environmental data are separated by a comma. Environmental variables are shown in blue.

3.3.2 Microbial assemblage diversity

Microbial assemblages were dominated by Cyanobacteria (18 rpS3 clusters), Bacteroidetes (97 rpS3 clusters), Proteobacteria (77 rpS3 clusters), and Verrucomicrobia (8 rpS3 clusters) but also contained Actinobacteria, Deinococcus-Thermus, Chloroflexi, bacteria from Candidate Phylum Kapabacteria and from three Candidate Phyla Radiation groups (CPR; Fig. 3.3). The genomic dataset for each sample included a relatively unique set of rpS3 sequence clusters, resulting in low species overlap (high beta diversity) among the sites with mean and median β_{sim} values of 0.73 and 0.8. Additionally, 25% of pairwise comparisons among sites had β_{sim} values of 1, indicating no shared rpS3 clusters among the samples. Additionally, no rpS3 cluster was detected in all samples.

Based on rpS3 clusters, Cyanobacteria were the most abundant organisms in all samples comprising 62-98% of the relative abundance within each sample (Fig. 3.4, Fig. 3.5A). The most common cyanobacterial rpS3 clusters were rpS3 66, 85, 152, and 244. These formed a clade with *Oscillatoria nigro-viridis* and *Microcoleus vaginatus* FGP-2 (Fig. 3.3), but not with any reference *Phormidium* rpS3 sequences (Fig. 3.3). (Few *Phormidium* rpS3 reference sequences are available, and the designations of the genera *Oscillatoria*, *Microcoleus*, and *Phormidium* are under revision (Sciuto et al. 2012, Strunecký et al. 2013, Komárek 2017a, 2017b). Therefore, I will continue to refer to the dominant Oscillatoriales genomes in each sample as *Phormidium*). Bacteroidetes were the most abundant non-cyanobacterial taxa, occurring in all 22 samples and representing 35-100% of the non-cyanobacterial assemblage (Figs. 3.4 and 3.5). Proteobacteria, primarily Burkholderiales and Sphingobacteriales, were also common in samples. Verrucomicrobia were detected in 10 samples at relative abundances approaching >40% (Fig. 3.5). The four CPR were identified as Peregrinibacteria (PER), Absconditabacteria (SR1) and Parcubacteria (OD1) (Fig. 3.3).

Draft genome results showed each of the 22 mats was dominated by Cyanobacteria from the order Oscillatoriales, as represented by a single draft genome for a population of very closely related organisms. In 12 samples, a second or third *Phormidium* genome was also recovered at lower coverage. Interestingly, these genomes formed four *Phormidium* species clusters sharing less than 96% nucleotide identity (the species level ANI threshold) among the clusters (Fig. 3.6A). *Phormidium* species 1-3 had 82-88% ANI from reference genomes. However, *Phormidium* species 4 had 96.1% ANI with the *Phormidium willei* BDU130971 reference genome, suggesting these might be the same species. In samples with more than one recovered *Phormidium* genome, the two genomes belonged to different species, with the second genome occurring at much lower coverage (Fig. 3.6A). Typically one or two rpS3 sequence clusters were associated with each *Phormidium* species.

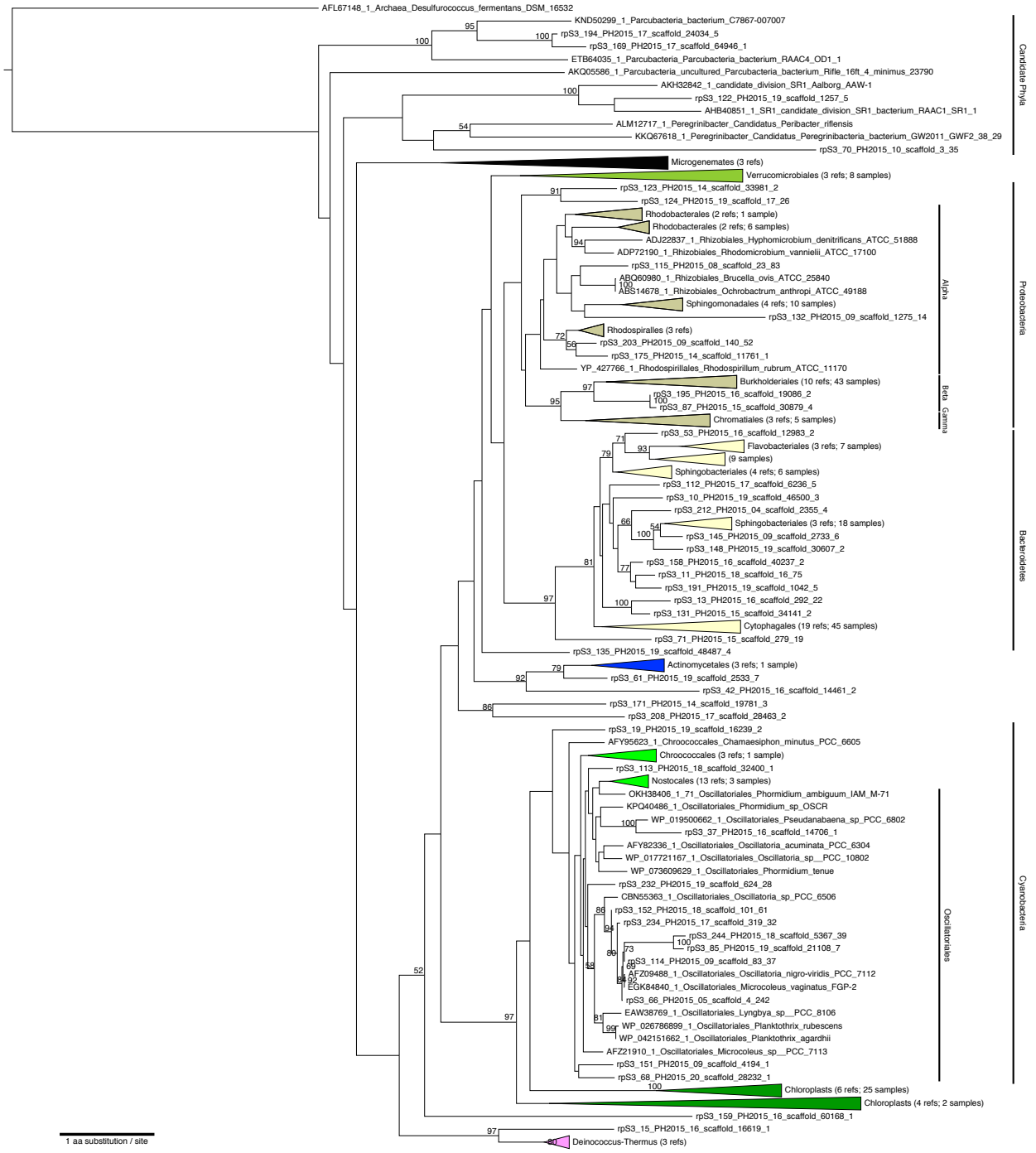

Fig. 3.3 Maximum likelihood phylogenetic tree of ribosomal protein S3 (rpS3) sequences with Archaea as the outgroup. Collapsed nodes are represented with colored triangles and the number of reference and sample sequences in the node indicated. Nodes with bootstrap values >50% are indicated on the tree.

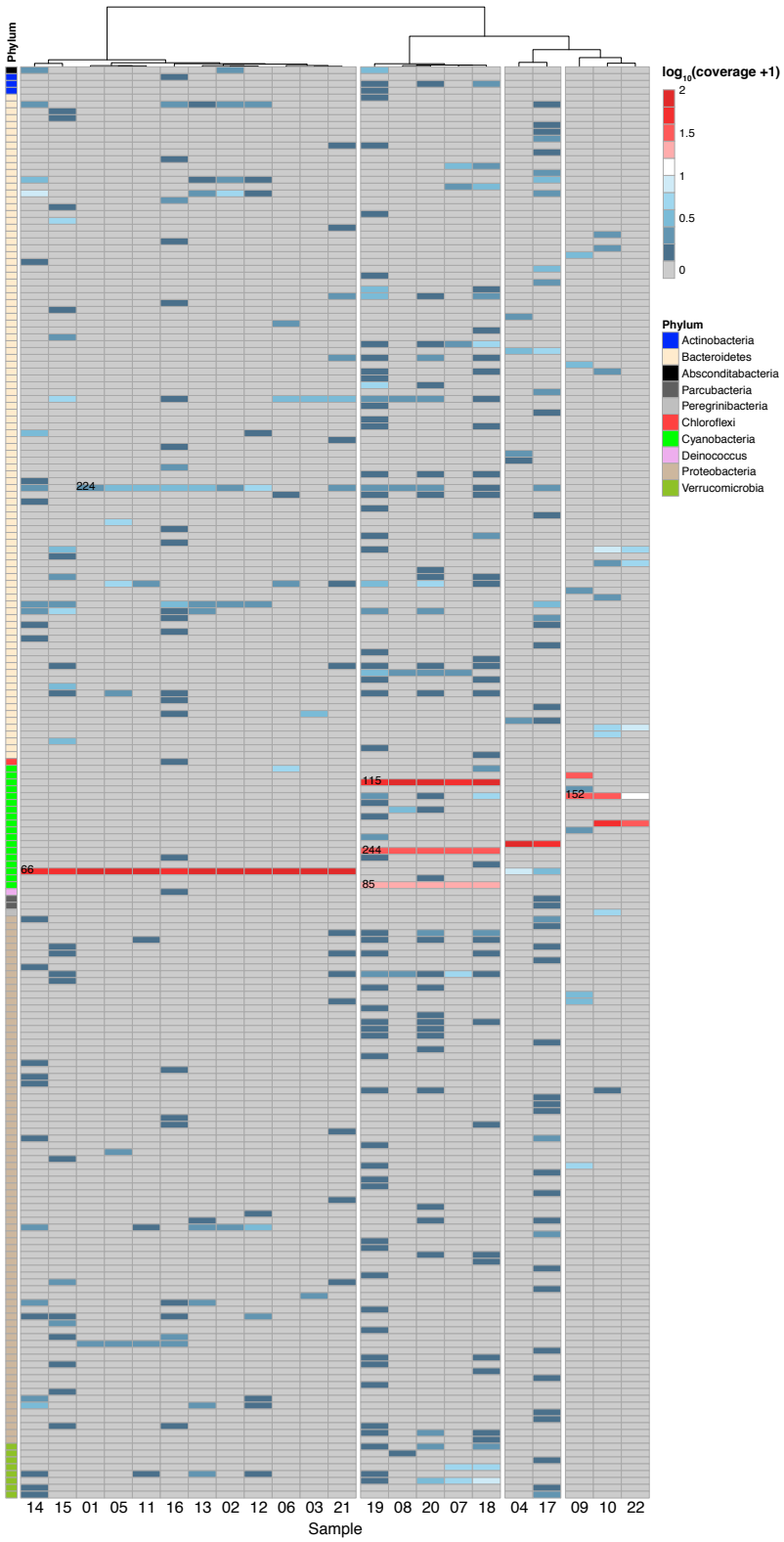

Fig. 3.4 Heatmap of ribosomal protein S3 (rpS3) coverage among the different samples. Each row is a unique rpS3 bin. The numbers of six rpS3 bins are labeled in black. Columns are clustered by Ward's distance.

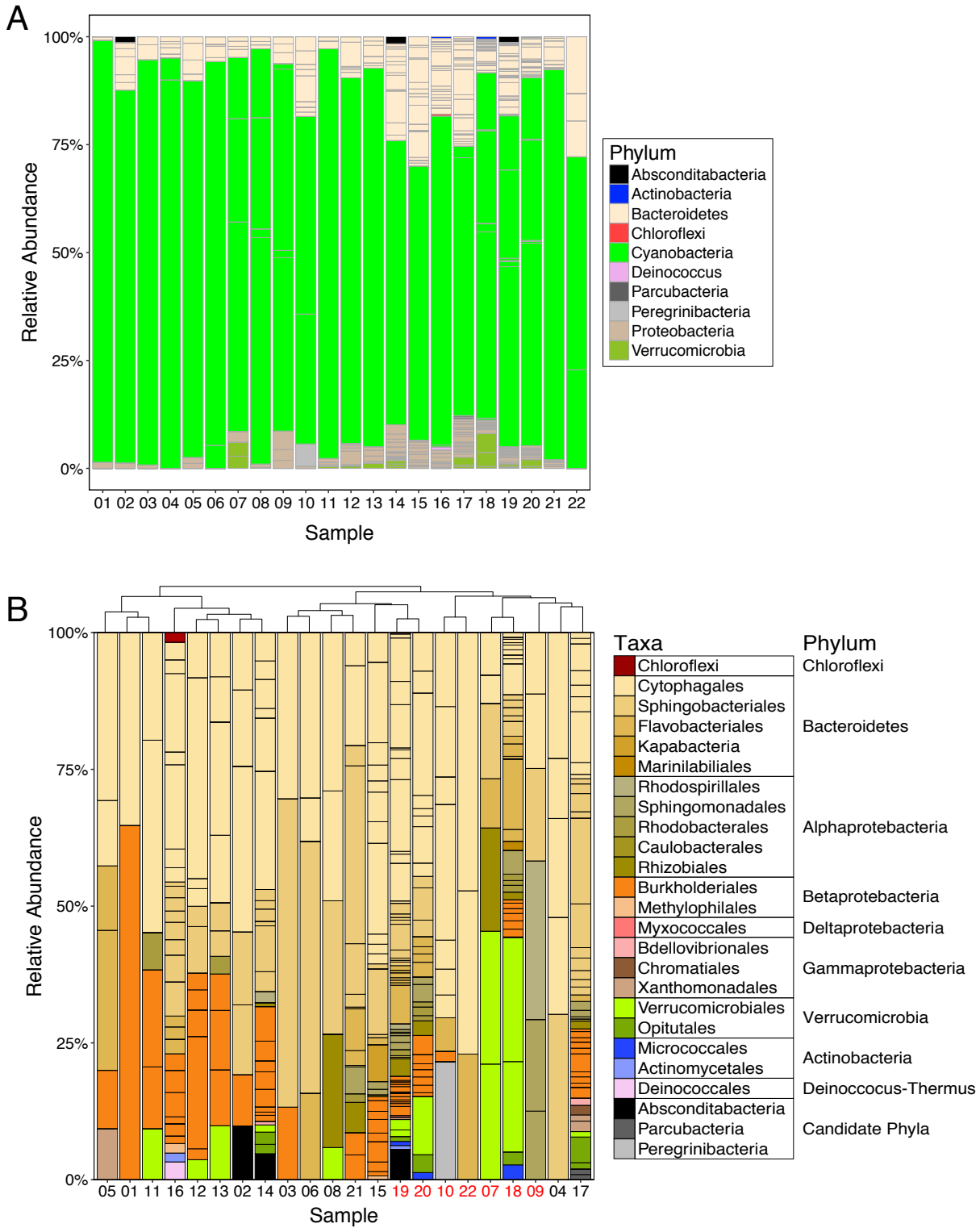

Fig. 3.5 Percent relative abundance of non-cyanobacterial rpS3 sequence clusters in samples. A) rpS3 clusters are colored by phyla. B) rpS3 clusters are colored at a variety of different taxonomic levels that indicate the best classification given the bin novelty. Columns are clustered by Ward's distance and samples in red indicate the recovery of the anatoxin-a gene operon in that sample.

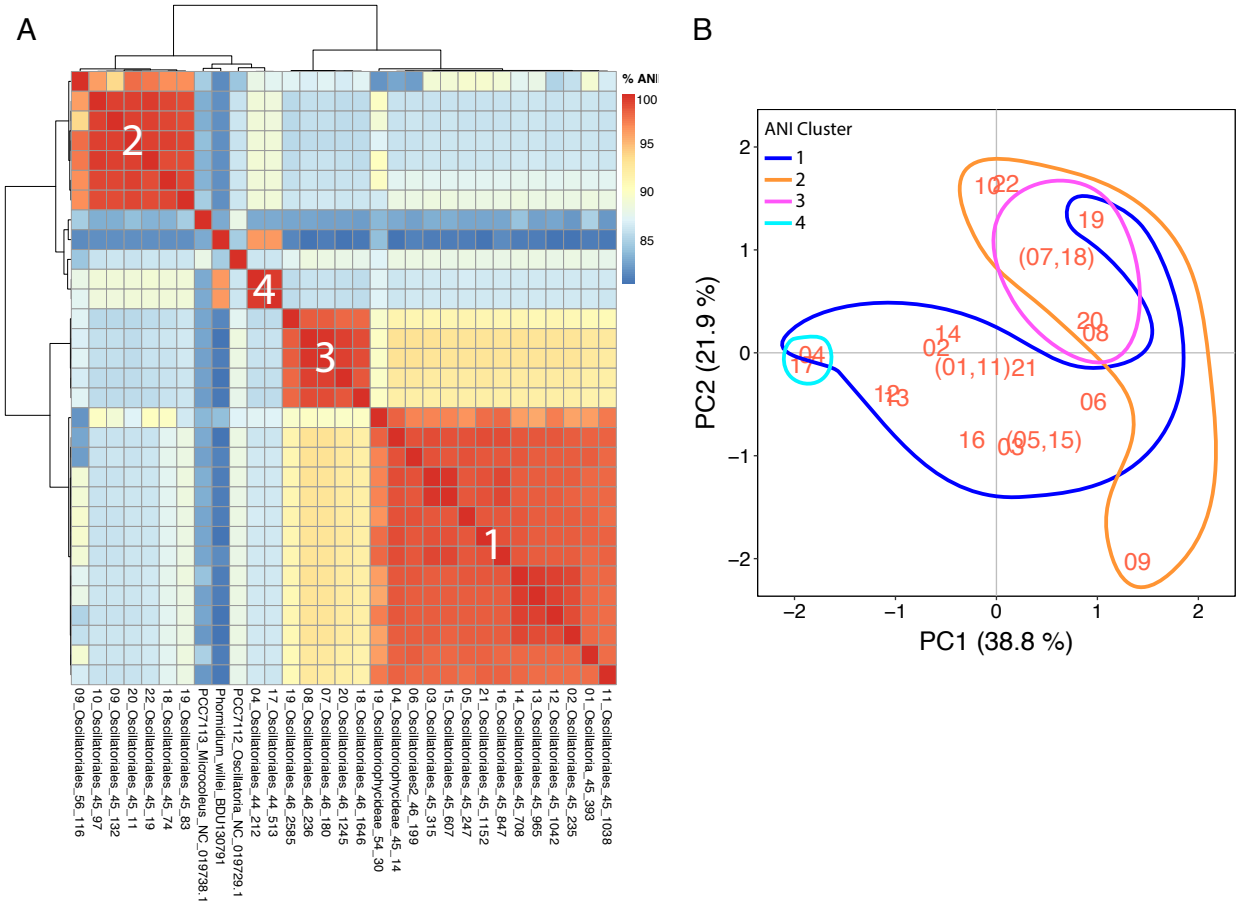

Fig. 3.6 A) Percent average nucleotide identity (ANI) of cyanobacterial genomes from samples and three reference genomes. The first number of the genome name identifies the sample location (see Fig. 3.1). The latter two numbers indicate the GC content and genome coverage. ANI results were clustered using Ward's distance and represent 4 species groups with <93% ANI among the clusters. B) Principal components axes of environmental variables from Fig. 3.2 with colored lines surrounding samples from each ANI cluster. Some samples generated genomes from multiple ANI clusters.

With the exception of *Phormidium* species 1, *Phormidium* species were limited to sub-regions in the watershed. Species 1 contained genomes collected from sites broadly distributed across the watershed (Figs. 3.1, 3.2B, and 3.6), including the eastern sites 05-06 and 15-16. However, species 1 also contained a sub-cluster of samples 02 and 12-14 with 99-100% ANI, all collected within 0.5 km in a single creek. Species 2 was found in the most downstream region (samples 09, 10, and 22) and in the middle reaches of the South Fork Eel (samples 18-20). Species 3 was limited to 3 sites in the South Fork Eel (samples 07-08 and 18-20), and Species 4 came from a single site (samples 04 and 17). Each *Phormidium* species also came from a wide range of environmental conditions, with only Species 3 and 4 found in a smaller environmental niche (Fig. 3.6B).

3.3.3 Anatoxin-a

The anatoxin-a synthesis gene operon (anaA – anaJ) was recovered from 7 samples: 07, 09, 10, 18, 19, 20, and 22 (Fig. 3.7A). Read mapping to the PH2015_19 anatoxin operon did not find any anatoxin synthesis genes in other samples (Table B.4). The non-cyanobacterial microbial assemblage was different in samples with and without the ATX operon (Fig. 3.7C, $p < 0.01$). This relationship is primarily driven by fewer Betaproteobacteria in samples without the ATX operon (Fig. 3.5B, $p < 0.01$).

In all samples but 07, the operons were found in the rpS3_152 bin and in *Phormidium* species 2 (Figs. 3.4 and 3.6A). In sample 07, the operon was partially recovered from the rpS3_85 bin in *Phormidium* species 3, with the anaC, J, and I genes assembled and annotated. Other scaffolds in sample 07 mapped to the PCC6506 operon, but the genes did not annotate to the assembled scaffolds at >50% identity. Most nucleotide identities of the ana genes to the PCC6506 reference sequence ranged from 88 to 94% similar (Table B.5), with lower values for a few scaffolds where LC-MS analyses detected anatoxin-a in 11 of the 19 samples (Fig. 3.7B), with median and maximum concentrations of 153 and 1,104 ng anatoxin-a / g DW, respectively. In four samples, anatoxin-a was detected with the LC-MS, but the operon was not recovered. There was no difference in the microbial assemblage among samples with and without LC-MS detection of anatoxin-a (Fig. 3.7, $p = 0.089$).

All gene annotations from these sequences matched those previously reported (Rantala-Ylinen et al. 2011, Méjean et al. 2014, Jiang et al. 2015, Brown et al. 2016). The arrangement of the anaB-G genes was similar to the three reference operons (Fig. 3.7A). However anaA, I, and J genes were located on the opposite end of the operon compared to PCC6506, and closer to anaG than the two Nostocales reference operons (*Anabaena* and *Cuspidothrix*) (Fig. 3.7A). In samples 09 and 10, anaJ was not assembled, but read mapping confirmed its presence in these samples. The transposase anaH gene was not found in any samples. The anaG gene was ~1670 base pairs shorter than in the three reference sequences. This missing region contained the ~300 base pair methyltransferase domain, proposed to affect the production of either anatoxin-a of homoanatoxin-a (Méjean et al. 2014, 2016). All samples also lacked the recently identified anaK gene, which enables production of dihydroanatoxin-a (Méjean et al. 2016).

Gene sequences in the operon were conserved among the samples, for example all amino acid sequences of the anaC genes from the samples were 100% identical to one another. However, some diverse loci in the operon do exist. In samples 9, 10, and 18 scaffolds terminated at the approximately the same location in the anaE gene (Fig. 3.7A). Read mapping showed that there was greater sequence variation among reads at this locus. Several paired end reads spanned this locus, so this high-variation loci is likely to be less than ~350 bp long (paired end insert size). This locus could also be a repeat region, as a recent completion of the *Anabaena* WA102 genome found triplicate tandem repeats within anaB gene of the operon (Brown et al. 2016).

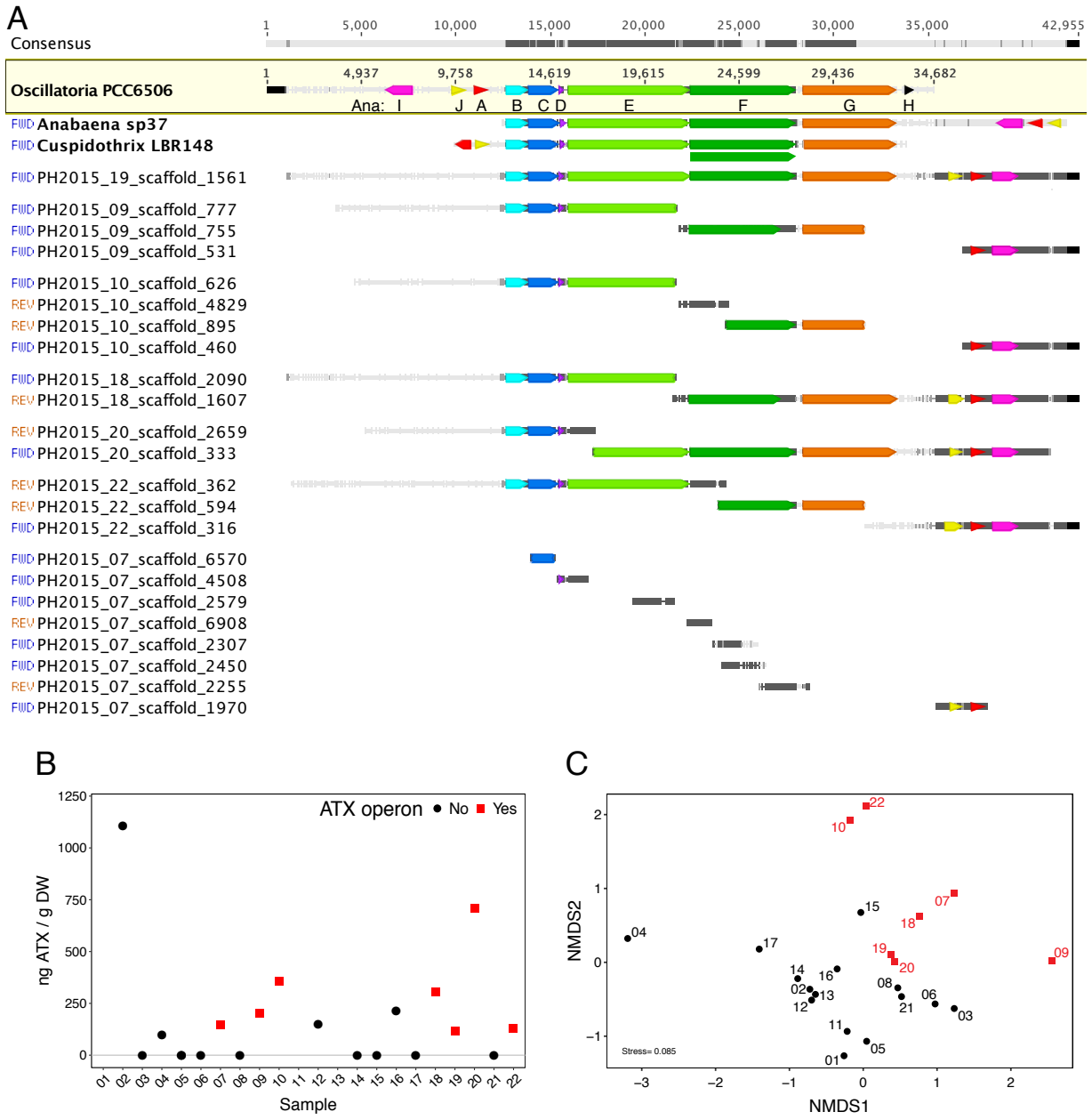

Fig. 3.7 A) Anatoxin-a operon from three reference sequences (bold) and samples 19, 09 10, 18, 20, 22, and 07. Sample scaffolds were mapped to Oscillatoria PCC6505, and gene annotations added at 50% identity to one of the 3 reference sequences. Different ana genes are different colors. B) Anatoxin-a (ATX) concentrations from *Phormidium* mat samples. ATX was not measured in samples 01, 11, and 13. C) Non-metric multidimensional scaling (NMDS) plot using Bray-Curtis dissimilarities of non-cyanobacterial assemblage showing samples with and without the anatoxin-a operon.

3.3.4 Metabolic potential and phosphorus acquisition

Considering the entire microbial community, samples were dominated by phototrophic, heterotrophic, nitrogen, and sulfur metabolisms (Fig. 3.8). Although genes associated with nitrogen fixation, hydrogenase, halogenated compounds, and formaldehyde were detected, the most common processes were carbon fixation, cytoQu_oxidase bo, nitrite reduction, urease, and sulfur oxidation. In addition to carbon fixation, *Phormidium* genomes contained genes for formaldehyde oxidation, urea breakdown, nitrite reduction, sulfur oxidation, and halogenated compounds breakdown. Across the 4 *Phormidium* species there was little variation in metabolic potential.

Bacteroidetes had the least metabolic diversity, based on analysis of 50 genomes, most genomes contain genes for carbon and sulfur oxidation. However, Bacteroidetes were the only organisms predicted to possess genes to oxidize methanol to formaldehyde. Verrucomicrobia primarily have genes for carbon oxidation and nitrite reduction. Bacteria from this phyla are the only organisms the mats with predicted genes for chlorite reduction (Fig. 3.8).

Among the organisms in the mats, Proteobacteria have the most diverse sulfur metabolic potential. Genes for sulfide oxidation (flavocytochrome c sulfide dehydrogenase), sulfur oxidation (sulfur dioxygenase), and thiosulfate oxidation (soxB, C, Y) were identified in genomes from both Alpha and Betaproteobacteria. Anoxygenic photosynthesis genes were found in a Sphingomonadales and Rhodobacterales genome. However, no sulfide oxidation genes (flavocytochrome c sulfide dehydrogenase) were associated with these genomes, suggesting these organisms are using an alternative electron donor for anoxygenic photosynthesis. A phylogeny of rpS3 sequences shows that the PH2015_09_Sphingomonadales_65_9 genome clusters with the freshwater aerobic anoxygenic phototrophic bacteria *Porphyrobacter* spp. (Yurkov and Beatty 1998, Koblizek 2015) and the PH2015_13_Rhodobacterales_65_6 genome with the purple non-sulfur bacteria *Rhodobacterales sphaeroides* and *Rhodobacterales capsulatus* (Fig. B.1).

Phosphorus uptake and transport genes were present in most genomes (Fig. 3.9). The non-cyanobacterial assemblage contains genes for alkaline phosphatase, while the most common phosphorus mineralization genes for *Phormidium* were acid phosphatase phoN and glycerophosphodiesterase ugpQ. The low-affinity inorganic phosphorus transport gene (pit) was most frequently identified in the Cyanobacteria and Bacteroidetes genomes, but all Verrucomicrobia and most Proteobacteria lacked this gene. *Phormidium* also contained the high affinity phosphate transport pst genes. Members of the Verrucomicrobia were different from other phyla as they only possess phoA and the pst transporter genes. The phosphorus-solubilization gene gcd was absent in all genomes.

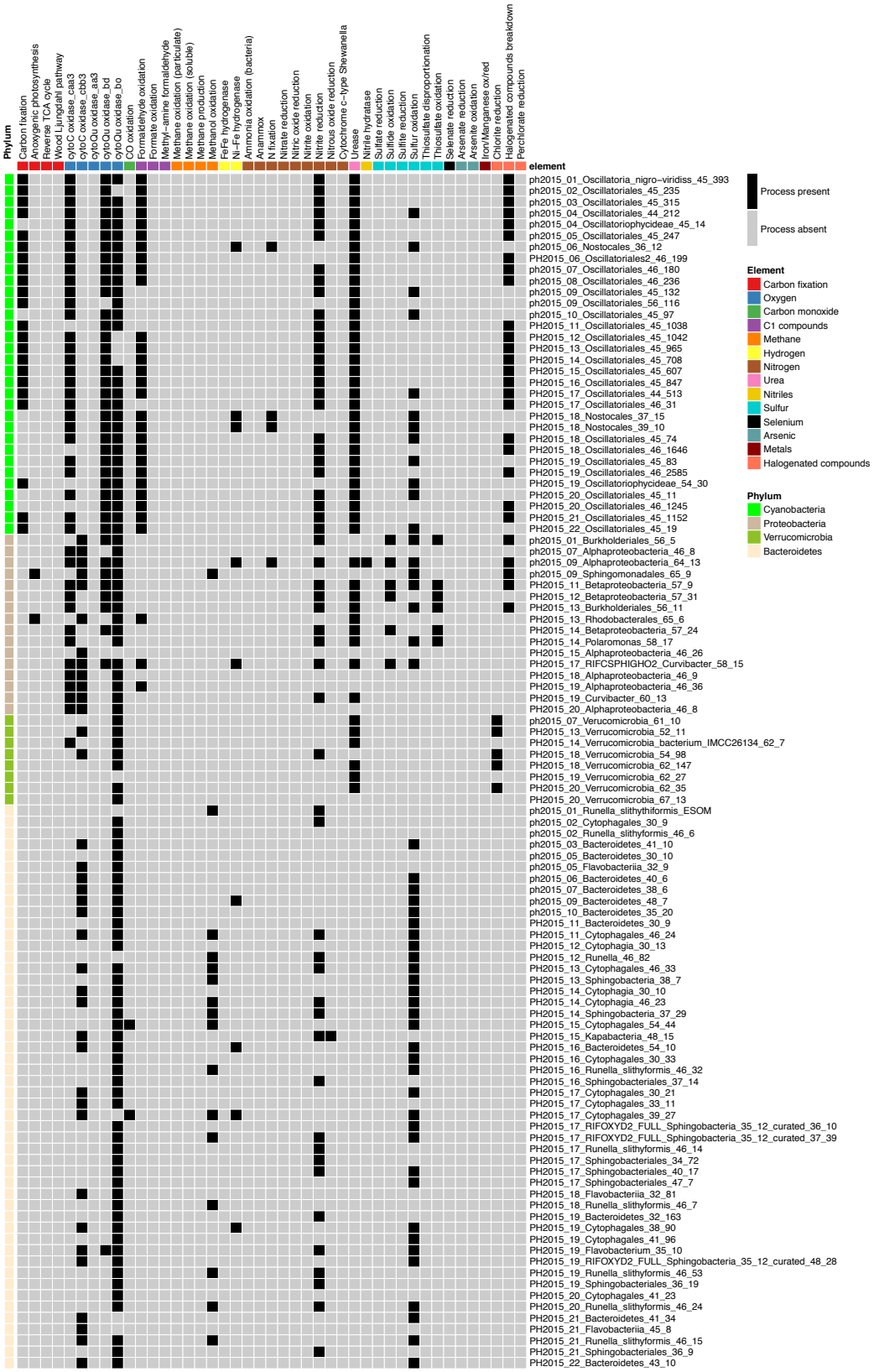

Fig. 3.8 Presence or absence of different metabolic processes in reconstructed genomes.

Fig. 3.9 Presence of genes for phosphorus acquisition and transport in recovered genomes.

3.4 Discussion

This is the first genome-resolved metagenomic analysis of toxin-producing freshwater benthic cyanobacterial mats. By recovering the genomes of bacteria within 22 *Phormidium* mats collected across a 9,547 km^2 watershed, I provide information about the microbes and genes potentially controlling energy flows, nutrient cycling, and toxin production within these benthic *Phormidium* mats.

3.4.1 Microbial diversity

The dominant phyla in my samples, Cyanobacteria, Bacteroidetes, Proteobacteria, and Verrucomicrobia, have been found to co-occur with freshwater planktonic cyanobacterial blooms (Pope and Patel 2008, Steffen et al. 2012, Mou et al. 2013, Louati et al. 2015, Parulekar et al. 2017), and were abundant in riverine *Phormidium* mat assemblages in New Zealand (Brasell et al. 2015). Prior studies of planktonic cyanobacterial blooms found a higher relative abundance of Proteobacteria, compared to Bacteroidetes, than I did in my benthic samples. In most prior studies, Alphaproteobacteria were the dominant group of Proteobacteria; only Louati et al. (2015) reported a higher relative abundance of Betaproteobacteria, as in my results. Increases in cyanobacterial biomass can affect microbial assemblages. As planktonic cyanobacteria blooms, or benthic *Phormidium* mats develop and thicken, the co-occurring microbial assemblage composition changes (Li et al. 2012, Parveen et al. 2013, Brasell et al. 2015). This successional change could account for some of the variation observed within and across sites and ecosystems.

In contrast to the non-cyanobacterial species, the *Phormidium* species showed higher overlap among the sites, and environmental conditions were not strongly associated with the presence of specific groups within each sample (Fig. 3.6B). *Phormidium* species 4 was the exception, being found only in the coolest shadiest site. More sampling of smaller tributaries could test the hypothesis that *Phormidium* species 4 is a cool-water, low sunlight *Phormidium* species, while *Phormidium* species 1-3 tend to occur in warmer sunnier environments. The *Phormidium* species had low ANI similarity to the reference genomes, suggesting each is a novel species, though there are few *Phormidium* reference genomes sequences (Shih et al. 2013, D'Agostino et al. 2016, Alvarenga et al. 2017). Therefore, the creation of these draft *Phormidium* genomes helps fill important gaps in our genomic understanding of cyanobacterial diversity and physiology.

3.4.2 Microbial assemblage and anatoxin-a

The difference in the non-cyanobacterial assemblage between samples with and without the anatoxin-a operon, suggests a relationship among anatoxin-a producing cyanobacteria and the non-cyanobacterial assemblage. Although it is possible that non-cyanobacterial organisms present in the environment influence selection for cyanobacterial strains, I consider the reverse more likely, that as cyanobacteria bloom changing environmental conditions from cyanobacterial produced compounds shapes microbial community composition. This could involve selection for associated bacteria with the capacity to degrade the toxin. Microcystin concentrations have been shown to affect bacterial assemblage composition (Mou et al. 2013), and the copies of microcystin degradation genes (mlr) in the overall community have been positively correlated with microcystin concentrations (Li et al. 2015, Lezcano 2016).

Little is known, however, about anatoxin-a degrading bacteria (Edwards and Lawton 2009, Kormas and Lymperopoulou 2013). Bacteria in sediments increase anatoxin-a degradation rates (Rapala et al. 1994) and a *Pseudomonas* sp. capable of degrading anatoxin-a has been isolated (Kiviranta et al. 1991). Mou et al. (2013) found a positive association between microcystin degradation rates and Burkholderiales, suggesting a role for these bacteria in toxin breakdown. Burkholderiales are important in some cyanobacterial blooms (Louati et al. 2015), although a decline in abundance of a Burkholderiales strain can be predictive of the onset of a Cyanobacterial bloom (Tromas et al. 2017). In the current study, samples with the anatoxin-a operon had fewer Burkholderiales, so it possible that the bacteria from this family in the Eel mats are negatively impacted by toxin production (unfortunately, the genes for anatoxin-a degradation are not known, so this cannot be deciphered genomically).

With the exception of samples 9 and 10, the other sample assemblages containing Cyanobacteria with the anatoxin-a operon had relatively more Sphingomonadales, an order with many known microcystin degrading species (Mou et al. 2013, Kormas and Lymperopoulou 2013, Briand et al. 2016). However, anatoxin-a and microcystin have different molecular structures. Anatoxin-a is bicyclic alkaloid, while microcystin is a cyclic peptide. It cannot be assumed that genes involved in microcystin degradation will confer the ability to degrade anatoxin-a. My findings motivate experiments to test impacts of co-occurring microbes on anatoxin-a degradation.

3.4.3 Microbial assemblage and metabolisms

Strong redox gradients occur in microbial mats in salt marshes, lakes and mudflats and result in diverse spatially structured metabolisms (Franks and Stolz 2009, Armitage et al. 2012). Although the epilithic *Phormidium* mats from this study clearly derive their energy from photosynthesis and carbon oxidation in an aerobic environment, a small fraction of bacteria in the assemblages appear to derive energy from sulfur and halogenated compounds. However, the epilithic growth on larger cobbles, compared to sand or silt substrates, limits the depth of the mat and likely prevents development of the permanent anoxic regions found in cyanobacterial dominated mats in estuaries (Franks and Stolz 2009). Within the Eel River mats, oxygen concentrations likely fluctuate on a diel cycle as they do in New Zealand (Wood et al. 2015), creating transient anoxic conditions (Paerl and Pinckney 1996) and limiting the relative abundance of organisms with anaerobic metabolisms. Overall, the mats studied here are metabolically simple, with few anaerobic or non-carbon metabolisms. This simplifies predictions about the environments in the river network in which mats may proliferate.

Genes for carbon respiration were common among reconstructed genomes from the mats, especially within Bacteroidetes genomes, the most abundant non-cyanobacteria in most samples. Bacteria from this phylum are sometimes heterotrophs, capable of breaking down complex organic compounds (Grondin et al. 2017). Consistent with this prediction, many of the genomes encode large inventories of genes for degradation of complex carbohydrates (e.g., many and diverse glycosyl-hydrolases). *Phormidium* mats are characterized by thick extracellular polymeric substances (EPS) that give structural integrity to the mat (Nicolaus et al. 1999). Therefore, it is likely that Bacteroidetes are metabolizing carbon compounds associated with the EPS produced by *Phormidium,* (Beraldi-Campesi et al. 2012). Bacteroidetes were the only bacteria predicted to possess methanol oxidation genes, which oxidize methanol to formaldehyde. This further

suggests a close carbon association of Bacteroidetes with *Phormidium,* as most *Phormidium* genomes contain formaldehyde oxidation genes. It is possible that some Bacteroidetes supply formaldehyde for *Phormidium* to metabolize to formate. However, as no formate metabolism genes were found, the fate of formate is unclear. Additionally, consistent with prior studies (Niemi et al. 2009), Burkholderiales are predicted to have some capacity to degrade complex organic compounds. This may also explain their high abundance in mats. CPR bacteria may also contribute to carbon cycling. As noted previously (Wrighton et al. 2012, Kantor et al. 2013, Nelson and Stegen 2015), the genomes of the bacteria from the three CPR groups are small and the organisms are predicted to have symbiotic anaerobic, fermentation-based lifestyles. Parcubacteria have been reported in planktonic cyanobacterial blooms (Parulekar et al. 2017), SM2F11 and 12 other Candidate Phyla reported in Antarctic Cyanobacteria/diatom mats (Stanish et al. 2013), and SR1 reported from various anaerobic aquatic habitats (Davis et al. 2009). Their identification in mats in a river network suggests that they play important and previously unrecognized roles in aquatic biofilms, both via carbon turnover and impacts on host organisms.

Many Cyanobacteria and Proteobacteria contained genes for sulfur and sulfide oxidation, both of which can occur in oxygenated environments, but often in proximity to anoxic regions where reduced sulfur compounds are formed or accumulate (Wasmund et al. 2017). However, most rivers do not have high concentrations of elemental or reduced sulfur in the water column (Meybeck 1993). Therefore, it is likely that these organisms are not using sulfur as a primary energy source, but are capable of metabolizing sulfur opportunistically when it may sporadically accumulate in anoxic microhabitats in the mats.

In the Eel River, nitrogen is considered a limiting nutrient in spring and early summer (Hill and Knight 1988, Finlay et al. 2011). For example, epilithic periphyton assemblages are often dominated by nitrogen fixing taxa (Power et al. 2009), such as Rhopalodiaceae diatoms (with endosymbiotic nitrogen fixing cyanobacteria), *Nostoc* spp. or *Anabaena* spp. However, few nitrogen fixation genes were predicted in the dataset analyzed here. Though some *Phormidium* species can fix nitrogen (Bergman et al. 1997), as expected based on samples in New Zealand (Heath et al. 2016), the *Phormidium* in Eel River mats do not fix nitrogen. Nitrogen fixing capacity was found in a single Alphaproteobacteria genome and three Nostocales genomes. *Phormidium* and most other bacteria in the Eel River mats likely derive their nitrogen exogenously from a combination of the water column and these sources.

All *Phormidium* genomes, and most Proteobacteria and Verrucomicrobia genomes, are predicted to contain urease genes. Dissolved organic nitrogen is hypothesized to be an important nitrogen source in the summer in the Eel River (Finlay et al. 2011). Urease genes may also suggest high rates of nitrogen cycling within mats, as organic nitrogenous waste products from organisms are taken up by other organisms. Therefore, once mats establish, internal cycling of organic nitrogen may decouple the mats from nitrogen dynamics in the overlying water column (Vadeboncoeur and Power 2017).

Phormidium mats proliferate in New Zealand rivers at low dissolved phosphorus concentrations (McAllister et al. 2016, Wood et al. 2017), and phosphorus may become more limiting in the

Eel River in late summer, when *Phormidium* mats are more commonly observed. Based on my genomic analyses, many of the organisms in the microbial assemblage likely contribute to phosphorus mineralization in mats. The pH levels within *Phormidium* mats in New Zealand oscillate daily due to changes in CO_2 and O_2 concentrations driven by cyanobacterial photosynthesis (Wood et al. 2015). *Phormidium* may use acid phosphatases to scavenge phosphorus at night when pH levels drop, and non-cyanobacteria use alkaline phosphatases scavenge during the day when pH is elevated. Phosphate weakly sorbed onto sediments trapped in mats may be an important phosphorus source to *Phormidium* mats (Wood et al. 2015). The lack of the solubilization gcd gene suggests that microbes are relying on pH and O2 gradients rather than extracellular enzymes to solubilize sorbed phosphorus. *Phormidium*, and some Proteobacteria, also contain the transporter pst genes, which are up-regulated at low inorganic phosphorus concentrations (Hirota et al. 2010). The presence of phosphatase genes and pst transporter genes may enable *Phormidium* to outcompete other organisms for phosphorus and enable it to dominate periphyton assemblages at low phosphorus concentrations.

3.4.4 Conclusions

The *de novo* genome assembly provided information about the community membership of *Phormidium*-dominated cyanobacterial mats in a river network and the metabolic capacities of the abundant organisms. Thus, it was possible to begin to define ecological exchanges of nutrients and energy in these mats. Similar to planktonic cyanobacterial blooms, but in contrast to laminated cyanobacterial mats on finer substrates, riverine mat metabolisms are primarily fueled by phototrophy and carbon degradation. Importantly, I directly identified the genes for cyanotoxin production and community compositional features that may predict the presence of this capacity. As humans put more pressure on water resources, through water extraction, nutrient pollution, and warming temperatures, cyanobacterial blooms are predicted to have increasing impacts on freshwater resources (Paerl et al. 2011, Taranu et al. 2015, Monteagudo and Moreno 2016). Understanding the relationships among toxigenic cyanobacteria and abiotic and biotic factors will be necessary to predict or mitigate cyanobacterial blooms in the future.

A: Supplementary information for chapter 1

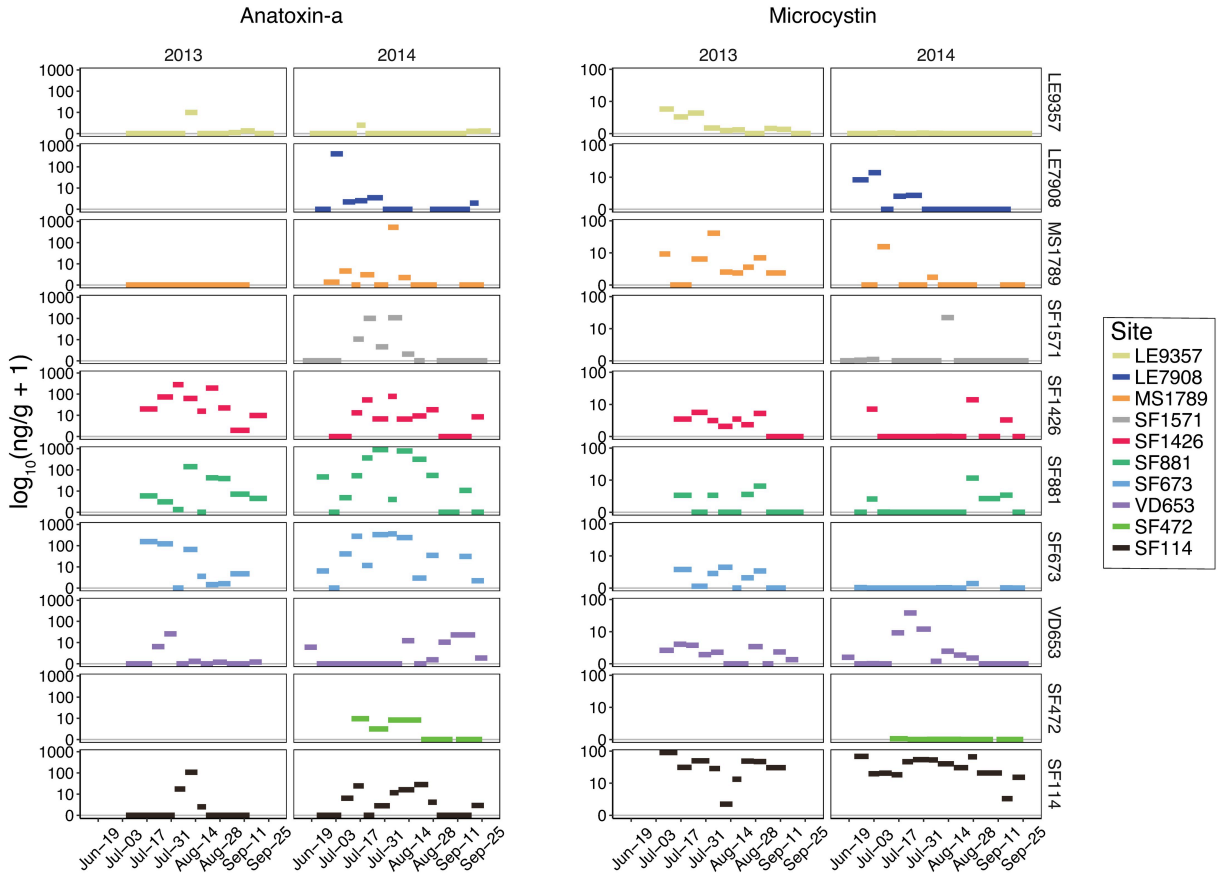

Fig. A.1 Time series of anatoxin-a and microcystin concentrations from SPATT samplers in 2013 and 2014. Sites are ordered top to bottom by watershed size. Each horizontal line represents an individual SPATT sampler and the length of the line corresponds to the number of days of deployment. LE79808, SF1571, and SF472 were only established in 2014.

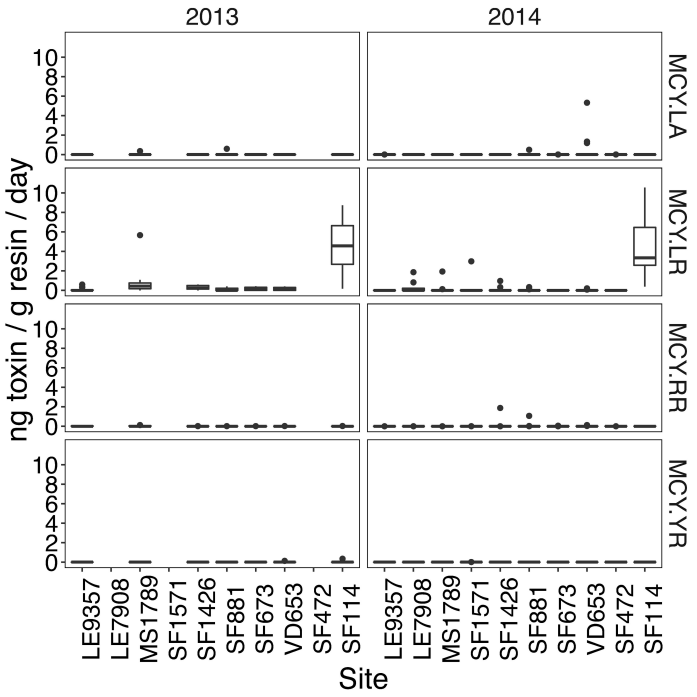

Fig. A.2 Boxplots of the four different microcystin (MCY) congeners measured from SPATT samplers in 2013 and 2014.

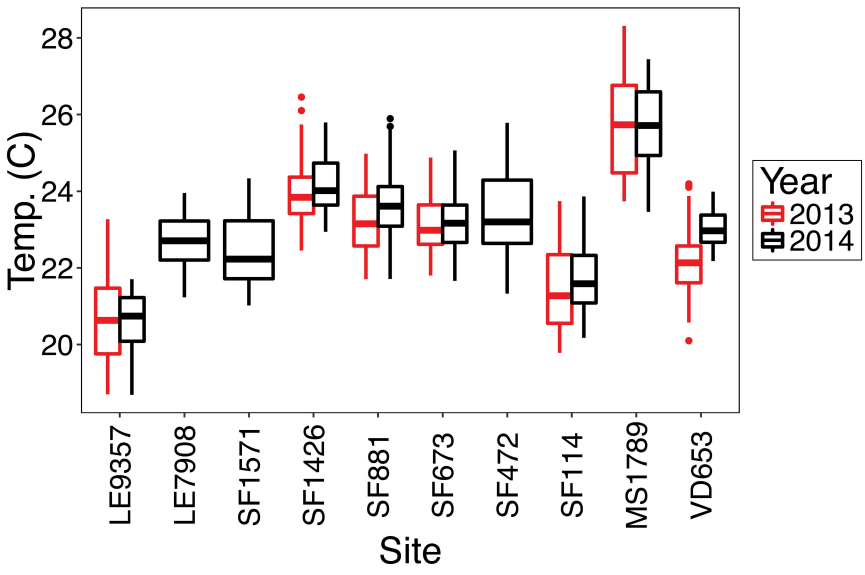

Fig. A.3 Boxplots of daily mean temperatures at SPATT sites from 3-Jul to 31-Aug in 2013 and 2014.

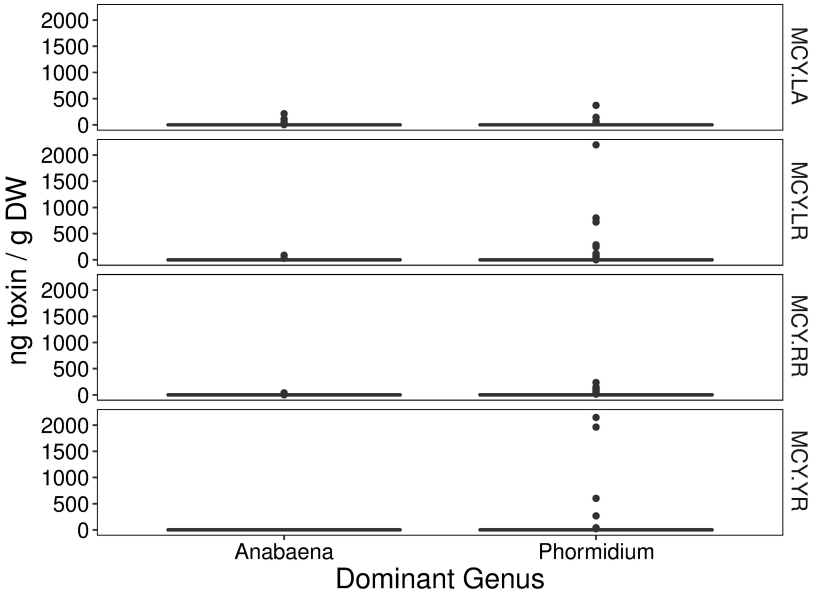

Fig. A.4 Microcystin (MCY) congeners from cyanobacterial mat samples collected in 2014 and 2015.

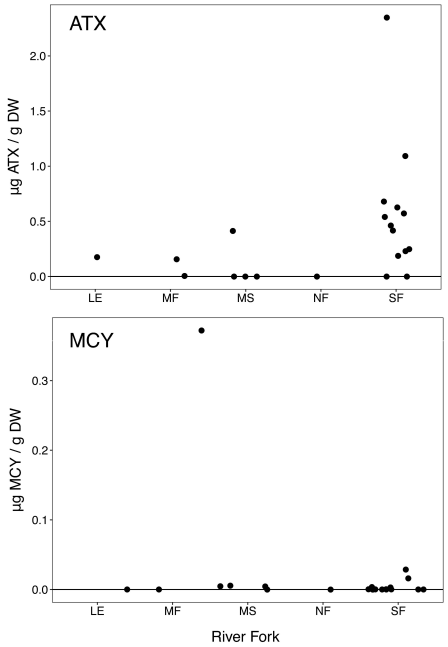

Fig. A.5 Anatoxin-a (ATX) and microcystin (MCY) concentrations in cyanobacterial mats. Samples collected in summer 2015 from Lower Eel (LE), Middle Fork (MF), Mainstem (MS), North Fork (NF), and South Fork (SF) Eel. (N= 21, 19 *Anabaena* samples and 2 *Phormidium* samples)

Table A.1 Cyanobacterial mat samples collected for microcystin (MCY) and anatoxin-a (ATX) analyses in Eel River watershed in 2014 and 2015.

Date collected	site	lat	long	Dominant cyano	ATX ng /g DW	MCY ng /g DW
8/15/15	17	39°43'44.54 "N	123°38'47.5 0"W	*Phormidium*	0	0
8/15/15	17	39°43'44.54 "N	123°38'47.5 0"W	*Phormidium*	0	0
8/15/15	17	39°43'44.54 "N	123°38'47.5 0"W	*Phormidium*	20.8083	14.4058
8/15/15	17	39°43'44.54 "N	123°38'47.5 0"W	*Phormidium*	39.8246	2220.6946
8/15/15	17	39°43'44.54 "N	123°38'47.5 0"W	*Phormidium*	0	2208.9402
8/3/15	527	39°50'22.71 "N	123°42'36.4 9"W	*Phormidium*	755.9775	0
8/3/15	527	39°50'22.71 "N	123°42'36.4 9"W	*Phormidium*	111.3299	30.2685
8/3/15	527	39°50'22.71 "N	123°42'36.4 9"W	*Phormidium*	797.5952	287.432
8/3/15	527	39°50'22.71 "N	123°42'36.4 9"W	*Phormidium*	0	794.3079
8/3/15	527	39°50'22.71 "N	123°42'36.4 9"W	*Phormidium*	0	761.7625
8/19/15	1391	40°11'10.81 "N	123°46'19.5 6"W	*Phormidium*	556.5136	76.4391
8/19/15	1391	40°11'10.81 "N	123°46'19.5 6"W	*Phormidium*	0	57.3982
8/19/15	1391	40°11'10.81 "N	123°46'19.5 6"W	*Phormidium*	314.3151	51.572
8/19/15	1391	40°11'10.81 "N	123°46'19.5 6"W	*Phormidium*	736.8056	127.5674
8/19/15	1391	40°11'10.81 "N	123°46'19.5 6"W	*Phormidium*	527.6416	837.2715
8/8/15	1397	40°11'31.51 "N	123°46'10.8 0"W	*Phormidium*	68.2447	0
8/8/15	1397	40°11'31.51 "N	123°46'10.8 0"W	*Phormidium*	0	102.3269
8/8/15	1397	40°11'31.51 "N	123°46'10.8 0"W	*Phormidium*	122.13	59.6111
8/8/15	1397	40°11'31.51 "N	123°46'10.8 0"W	*Phormidium*	436.1311	420.1088
8/8/15	1397	40°11'31.51 "N	123°46'10.8 0"W	*Phormidium*	146.3988	800.392
7/7/14	AN	39°44'30.74 "N	123°38'11.2 4"W	*Anabaena*	0	NA
7/17/14	AN	39°44'30.74 "N	123°38'11.2 4"W	*Anabaena*	0	0
7/17/14	AN	39°44'30.74 "N	123°38'11.2 4"W	*Anabaena*	1649.423	0

7/17/14	AN	39°44'30.74"N	123°38'11.24"W	*Anabaena*	NA	0
7/17/14	AN	39°44'30.74"N	123°38'11.24"W	*Anabaena*	0	4.122
7/17/14	AN	39°44'30.74"N	123°38'11.24"W	*Anabaena*	0	7.777
7/21/14	AN	39°44'30.74"N	123°38'11.24"W	*Anabaena*	0	0
7/21/14	AN	39°44'30.74"N	123°38'11.24"W	*Anabaena*	0	2.605
7/22/14	AN	39°44'30.74"N	123°38'11.24"W	*Phormidium*	0	1.405
8/4/15	CedarCr Confluence	39°50'21.83"N	123°42'29.24"W	*Phormidium*	147.482	79.1367
8/5/15	CedarCr Weir	39°50'25.90"N	123°42'25.84"W	*Phormidium*	1104.8951	0
8/5/15	CedarCr Weir	39°50'28.24"N	123°42'22.88"W	*Phormidium*	3304.7896	0
8/5/15	CedarCr Weir	39°50'28.24"N	123°42'22.88"W	*Phormidium*	111.5385	144.8718
8/12/15	Chimney Tree_DS	40°11'36.26"N	123°46'10.42"W	*Phormidium*	307.0709	5.7541
8/12/15	Chimney Tree_US	40°11'33.60"N	123°46'10.86"W	*Phormidium*	144.6465	0
7/12/14	CL	40°29'26.80"N	123°59'38.44"W	*Anabaena*	0	0
8/6/15	Dobbyn AP1	40°11'29.17"N	123°35'21.14"W	*Phormidium*	0	41.7189
8/6/15	Dobbyn AP2	40°11'29.17"N	123°35'21.14"W	*Phormidium*	215.0611	95.8842
8/6/15	Dobbyn_FS1	40°14'6.91"N	123°37'59.30"W	*Phormidium*	652.9923	0
8/6/15	Dobbyn FS2	40°14'6.91"N	123°37'59.30"W	*Phormidium*	28.0447	0
8/6/15	Dobbyn FS3	40°14'6.55"N	123°37'58.86"W	*Phormidium*	0	0
7/18/14	Dora	39°53'55.60"N	123°45'8.15"W	*Anabaena*	2744.361	0
7/17/15	Dora Creek	39°53'55.60"N	123°45'8.15"W	*Anabaena*	0	2.8798
8/10/15	Elder_Cob1	39°43'44.54"N	123°38'47.50"W	*Phormidium*	38.3505	386.8041
8/10/15	Elder_Cob2	39°43'44.54"N	123°38'47.50"W	*Phormidium*	98.2414	36.3857
7/10/15	Girlymon	39°44'30.84"N	123°38'4.54"W	*Anabaena*	152.8126	0
7/10/15	Girlymon	39°44'30.84"N	123°38'4.54"W	*Anabaena*	607.804	0
7/10/15	Girlymon	39°44'30.84"N	123°38'4.54"W	*Anabaena*	463.5115	42.1374
7/12/14	HF	40°25'13.50"N	123°56'7.10"W	*Anabaena*	0	42.076

8/18/15	Holmes Flat	40°25'13.50"N	123°56'7.10"W	*Phormidium*	202.5604	0
7/17/15	Howe Creek Pool	40°30'48.96"N	124° 9'27.27"W	*Anabaena*	175.9208	0
8/18/15	Larabee Creek DS	40°24'31.67"N	123°55'56.80"W	*Phormidium*	129.1107	21.1409
8/18/15	Larabee Creek US	40°24'32.57"N	123°55'53.13"W	*Phormidium*	357.8514	0
7/18/14	LG	39°52'31.49"N	123°43'33.01"W	*Phormidium*	0	150.184
7/24/14	LG	39°52'31.49"N	123°43'33.01"W	*Phormidium*	0	NA
8/2/14	LG	39°52'31.49"N	123°43'33.01"W	*Phormidium*	3330.579	21.429
8/24/14	LG	39°52'31.49"N	123°43'33.01"W	*Phormidium*	1226.326	45.744
9/12/14	LG	39°52'31.49"N	123°43'33.01"W	*Phormidium*	1745.613	30.342
8/12/15	Lumber Bridge_1	39°58'25.60"N	123°48'10.28"W	*Phormidium*	118.2005	0
7/19/15	Main Stem, Dos Rios	39°42'47.96"N	123°21'12.40"W	*Anabaena*	0	0
7/19/15	Main Stem, Dos Rios	39°42'47.96"N	123°21'12.40"W	*Anabaena*	0	5.2403
7/17/15	McCann	40°19'34.84"N	123°50'21.46"W	*Anabaena*	0	4.7075
7/17/15	McCann	40°19'34.84"N	123°50'21.46"W	*Anabaena*	412.7702	4.0767
7/8/15	Merganser	39°44'30.74"N	123°38'11.24"W	*Anabaena*	229.8936	0
7/8/15	Merganser	39°44'30.74"N	123°38'11.24"W	*Anabaena*	679.1059	0
7/8/15	Merganser	39°44'30.74"N	123°38'11.24"W	*Anabaena*	416.9058	0
7/8/15	Merganser	39°44'30.74"N	123°38'11.24"W	*Anabaena*	2347.2803	28.4519
7/10/15	Merganser	39°44'30.74"N	123°38'11.24"W	*Anabaena*	607.5183	0
7/10/15	Merganser	39°44'30.74"N	123°38'11.24"W	*Anabaena*	617.4818	0
7/10/15	Merganser	39°44'30.74"N	123°38'11.24"W	*Anabaena*	553.0549	0
7/10/15	Merganser	39°44'30.74"N	123°38'11.24"W	*Anabaena*	1513.1995	0
7/10/15	Merganser	39°44'30.74"N	123°38'11.24"W	*Anabaena*	571.6265	0
7/10/15	Merganser	39°44'30.74"N	123°38'11.24"W	*Anabaena*	575.0943	0
7/10/15	Merganser	39°44'30.74"N	123°38'11.24"W	*Anabaena*	378.1074	110.2813
7/10/15	Merganser	39°44'30.74"N	123°38'11.24"W	*Anabaena*	1100.6369	212.7898

7/10/15	Merganser	39°44'30.74"N	123°38'11.24"W	*Anabaena*	0	1.1603
7/10/15	Merganser	39°44'30.74"N	123°38'11.24"W	*Anabaena*	894.6746	44.1815
7/12/14	MF	39°42'48.06"N	123°21'7.02"W	*Anabaena*	0	0
7/12/14	MF	39°42'48.06"N	123°21'7.02"W	*Anabaena*	171.911	0
8/11/15	MF_BB	39°49'28.88"N	123°5'24.20"W	*Phormidium*	3.6835	0
8/11/15	MF USGS_1	39°49'44.12"N	123°4'19.55"W	*Phormidium*	6.3552	2.1184
8/11/15	MF USGS_2	39°49'44.12"N	123°4'19.55"W	*Phormidium*	6.6199	16.8744
8/11/15	MF USGS_3	39°49'44.12"N	123°4'19.55"W	*Phormidium*	0	0
7/19/15	Middle Fork, Dos Rios	39°42'48.06"N	123°21'7.02"W	*Anabaena*	5.7143	0
7/19/15	Middle Fork, upstream	39°42'48.06"N	123°21'7.02"W	*Phormidium*	156.4848	371.9348
7/17/15	Miranda Bridge	40°13'4.55"N	123°48'59.50"W	*Anabaena*	247.9976	0
7/17/15	Miranda Bridge	40°13'4.55"N	123°48'59.50"W	*Anabaena*	187.0875	0
7/19/15	North Fork	39°56'17.11"N	123°20'58.76"W	*Anabaena*	0	0
7/8/15	Piercy	40°0'1.53"N	123°47'15.74"W	*Phormidium*	571.8324	0
8/13/15	Piercy_DS	40°0'0.94"N	123°47'13.17"W	*Phormidium*	710.2764	0
8/13/15	Piercy_US	39°59'58.65"N	123°47'36.74"W	*Phormidium*	13.0678	0
7/12/14	PR			*Anabaena*	0	0
7/18/14	PR			*Anabaena*	88.371	0
7/18/14	PR	40°0'3.02"N	123°47'19.46"W	*Anabaena*	30692.761	0
7/18/14	PR	40°0'3.02"N	123°47'19.46"W	*Anabaena*	70934.751	0
7/18/14	PR	40°0'4.45"N	123°47'23.72"W	*Phormidium*	0	41.89
7/24/14	PR	40°0'3.02"N	123°47'19.46"W	*Anabaena*	0	0
8/2/14	PR	40°0'3.02"N	123°47'19.46"W	*Phormidium*	0	0
8/7/14	PR	40°0'3.02"N	123°47'19.46"W	*Anabaena*	0	0
8/7/14	PR	40°0'6.89"N	123°47'29.10"W	*Phormidium*	0	0
8/7/14	PR	40°0'4.45"N	123°47'23.72"W	*Phormidium*	51.616	0
8/24/14	PR			*Phormidium*	0	161.133

8/31/14	PR	40°0'3.02"N	123°47'19.46"W	*Phormidium*	0	0
8/31/14	PR			*Phormidium*	0	0
9/19/14	PR	40°0'3.02"N	123°47'19.46"W	*Anabaena*	0	0
6/3/14	PV	40°12'18.08"N	123°47'14.72"W	*Anabaena*	0	0
6/29/14	PV	40°12'18.79"N	123°47'18.29"W	*Anabaena*	0	0
6/29/14	PV	40°12'18.08"N	123°47'14.72"W	*Anabaena*	0	0
6/29/14	PV	40°12'18.08"N	123°47'14.72"W	*Anabaena*	0	0
6/29/14	PV	40°12'18.08"N	123°47'14.72"W	*Anabaena*	0	0
6/29/14	PV	40°12'19.32"N	123°47'18.40"W	*Anabaena*	0	0
6/29/14	PV	40°12'19.32"N	123°47'18.40"W	*Anabaena*	0	0
6/29/14	PV	40°12'18.08"N	123°47'14.72"W	*Anabaena*	NA	0
7/5/14	PV			*Anabaena*	0	0
7/5/14	PV			*Anabaena*	0	0
7/5/14	PV			*Anabaena*	0	0
7/5/14	PV			*Anabaena*	0	0
7/5/14	PV			*Anabaena*	NA	0
7/5/14	PV	40°12'18.79"N	123°47'18.29"W	*Phormidium*	NA	0
7/5/14	PV			*Anabaena*	NA	0
7/12/14	PV	40°12'19.32"N	123°47'18.40"W	*Anabaena*	116.525	0
7/12/14	PV	40°12'18.08"N	123°47'14.72"W	*Anabaena*	741.78	0
7/12/14	PV	40°12'18.79"N	123°47'18.29"W	*Anabaena*	646.929	0
7/12/14	PV	40°12'18.47"N	123°47'18.29"W	*Anabaena*	3647.146	0
7/12/14	PV	40°12'19.32"N	123°47'18.40"W	*Anabaena*	0	0.957
7/12/14	PV	40°12'19.32"N	123°47'18.40"W	*Anabaena*	0	154.412
7/18/14	PV	40°12'18.08"N	123°47'14.72"W	*Anabaena*	0	0
7/18/14	PV	40°12'19.32"N	123°47'18.40"W	*Anabaena*	0	0
7/18/14	PV	40°12'19.32"N	123°47'18.40"W	*Anabaena*	0	0
7/18/14	PV	40°12'19.32"N	123°47'18.40"W	*Anabaena*	0	0

7/18/14	PV	40°12'18.08"N	123°47'14.72"W	*Anabaena*	0	0
7/18/14	PV	40°12'18.08"N	123°47'14.72"W	*Anabaena*	2134.847	0
7/18/14	PV	40°12'19.29"N	123°47'19.36"W	*Anabaena*	739.84	0
7/18/14	PV	40°12'18.79"N	123°47'18.29"W	*Anabaena*	3184.371	0
7/18/14	PV	40°12'18.08"N	123°47'14.72"W	*Anabaena*	3703.03	0
7/24/14	PV	40°12'19.32"N	123°47'18.40"W	*Anabaena*	0	0
7/24/14	PV	40°12'18.79"N	123°47'18.29"W	*Anabaena*	0	0
8/2/14	PV	40°12'19.32"N	123°47'18.40"W	*Anabaena*	0	0
8/2/14	PV	40°12'16.88"N	123°47'16.46"W	*Anabaena*	0	0
8/2/14	PV	40°12'18.79"N	123°47'18.29"W	*Anabaena*	14.622	0
8/2/14	PV	40°12'19.32"N	123°47'18.40"W	*Anabaena*	35.9	0
8/2/14	PV	40°12'19.32"N	123°47'18.40"W	*Anabaena*	101.089	0
8/2/14	PV	40°12'18.79"N	123°47'18.29"W	*Anabaena*	4984.99	0
8/7/14	PV	40°12'18.79"N	123°47'18.29"W	*Anabaena*	0	0
8/7/14	PV	40°12'18.79"N	123°47'18.29"W	*Anabaena*	0	0
8/7/14	PV	40°12'19.32"N	123°47'18.40"W	*Anabaena*	15.652	0
8/7/14	PV	40°12'19.32"N	123°47'18.40"W	*Anabaena*	NA	0
8/7/14	PV	40°12'19.32"N	123°47'18.40"W	*Anabaena*	NA	0
8/7/14	PV	40°12'16.88"N	123°47'16.46"W	*Anabaena*	745.916	0
8/7/14	PV	40°12'18.08"N	123°47'14.72"W	*Anabaena*	437.641	6.772
8/16/14	PV	40°12'19.29"N	123°47'19.36"W	*Anabaena*	560.226	0
8/16/14	PV	40°12'16.88"N	123°47'16.46"W	*Anabaena*	59140.619	0
8/16/14	PV	40°12'19.32"N	123°47'18.40"W	*Anabaena*	159.289	10.185
8/16/14	PV	40°12'16.88"N	123°47'16.46"W	*Phormidium*	2653.422	68.947
8/16/14	PV	40°12'18.79"N	123°47'18.29"W	*Anabaena*	415.725	30.057
8/24/14	PV	40°12'16.88"N	123°47'16.46"W	*Phormidium*	1823.449	0

8/24/14	PV	40°12'16.88"N	123°47'16.46"W	*Anabaena*	1370.283	0
8/24/14	PV	40°12'16.88"N	123°47'16.46"W	*Anabaena*	50965.372	0
8/24/14	PV	40°12'19.29"N	123°47'19.36"W	*Anabaena*	11203.42	9.001
8/24/14	PV	40°12'18.08"N	123°47'14.72"W	*Anabaena*	82.655	8.77
8/24/14	PV	40°12'19.32"N	123°47'18.40"W	*Anabaena*	102.064	8.935
8/24/14	PV	40°12'19.32"N	123°47'18.40"W	*Anabaena*	127.527	16.716
8/24/14	PV	40°12'18.08"N	123°47'14.72"W	*Anabaena*	327.954	38.411
8/24/14	PV	40°12'18.79"N	123°47'18.29"W	*Anabaena*	779.878	36.514
8/31/14	PV	40°12'19.32"N	123°47'18.40"W	*Anabaena*	0	0
8/31/14	PV	40°12'18.08"N	123°47'14.72"W	*Anabaena*	0	0
8/31/14	PV	40°12'19.32"N	123°47'18.40"W	*Anabaena*	175.876	0
8/31/14	PV	40°12'16.88"N	123°47'16.46"W	*Phormidium*	6123.454	0
8/31/14	PV	40°12'18.79"N	123°47'18.29"W	*Anabaena*	6464.727	0
8/31/14	PV	40°12'16.88"N	123°47'16.46"W	*Phormidium*	24194.243	0
8/31/14	PV	40°12'19.32"N	123°47'18.40"W	*Anabaena*	13.038	4.179
8/31/14	PV	40°12'18.08"N	123°47'14.72"W	*Anabaena*	7071.041	0.731
9/19/14	PV	40°12'19.29"N	123°47'19.36"W	*Anabaena*	0	0
9/19/14	PV	40°12'19.32"N	123°47'18.40"W	*Anabaena*	469.678	0
9/19/14	PV	40°12'19.32"N	123°47'18.40"W	*Anabaena*	3107.692	0
9/19/14	PV	40°12'19.32"N	123°47'18.40"W	*Anabaena*	0	0.407
7/8/15	PV	40°12'19.32"N	123°47'18.40"W	*Anabaena*	1092.0307	0
7/8/15	PV	40°12'19.29"N	123°47'19.36"W	*Anabaena*	461.5718	0
7/10/15	Salser Bar	39°44'30.69"N	123°38'17.30"W	*Anabaena*	626.1905	0
7/10/15	Salser Bar	39°44'30.69"N	123°38'17.30"W	*Anabaena*	125.3968	0
7/10/15	Salser Bar	39°44'30.69"N	123°38'17.30"W	*Anabaena*	237.69	0
7/10/15	Salser Bar	39°44'30.69"N	123°38'17.30"W	*Anabaena*	367.5676	0

7/10/15	Salser Bar	39°44'30.69"N	123°38'17.30"W	*Anabaena*	482.8402	0
7/10/15	Salser Bar	39°44'30.69"N	123°38'17.30"W	*Anabaena*	33.3333	3.5842
8/13/15	Standish Hickey	39°52'31.49"N	123°43'33.01"W	*Phormidium*	0	2295.9086
7/8/15	USGS Miranda	40°10'55.56"N	123°46'35.50"W	*Anabaena*	539.5523	16.0141
7/17/15	USGS Miranda	40°10'55.56"N	123°46'35.50"W	*Anabaena*	0	3.488
7/12/14	HF	40°24'59.74"N	123°56'6.19"W	Nostoc	0	0
7/22/14	SF.TM	39°45'16.60"N	123°37'52.98"W	Nostoc	0	0
7/22/14	SF.TM	39°45'16.60"N	123°37'52.98"W	Nostoc	0	0
7/24/14	LG	39°52'29.35"N	123°44'4.20"W	Nostoc	0	0
8/2/14	PV	40°12'19.15"N	123°47'18.99"W	Nostoc	0	0
8/16/14	PV	40°12'19.15"N	123°47'18.99"W	Nostoc	0	0
8/31/14	LG	39°52'31.75"N	123°43'33.11"W	Nostoc	63.427	0
8/31/14	PV	40°12'19.15"N	123°47'18.99"W	Nostoc	883.154	0
9/19/14	PV	40°12'19.15"N	123°47'18.99"W	Nostoc	0	0

Table A.2 Cell counts of cyanobacterial cells from filtered water samples.

Date Collected	Location	Filtered Vol (mL)	*Anabaena* Filaments	Average *Anabaena* Cells / filament	Filaments / mL	Cells / mL
19-Jul-16	Chimney Tree	500	17	15.1	2	29
21-Jul-16	SFCed_DS	500	15	13.4	2	22
21-Jul-16	SFCed_US	500	29	15.9	3	54
27-Jun-16	SFSC	400	0	0.0	0	0
27-Jun-16	White House Pool	400	14	14.2	1	15
27-Jun-16	Salser Bar	400	11	15.0	1	12
27-Jun-16	Turtle Teacup Head	400	2	20.0	0	3
27-Jun-16	Wild Pool Tail	400	1	5.0	0	0
27-Jun-16	Wild Pool Head	400	0	0.0	0	0
27-Jun-16	SF_McKinley	400	2	13.0	0	2
27-Jun-16	SF_Elder	400	2	13.0	0	2
29-Jun-16	White House Pool_Deep	340	120	19.1	23	441
29-Jun-16	White House Pool_Surf	340	32	17.3	6	107
29-Jul-16	SFP_1	300	49	23.4	7	153
29-Jul-16	SFP_2	300	68	24.5	9	221

Table A.3 Relative percent abundance of different taxa in *Anabaena* and *Phormidium* dominated benthic mats based on microscopic cell counts.

Date	ID	lat	long	Dominant Cyano	*Cladophora* .gl	Spirogyra .spp	Epithemia. spp	Diatom .spp	*Anabaena* .spp	Phorm .spp	Cyano .spp	OtherTaxa
7/12 /14	SC1	40°12' 18.79" N	123°47' 18.29" W	*Anabaena*	0.2%	0.7%	37.1%	24.9%	10.2%	0.5%	24.5%	2.0%
7/18 /14	SC10	40° 0'3.02" N	123°47' 19.46" W	*Anabaena*	0.1%	0.6%	55.2%	20.1%	3.6%	1.0%	17.7%	1.7%
7/17 /14	SC102	39°44' 30.74" N	123°38' 11.24" W	*Anabaena*	0.8%	0.6%	33.3%	41.5%	8.6%	1.1%	7.9%	6.2%
8/31 /14	SC11	40°12' 18.79" N	123°47' 18.29" W	*Anabaena*	0.0%	0.4%	42.2%	25.2%	17.9%	0.1%	13.3%	0.8%
8/24 /14	SC114	40°12' 18.79" N	123°47' 18.29" W	*Anabaena*	1.1%	5.0%	23.8%	20.8%	16.9%	3.8%	24.9%	3.7%
8/16 /14	SC124	40°12' 18.79" N	123°47' 18.29" W	*Anabaena*	0.0%	0.0%	15.6%	10.2%	33.5%	1.8%	37.0%	2.0%
8/24 /14	SC126	40°12' 18.79" N	123°47' 18.29" W	*Anabaena*	0.0%	0.2%	18.7%	17.4%	20.9%	3.8%	37.1%	1.9%
8/31 /14	SC14	40°12' 18.79" N	123°47' 18.29" W	*Anabaena*	2.8%	5.9%	23.7%	25.3%	18.5%	6.5%	17.1%	0.2%
8/31 /14	SC17	40°12' 18.79" N	123°47' 18.29" W	*Anabaena*	3.1%	9.6%	40.5%	15.4%	22.6%	1.3%	6.8%	0.8%
7/18 /14	SC24	40°12' 18.79" N	123°47' 18.29" W	*Anabaena*	0.0%	2.5%	30.2%	16.9%	38.7%	1.4%	10.1%	0.2%

7/18/14	SC25	40°12' 18.79" N	123°47' 18.29" W	*Anabaena*	0.4%	0.0%	74.2%	4.1%	19.6%	0.1%	0.8%	0.7%
7/18/14	SC27	40°12' 18.79" N	123°47' 18.29" W	*Anabaena*	2.1%	0.5%	64.6%	8.4%	17.7%	0.0%	6.2%	0.6%
7/18/14	SC30	40°12' 18.79" N	123°47' 18.29" W	*Anabaena*	0.0%	0.0%	43.4%	14.6%	34.8%	0.2%	5.7%	1.2%
7/17/14	SC32	39°44' 30.74" N	123°38' 11.24" W	*Anabaena*	1.1%	0.0%	76.5%	11.1%	3.2%	0.0%	6.1%	2.0%
7/18/14	SC34	39°53' 55.60" N	123°45' 8.15" W	*Anabaena*	0.0%	0.0%	45.2%	18.7%	27.0%	0.0%	7.7%	1.4%
8/2/14	SC40	40°12' 18.79" N	123°47' 18.29" W	*Anabaena*	0.0%	0.2%	29.5%	18.4%	27.5%	1.3%	22.7%	0.4%
7/18/14	SC42	40°12' 18.79" N	123°47' 18.29" W	*Anabaena*	0.6%	2.1%	37.1%	17.7%	16.2%	1.8%	23.6%	0.9%
7/12/14	SC44	39°42' 48.06" N	123°21' 7.02" W	*Anabaena*	0.0%	1.1%	60.3%	13.9%	11.4%	0.0%	11.9%	1.4%
7/12/14	SC46	39°42' 48.06" N	123°21' 7.02" W	*Anabaena*	0.6%	13.4%	13.1%	16.8%	34.1%	0.0%	20.1%	2.0%
7/12/14	SC47	40°12' 18.79" N	123°47' 18.29" W	*Anabaena*	0.0%	0.2%	63.3%	6.1%	12.3%	0.0%	15.8%	2.4%
7/7/14	SC50	39°44' 30.69" N	123°38' 17.30" W	*Anabaena*	4.2%	0.2%	27.9%	32.1%	5.0%	0.2%	28.6%	1.8%
7/12/14	SC51	40°12' 18.79" N	123°47' 18.29" W	*Anabaena*	0.0%	2.4%	29.0%	23.1%	36.9%	2.2%	4.0%	2.4%

7/17/14	SC6	39°44' 30.74" N	123°38' 11.24" W	*Anabaena*	0.0%	0.5%	25.9%	30.4%	14.7%	0.3%	26.9%	1.2%
8/31/14	SC61	40°12' 18.79" N	123°47' 18.29" W	*Anabaena*	0.0%	0.0%	61.4%	9.4%	15.9%	0.5%	12.4%	0.4%
7/18/14	SC67	40° 0'3.02" N	123°47' 19.46" W	*Anabaena*	1.0%	0.8%	55.9%	27.3%	7.7%	0.0%	7.1%	0.3%
7/5/14	SC68	40°12' 18.79" N	123°47' 18.29" W	*Anabaena*	0.2%	0.7%	42.7%	13.7%	17.6%	0.6%	22.8%	1.6%
7/12/14	SC70	39°42' 48.06" N	123°21' 7.02" W	*Anabaena*	0.0%	0.2%	30.9%	24.2%	0.7%	0.9%	42.6%	0.5%
8/31/14	SC71	40°12' 18.79" N	123°47' 18.29" W	*Anabaena*	0.2%	0.0%	26.2%	8.3%	13.5%	0.2%	49.7%	1.9%
7/24/14	SC84	40° 0'3.02" N	123°47' 19.46" W	*Anabaena*	0.7%	2.4%	66.3%	21.1%	3.9%	4.1%	0.9%	0.6%
8/2/14	SC88	40°12' 18.79" N	123°47' 18.29" W	*Anabaena*	1.3%	2.6%	48.8%	6.2%	15.4%	0.9%	22.2%	2.6%
7/18/14	SC97	40° 0'3.02" N	123°47' 19.46" W	*Anabaena*	0.0%	0.6%	52.9%	27.8%	8.0%	1.2%	6.7%	2.7%
8/16/14	SC118	40°12' 18.79" N	123°47' 18.29" W	*Phormidium*	0.0%	0.0%	18.1%	10.9%	9.2%	35.9%	24.4%	1.5%
8/31/14	SC22	40° 0'3.02" N	123°47' 19.46" W	*Phormidium*	0.0%	0.0%	1.4%	3.8%	0.0%	91.6%	2.7%	0.5%
8/31/14	SC3	40°12' 18.79" N	123°47' 18.29" W	*Phormidium*	0.0%	0.0%	2.7%	11.1%	0.0%	79.7%	5.9%	0.5%

9/12/14	SC5	39°52'31.49" N	123°43'33.01" W	*Phormidium*	0.0%	0.0%	0.2%	35.4%	0.0%	46.2%	16.8%	1.4%
8/7/14	SC76	40°0'3.02" N	123°47'19.46" W	*Phormidium*	0.0%	0.2%	5.7%	12.6%	1.7%	37.0%	41.8%	1.0%
8/31/14	SC9	40°12'18.79" N	123°47'18.29" W	*Phormidium*	0.2%	0.2%	21.5%	41.0%	3.8%	4.0%	25.6%	3.6%
8/2/14	SC91	39°52'31.49" N	123°43'33.01" W	*Phormidium*	0.0%	0.2%	17.3%	21.9%	0.5%	56.9%	2.4%	0.7%
7/18/14	SC95	40°0'3.02" N	123°47'19.46" W	*Phormidium*	0.0%	0.4%	26.7%	15.9%	2.4%	45.0%	8.1%	1.5%

B: Supplementary information for chapter 3

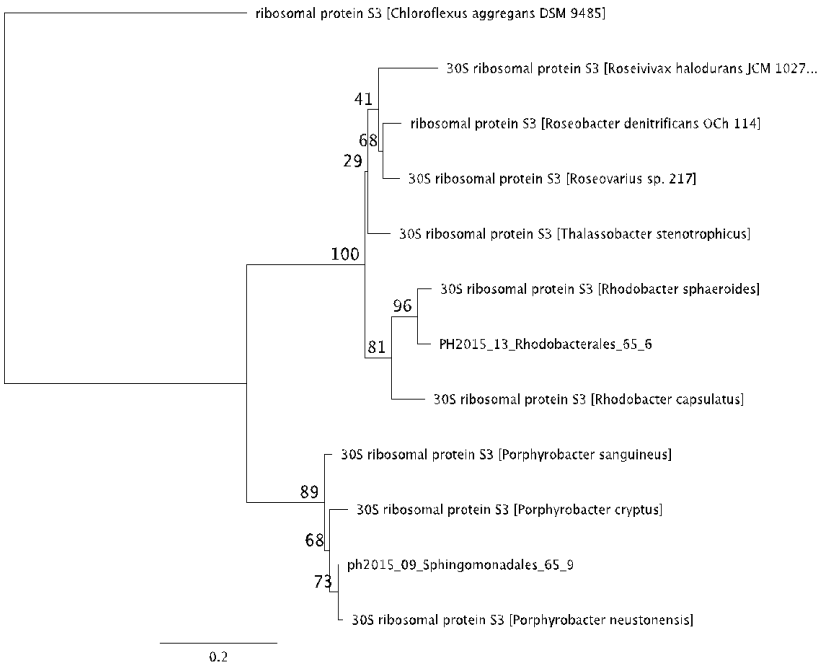

Fig. B.1 Maximum likelihood tree (PHYLM) of ribosomal protein S3 amino acid sequences of Alphaproteobacteria. This shows PH2015_13_Rhodobacterales_65_6 genome clustering with the non-sulfur purple bacteria *Rhodobacter capsulatus* and PH2015_09_Sphingomonadales_65_9 clustering with aerobic anoxygenic phototrophs *Porphyrobacter* spp. Node values show bootstrap support out of 100 iterations.

Table B.1 Hidden Markov model (HMM) identifications and cutoff scores for metabolism genes. Cutoff scores and custom HMMs from Anantharaman et al. (2016).

process	gene	hmm_id	cutoff score
reverse TCA cycle	acetate_citrate_lyase aclA_alignment	Custom	215
reverse TCA cycle	acetate_citrate_lyase aclB_alignment	Custom	177
sulfate_reduction	aprA	TIGR02061	326
arsenate_reduction	ars_glutaredoxin	TIGR02689	113
arsenate_reduction	ars_ox	TIGR02693	357
arsenate_reduction	ars_ox	TIGR02694	61
arsenate_reduction	ars_thioredoxin	TIGR02691	112
sulfate_reduction	asrA	TIGR02910	223
sulfate_reduction	asrB	TIGR02911	226
sulfate_reduction	asrC	TIGR00014	61
sulfate_reduction	asrC	TIGR02912	194
CO_oxidation	carbon_monoxide_dehydrogenase coxM_alignment	Custom	184
CO_oxidation	carbon_monoxide_dehydrogenase coxS_alignment	Custom	198
cytoC_oxidase_cbb3	ccoN	TIGR00780	168
cytoC_oxidase_cbb3	ccoO	TIGR00781	62
cytoC_oxidase_cbb3	ccoP	TIGR00782	54
chlorite_reduction	cld	PF06778	65
wood_lungdahl_pathway	codh_catalytic	TIGR01702	210
wood_lungdahl_pathway	codhC	TIGR00316	355
wood_lungdahl_pathway	codhD	TIGR00381	197
cytoC_oxidase_caa3	coxA	TIGR02891	617
cytoC_oxidase_caa3	coxB	TIGR02866	144
cytoC_oxidase_caa3	coxL	TIGR02416	300
cytoQu_oxidase_bd	cydA	PF01654	118
cytoQu_oxidase_bd	cydB	TIGR00203	88
cytoQu_oxidase_bo	cyoA	TIGR01433	218
cytoQu_oxidase_bo	cyoD	TIGR02847	64
cytoQu_oxidase_bo	cyoE	TIGR01473	138
sulfate_reduction	cysC	TIGR00455	133
sulfate_reduction	cysN	TIGR02034	327
sulfur_oxidation	dsrA	TIGR02064	223
sulfur_oxidation	dsrB	TIGR02066	205
sulfite_reduction	dsrD	PF08679	50

formaldehyde_oxidation	fae	TIGR03126	31
sulfide_oxidation	fccB	Pfam	266
formate_oxidation	fdh_thiol_id	TIGR02819	425
formate_oxidation	fdhA	TIGR01591	610
formate_oxidation	fdhB	TIGR01582	152
formate_oxidation	fdhC	TIGR01583	56
Ni_Fe_hydrogenase	FeFeHydrogenase	TIGR02512	300
Ni_Fe_hydrogenase	FeFeHydrogenase	TIGR04105	380
formaldehyde_oxidation	fmtf	TIGR03119	94
halogenated_compounds_breakdown	hdh	TIGR01428	72
anammox	hydrazine_oxidase_hzoA	Custom	325
nitrile_hydratase	hydrazine_synthase_hzsA	Custom	466
Ni_Fe_hydrogenase	Hydrogenase_Group_1	Custom	411
Ni_Fe_hydrogenase	Hydrogenase_Group_2a	Custom	472
Ni_Fe_hydrogenase	Hydrogenase_Group_2b	Custom	555
Ni_Fe_hydrogenase	Hydrogenase_Group_3a	Custom	368
Ni_Fe_hydrogenase	Hydrogenase_Group_3b	Custom	303
Ni_Fe_hydrogenase	Hydrogenase_Group_3c	Custom	575
Ni_Fe_hydrogenase	Hydrogenase_Group_3d	Custom	541
Ni_Fe_hydrogenase	Hydrogenase_Group_4	Custom	430
methylamine_formaldehyde	madA	TIGR02659	85
methylamine_formaldehyde	madB	TIGR02658	90
methane_production	mcrA	TIGR03256	314
methane_production	mcrB	TIGR03257	173
methane_production	mcrC	TIGR03259	171
methanol_oxidation	methanol_dehydrogenase pqq_xoxF_mxaF_alignment	Custom	166
methanol_oxidation	mmoB	PF02406	-
methanol_oxidation	mmoD	TIGR04550	-
formaldehyde_oxidation	mtmc	TIGR03120	147
iron_manganese_oxidation	mtrA	TIGR03507	60
iron_manganese_oxidation	mtrC	TIGR03509	165
nitrate_reduction	napA	TIGR01706	472
nitrate_reduction	napB	PF03892	23.9
nitrate_reduction	narG	TIGR01580	600
nitrate_reduction	narH	TIGR01660	348
nitrate_reduction	ndma	TIGR04266	400
N_fixation	nifA_Fe	TIGR01861	873
N_fixation	nifA_Mo	TIGR01282	503

N_fixation	nifA_Va	TIGR01860	822
N_fixation	nifB_Fe	TIGR02931	853
N_fixation	nifB_Mo	TIGR01286	414
N_fixation	nifB_V	TIGR02932	821
N_fixation	nifD_Fe	TIGR02929	124
N_fixation	nifD_V	TIGR02930	122
N_fixation	nifH	TIGR01287	261
nitrite_reduction	nirB	TIGR02374	442
nitrite_reduction	nirD	TIGR02378	69
nitrite_reduction	nirK	TIGR02376	169
nitric_oxide_reduction	nitric_oxide_reductase norB_alignment	Custom	79
nitric_oxide_reduction	nitric_oxide_reductase norC_alignment	Custom	50
nitrite_oxidation	nitrite_oxidoreductase nxrA_alignment	Custom	370
nitrite_oxidation	nitrite_oxidoreductase nxrB_alignment	Custom	252
nitrite_reduction	nitrite_reductase nirS_alignment	Custom	200
nitrous_oxide_reduction	nosD	PF05048/TIGR04247	290
nitrous_oxide_reduction	nosZ	TIGR04246	550
nitrite_reduction	nrfA	PF02335	57
nitrite_reduction	nrfA	PF02335/TIGR03152	576
nitrite_reduction	nrfD	TIGR03148	300
nitrite_reduction	nrfH	TIGR03153	75
nitrile_hydratase	nthA	TIGR01323	239
nitrile_hydratase	nthB	TIGR03888	136
Octaheme c-type cytochrome Shewanella-type	octR	TIGR04315	325
perchlorate_reduction	pcrA	TIGR03479	559
perchlorate_reduction	pcrB	TIGR03478	319
methane_oxidation	pmoA	TIGR03080	92
methane_oxidation	pmoB	TIGR03079	202
methane_oxidation	pmoC	TIGR03078	124
cytochrome (quinone) oxidase, aa3 type, QoxABCD	qoxA	TIGR01432	204
cytochrome (quinone) oxidase, aa3 type, QoxABCD	qoxB	TIGR02882	954
Reductive dehalogenase	rdh	TIGR02486	132
carbon_fixation	rubisco_form_I_alignment	Custom	500
carbon_fixation	rubisco_form_II_III_alignment	Custom	500

carbon_fixation	rubisco_form_II_alignment	Custom	500
carbon_fixation	rubisco_form_III_alignment	Custom	450
sulfate_reduction	sat	TIGR00339	181
selenate_reduction	sel_mo	TIGR03313	526
formaldehyde_oxidation	sfh	TIGR02821	131
formaldehyde_oxidation	sgdh	TIGR02818	509
formaldehyde_oxidation	smdh	TIGR03451	512
sulfur_oxidation	sor	PF07682	300
thiosulfate_oxidation	soxB	TIGR04486	375
thiosulfate_oxidation	soxC	TIGR04555	330
thiosulfate_oxidation	soxY	TIGR04488	125
sulfide_oxidation	sulfide_quinone_oxidoreductase sqr_alignment	Custom	300
sulfur_oxidation	sulfur_dioxygenase sdo_alignment	Custom	120
thiosulfate_disproportionation	thiosulfate_reductase phsA_alignment	Custom	323
urease	ureA	TIGR00193	31
urease	ureB	TIGR00192	40
urease	ureC	TIGR01792	212
selenate_reduction	ygfK	TIGR03315	354
selenate_reduction	ygfM	TIGR03312	87

Table B.2 Hidden Markov model (HMM) matrix used for identification of phosphorus genes.

process	enzyme_name	HMM_ID	gene	cutoff
M	Acid Phosphatase (Class A)	PF01569	phoN	40
M	Acid Phosphatase (Class B)	PF03767	aphA	40
M	Alkaline Phosphatase (PhoA)	PF00245	phoA	100
M	Alkaline Phosphatase (PhoD)	PF09423	phoD	50
M	Glycerophosphoryl Diester Phosphodiesterase	PF03009	ugpQ	100
S	PQQGDH (Quinoprotein Glucose Dehydrogenase)	TIGR03074	gcd	800
T	Phosphate Inorganic Transporter (Pit)	PF01384	pit	180
T	Phosphate–Specific Transport System Subunit (PstA)	TIGR00974	pstA	193
T	Phosphate–Specific Transport System Subunit (PstB)	TIGR00972	pstB	343
T	Phosphate–Specific Transport System Subunit (PstC)	TIGR02138	pstC	196
T	Phosphate–Specific Transport System Subunit (PstS)	TIGR00975	pstS	205
R	Phosphate Regulon Response Regulator (PhoB)	TIGR02154	phoB	296
R	Phosphate Regulon Sensor Histidine Kinase (PhoR)	TIGR02966	phoR	330
R	PhoR/PhoB Inhibitor Protein (PhoU)	TIGR02135	phoU	130

Table B.3 Environmental parameters measured at each metagenomics sampling site in 2015.

Date collected	Sample ID	Drainage Area km^2	Depth cm	Flow cm/s	Temp C	pH	Cond µs	DO mgL	Canopy cover avg	DOC mgL	TDN ugL	NH4 ugL	NO3 ugL	TDP ugL
4-Aug-15	PH2015_01	527	15-20	30-50	19.6	8.68	214	9.63	1.82%	0.728	44.541	1.435	30.278	9.067
4-Aug-15	PH2015_11	527	15-20	30-50	19.6	8.68	214	9.63	1.82%	0.728	44.541	1.435	30.278	9.067
4-Aug-15	PH2015_12	39	10	10-20	17.2	8.66	196	9.71	21.32%	0.472	26.473	1.001	43.637	8.237
4-Aug-15	PH2015_13	39	10	10-20	17.2	8.66	196	9.71	0.26%	0.472	26.473	1.001	43.637	8.237
5-Aug-15	PH2015_02	39	13	30-50	18.6	8.63	202.2	9.35	55.90%	0.728	44.541	1.435	30.278	8.237
5-Aug-15	PH2015_14	39	25	30-50	18.6	8.63	202.2	9.35	50.70%	0.728	44.541	1.435	30.278	8.237
6-Aug-15	PH2015_15	160	10-15	30-50	22.4	8.91	273.8	9.75	1.30%	1.022	44.821	1.173	11.531	6.660
6-Aug-15	PH2015_03	160	5-10	20-30	22.4	8.91	273.8	9.75	11.96%	1.022	44.821	1.173	11.531	6.660
6-Aug-15	PH2015_16	96	5-10	30-50	24.8	8.92	253.3	10.03	46.80%	0.726	35.437	0.967	20.322	10.912
10-Aug-15	PH2015_17	17	5	5-10	17.6	8.53	136	8.5	60.84%	0.608	28.153	0.921	14.052	27.805
10-Aug-15	PH2015_04	17	15	10-15	17.6	8.53	136	8.5	61.10%	0.608	28.153	0.921	14.052	27.805
11-Aug-15	PH2015_05	531	15-20	30-50	22.1	8.84	345.9	9.38	1.30%	0.891	39.779	0.761	13.737	5.677
11-Aug-15	PH2015_06	951	10-15	20-30	26.0	9.08	345	9.44	0.00%	1.066	58.408	1.995	26.718	5.377
12-Aug-15	PH2015_07	1417	18	30-50	25.0	8.46	249.9	8.53	4.94%	0.944	72.835	2.040	52.900	10.742
12-Aug-15	PH2015_18	1417	20	30-50	25.0	8.46	249.9	8.53	1.82%	0.944	72.835	2.040	52.900	10.742
12-Aug-15	PH2015_19	795	34	50-70	24.3	8.56	249.3	10.1	39.78%	0.945	72.135	1.504	98.939	8.878
13-Aug-15	PH2015_20	881	20	50-100	23.8	8.75	243.6	10.02	22.88%	0.995	71.434	2.452	27.474	6.953
13-Aug-15	PH2015_08	881	15	100	23.8	8.75	243.6	10.02	0.78%	0.995	71.434	2.452	27.474	6.953
13-Aug-15	PH2015_21	653	5-15	30-50	23.4	8.51	244.5	9.35	2.34%	0.951	50.564	1.629	17.983	5.558
18-Aug-15	PH2015_09	7908	10-15	30-50	24.1	8.84	249	12.4	0.00%	1.201	83.620	0.533	7.868	5.434
18-Aug-15	PH2015_10	228	2-10	20-30	20.8	8.01	260.4	8.1	30.42%	0.879	72.555	2.063	72.624	9.370
18-Aug-15	PH2015_22	228	15	20-30	20.8	8.01	260.4	8.1	0.26%	0.879	72.555	2.063	72.624	9.370

Table B.4 Read mapping coverage to anatoxin-a synthesis operon genes in PH2015_19_scaffold_1561.

Ana gene and bp	anaE: 5739	anaJ: 174	anaD: 264	anaG: 3219	anaB: 1146	anaF: 5619	anaC: 1620	anaI: 1401	anaA: 762
PH2015_01	1.2	0.0	0.0	0.3	0.4	0.6	0.0	0.2	0.6
PH2015_02	0.2	0.0	1.1	0.2	0.3	0.0	0.4	0.0	1.2
PH2015_03	0.0	0.0	0.0	0.0	0.0	0.1	0.4	0.0	0.0
PH2015_04	0.0	0.0	0.0	0.0	0.0	0.1	0.0	0.0	0.0
PH2015_05	0.1	0.0	0.0	0.1	0.0	0.2	0.2	0.0	0.4
PH2015_06	0.3	0.0	0.6	0.4	0.5	0.1	0.3	0.2	0.0
PH2015_07	2.8	1.7	2.3	2.9	2.8	3.6	3.3	2.8	3.5
PH2015_08	1.3	0.0	4.5	1.5	2.0	1.4	2.9	0.6	0.7
PH2015_09	138.0	89.6	152.8	137.6	143.5	136.3	136.4	144.7	152.6
PH2015_10	100.8	56.7	105.0	106.5	99.7	101.6	107.3	113.8	105.8
PH2015_11	0.8	0.0	0.0	0.7	0.8	0.7	0.4	1.2	1.2
PH2015_12	0.1	0.0	0.0	0.0	0.3	0.0	0.4	0.0	0.0
PH2015_13	0.1	0.0	0.0	0.0	0.0	0.1	0.0	0.1	0.0
PH2015_14	0.0	0.0	0.0	0.0	0.0	0.0	0.2	0.0	0.0
PH2015_15	0.1	0.0	0.0	0.1	0.0	0.0	0.0	0.0	0.0
PH2015_16	0.2	0.0	0.0	0.2	0.0	0.0	0.0	0.0	0.0
PH2015_17	0.1	0.0	0.0	0.1	0.3	0.1	0.0	0.0	0.0
PH2015_18	62.7	38.7	71.4	67.7	67.5	63.3	66.6	63.8	61.9
PH2015_19	65.1	24.6	63.0	66.8	55.4	62.2	61.6	62.2	63.3
PH2015_20	9.3	8.1	9.8	9.1	9.6	11.8	12.6	8.0	12.9
PH2015_21	0.4	0.0	0.0	0.3	0.8	0.5	0.0	0.2	0.4
PH2015_22	21.1	11.8	20.7	19.8	25.4	20.1	23.7	26.0	26.7

Table B.5 Percent nucleotide similarity of ana genes with the Oscillatoria PCC6506 operon.

Sample	anaA	anaB	anaC	anaD	anaE	anaF	anaG	anaI	anaJ
Oscillatoria PCC6506	100%	100%	100%	100%	100%	100%	100%	100%	100%
Anabaena sp 37	89%	84%	82%	86%	86%	86%	88%	81%	88%
Cuspidothrix LBR148	86%	83%	83%	83%	86%	86%	88%	89%	NA
PH2015_07_scaffold_1970	88%	NA	90%	89%	94%	87%	91%	NA	88%
PH2015_09_scaffold_531	88%	93%	90%	89%	94%	85%	58%	89%	NA
PH2015_10_scaffold_460	88%	93%	90%	89%	94%	87%	58%	89%	NA
PH2015_18_scaffold_1607	88%	93%	90%	89%	94%	87%	57%	89%	79%
PH2015_19_scaffold_1561	88%	93%	90%	89%	93%	87%	58%	89%	85%
PH2015_20_scaffold_333	88%	93%	90%	89%	94%	87%	58%	89%	88%
PH2015_22_scaffold_316	88%	93%	90%	89%	94%	85%	58%	89%	60%

References

Aboal, M., M. Á. Puig, and A. D. Asencio. 2005. Production of microcystins in calcareous Mediterranean streams: The Alharabe River, Segura River basin in south-east Spain. Journal of Applied Phycology 17:231–243.

Allen, M. B. 1952. The Cultivation of Myxophyeeae. Arch. Milcrobiol 53:34–53.

Alvarenga, D. O., M. F. Fiore, and A. M. Varani. 2017. A metagenomic approach to cyanobacterial genomics. Frontiers in Microbiology 8:1–16.

Anantharaman, K., C. T. Brown, L. A. Hug, I. Sharon, C. J. Castelle, A. J. Probst, B. C. Thomas, A. Singh, M. J. Wilkins, U. Karaoz, E. L. Brodie, K. H. Williams, S. S. Hubbard, and J. F. Banfield. 2016. Thousands of microbial genomes shed light on interconnected biogeochemical processes in an aquifer system. Nature Communications 7:13219.

Van Apeldoorn, M. E., H. P. Van Egmond, G. J. A. Speijers, and G. J. I. Bakker. 2007. Toxins of cyanobacteria. Molecular Nutrition and Food Research 51:7–60.

Aristi, I., J. E. Clapcott, V. Acuña, A. Elosegi, H. Mills, S. A. Wood, and R. G. Young. 2017. Forestry affects the abundance of *Phormidium*-dominated biofilms and the functioning of a New Zealand river ecosystem. Marine and Freshwater Research:MF16208.

Armitage, D. W., K. L. Gallagher, N. D. Youngblut, D. H. Buckley, and S. H. Zinder. 2012. Millimeter-scale patterns of phylogenetic and trait diversity in a salt marsh microbial mat. Frontiers in Microbiology 3:1–16.

Backer, L. C., J. H. Landsberg, M. Miller, K. Keel, and T. K. Taylor. 2013. Canine cyanotoxin poisonings in the United States (1920s-2012): review of suspected and confirmed cases from three data sources. Toxins 5:1597–1628.

Bagatini, I. L., A. Eiler, S. Bertilsson, D. Klaveness, P. Tessarolli, and A. A. H. Vieira. 2014. Host-Specificity and Dynamics in Bacterial Communities Associated with Bloom-Forming Freshwater Phytoplankton. PLoS ONE 9:e85950.

Bates, D., M. Maechler, B. Bolker, and W. Steve. 2015. Fitting linear mixed-effects models using lme4. Journal of Statistical Software 67:1–48.

Beraldi-Campesi, H., C. Arenas-Abad, F. Garcia-Pichel, O. Arellano-Aguilar, L. Auqué, M. Vázquez-Urbez, C. Sancho, C. Osácar, and S. Ruiz-Velasco. 2012. Benthic bacterial diversity from freshwater tufas of the Iberian Range (Spain). FEMS Microbiology Ecology 80:363–379.

Berg, K. A., C. Lyra, K. Sivonen, L. Paulin, S. Suomalainen, P. Tuomi, and J. Rapala. 2009. High diversity of cultivable heterotrophic bacteria in association with cyanobacterial water blooms. The ISME journal 3:314–25.

Bergkemper, F., A. Schöler, M. Engel, F. Lang, J. Krüger, M. Schloter, and S. Schulz. 2016. Phosphorus depletion in forest soils shapes bacterial communities towards phosphorus recycling systems. Environmental Microbiology 18:1988–2000.

Bergman, B., J. R. Gallon, A. N. Rai, and L. J. Stal. 1997. N2 Fixation by non-heterocystous cyanobacteria. FEMS Microbiology Reviews 19:139–185.

Bormans, M., and S. A. Condie. 1997. Modelling the distribution of Anabaena and Melosira in a stratified river wier pool. Hydrobiologia 364:3–13.

Bormans, M., B. S. Sherman, and I. T. Webster. 1999. Is buoyancy regulation in cyanobacteria an adaptation to exploit separation of light and nutrients? Marine and Freshwater Research 50:897.

Bosak, T., J. W. M. Bush, M. R. Flynn, B. Liang, S. Ono, A. P. Petroff, and M. S. Sim. 2010. Formation and stability of oxygen-rich bubbles that shape photosynthetic mats. Geobiology 8:45–55.

Bouma-Gregson, K., M. E. Power, and M. Bormans. 2017. Rise and fall of toxic benthic freshwater cyanobacteria (*Anabaena* spp.) in the Eel river: Buoyancy and dispersal. Harmful Algae 66:79–87.

Brasell, K. A., M. W. Heath, K. G. Ryan, and S. A. Wood. 2015. Successional Change in Microbial Communities of Benthic *Phormidium*-Dominated Biofilms. Microbial Ecology 69:254–266.

Briand, E., J. Humbert, K. Tambosco, M. Bormans, and W. H. Gerwick. 2016. Role of bacteria in the production and degradation of *Microcystis* cyanopeptides. MicrobiologyOpen 5:469–478.

Brown, N. M., R. S. Mueller, J. W. Shepardson, Z. C. Landry, J. T. Morré, C. S. Maier, F. J. Hardy, and T. W. Dreher. 2016. Structural and functional analysis of the finished genome of the recently isolated toxic *Anabaena* sp. WA102. BMC Genomics 17:457.

Cadel-Six, S., I. Iteman, C. Peyraud-Thomas, S. Mann, O. Ploux, and A. Méjean. 2009. Identification of a polyketide synthase coding sequence specific for anatoxin-a-producing Oscillatoria cyanobacteria. Applied and Environmental Microbiology 75:4909–4912.

Cadel-Six, S., C. Peyraud-Thomas, L. Brient, N. T. De Marsac, R. Rippka, and A. Méjean. 2007. Different genotypes of anatoxin-producing cyanobacteria coexist in the Tarn River, France. Applied and Environmental Microbiology 73:7605–7614.

Cantoral Uriza, E., A. Asencio, and M. Aboal. 2017. Are We Underestimating Benthic Cyanotoxins? Extensive Sampling Results from Spain. Toxins 9:385.

Carey, C. C., B. W. Ibelings, E. P. Hoffmann, D. P. Hamilton, and J. D. Brookes. 2012. Eco-physiological adaptations that favour freshwater cyanobacteria in a changing climate. Water research 46:1394–407.

Carmichael, W. W., D. F. Biggs, and M. A. Peterson. 1979. Pharmacology of anatoxin-a, produced by the freshwater cyanophyte *Anabaena flos-aquae* NRC-44-1. Toxicon 17:229–236.

Cayan, D. R., E. P. Maurer, M. D. Dettinger, M. Tyree, and K. Hayhoe. 2008. Climate change scenarios for the California region. Climatic Change 87:21–42.

Chorus, I., and J. Bartram. 1999. Toxic cyanobacteria in water: a guide to their public health consequences, monitoring, and management. (I. Chorus and J. Bartram, Eds.). E & FN Spon, London.

Chu, Z., X. Jin, B. Yang, and Q. Zeng. 2007. Buoyancy regulation of Microcystis flos-aquae during phosphorus-limited and nitrogen-limited growth. Journal of Plankton Research 29:739–745.

Cirés, S., L. Wörmer, C. Wiedner, and A. Quesada. 2013. Temperature-dependent dispersal strategies of *Aphanizomenon ovalisporum* (Nostocales, Cyanobacteria): implications for the annual life cycle. Microbial Ecology 65:12–21.

Cowell, B. C., and P. S. Botts. 1994. Factors influencing the distribution, abundance and growth of *Lyngbya wollei* in central Florida. Aquatic Botany 49:1–17.

D'Agostino, P. M., J. N. Woodhouse, A. K. Makower, A. C. Y. Yeung, S. E. Ongley, M. L. Micallef, M. C. Moffitt, and B. A. Neilan. 2016. Advances in genomics, transcriptomics and proteomics of toxin-producing cyanobacteria. Environmental Microbiology Reports 8:3–13.

Davis, J. P., N. H. Youssef, and M. S. Elshahed. 2009. Assessment of the diversity, abundance, and ecological distribution of members of candidate division SR1 reveals a high level of phylogenetic diversity but limited morphotypic diversity. Applied and environmental microbiology 75:4139–48.

Dervaux, J., A. Mejean, and P. Brunet. 2015. Irreversible collective migration of cyanobacteria in eutrophic conditions. PLOS ONE 10:e0120906.

Devlin, J., and O. Edwards. 1977. Anatoxin-a, a toxic alkaloid from *Anabaena flos-aquae* NRC-44h. Canadian Journal of Chemistry:1–5.

Edgar, R. C. 2004. MUSCLE: multiple sequence alignment with high accuracy and high throughput. Nucleic Acids Research 32:1792–1797.

Edgar, R. C. 2010. Search and clustering orders of magnitude faster than BLAST. Bioinformatics 26:2460–2461.

Edwards, C., K. A. Beattie, C. M. Scrimgeour, and G. A. Codd. 1992. Identification of anatoxin-a in benthic cyanobacteria (blue-green algae) and in associated dog poisonings at Loch Insh, Scotland. Toxicon 30:1165–1175.

Edwards, C., and L. A. Lawton. 2009. Bioremediation of Cyanotoxins. Pages 109–129Advances in Applied Microbiology. First edition. Elsevier Inc.

Fetscher, A. E., M. D. A. Howard, R. Stancheva, R. M. Kudela, E. D. Stein, M. A. Sutula, L. B. Busse, and R. G. Sheath. 2015. Wadeable streams as widespread sources of benthic cyanotoxins in California, USA. Harmful Algae 49:105–116.

Finlay, J. C., J. M. Hood, M. P. Limm, M. E. Power, J. D. Schade, and J. R. Welter. 2011. Light-mediated thresholds in stream-water nutrient composition in a river network. Ecology 92:140–50.

Fraisse, S., M. Bormans, and Y. Lagadeuc. 2015. Turbulence effects on phytoplankton morphofunctional traits selection. Limnology and Oceanography 60:872–884.

Francis, G. 1878. Poisonous Australian lake. Nature 18:11–12.

Franks, J., and J. F. Stolz. 2009. Flat laminated microbial mat communities. Earth-Science Reviews 96:163–172.

Gibble, C. M., and R. M. Kudela. 2014. Detection of persistent microcystin toxins at the land–sea interface in Monterey Bay, California. Harmful Algae 39:146–153.

Grondin, J. M., K. Tamura, G. Déjean, D. W. Abbott, and H. Brumer. 2017. Polysaccharide Utilization Loci: Fueling Microbial Communities. Journal of Bacteriology 199:e00860-16.

Gugger, M., S. Lenoir, C. Berger, A. Ledreux, J.-C. Druart, J.-F. Humbert, C. Guette, and C. Bernard. 2005. First report in a river in France of the benthic cyanobacterium *Phormidium favosum* producing anatoxin-a associated with dog neurotoxicosis. Toxicon 45:919–28.

Haft, D. H., J. D. Selengut, and O. White. 2003. The TIGRFAMs database of protein families. Nucleic acids research 31:371–3.

Halinen, K., D. P. Fewer, L. M. Sihvonen, C. Lyra, E. Eronen, and K. Sivonen. 2008. Genetic diversity in strains of the genus *Anabaena* isolated from planktonic and benthic habitats of the Gulf of Finland (Baltic Sea). FEMS Microbiology Ecology 64:199–208.

Halinen, K., J. Jokela, D. P. Fewer, M. Wahlsten, and K. Sivonen. 2007. Direct evidence for production of microcystins by *Anabaena* strains from the Baltic Sea. Applied and Environmental Microbiology 73:6543–6550.

Heath, M. W., S. A. Wood, and K. G. Ryan. 2011. Spatial and temporal variability in *Phormidium* mats and associated anatoxin-a and homoanatoxin-a in two New Zealand rivers. Aquatic Microbial Ecology 64:69–79.

Heath, M., S. A. Wood, R. G. Young, and K. G. Ryan. 2016. The role of nitrogen and phosphorus in regulating *Phormidium* sp. (cyanobacteria) growth and anatoxin production. FEMS Microbiology Ecology 92:fiw021.

Hill, W. R., and A. W. Knight. 1988. Nutrient and Light Limitation of Algae in Two Northern California Streams. Journal of Phycology 24:125–132.

Hirota, R., A. Kuroda, J. Kato, and H. Ohtake. 2010. Bacterial phosphate metabolism and its application to phosphorus recovery and industrial bioprocesses. Journal of Bioscience and Bioengineering 109:423–432.

Hoiczyk, E. 2000. Gliding motility in cyanobacterial: observations and possible explanations. Archives of microbiology 174:11–17.

Holmes, R. M., A. Aminot, R. Kérouel, B. A. Hooker, and B. J. Peterson. 1999. A simple and precise method for measuring ammonium in marine and freshwater ecosystems. Canadian Journal of Fisheries and Aquatic Sciences 56:1801–1808.

Horne, A. J., and C. J. W. Carmiggelt. 1975. Algal nitrogen fixation in Californian streams: seasonal cycles. Freshwater Biology 5:461–470.

Hug, L. A., B. J. Baker, K. Anantharaman, C. T. Brown, A. J. Probst, C. J. Castelle, C. N. Butterfield, A. W. Hernsdorf, Y. Amano, K. Ise, Y. Suzuki, N. Dudek, D. A. Relman, K. M. Finstad, R. Amundson, B. C. Thomas, and J. F. Banfield. 2016. A new view of the tree of life. Nature Microbiology 1:16048.

Hyatt, D., G.-L. Chen, P. F. Locascio, M. L. Land, F. W. Larimer, and L. J. Hauser. 2010. Prodigal: prokaryotic gene recognition and translation initiation site identification. BMC bioinformatics 11:119.

Ibelings, B. W., L. R. Mur, and A. E. Walsby. 1991. Diurnal changes in buoyancy and vertical distribution in populations of *Microcystis* in two shallow lakes. Journal of Plankton Research 13:419–436.

Jaworski, G. H. M., S. W. Wiseman, and C. S. Reynolds. 1988. Variability in sinking rate of the freshwater diatom *Asterionella formosa*: the influence of colony morphology. British Phycological Journal 23:167–176.

Jiang, Y., G. Song, Q. Pan, Y. Yang, and R. Li. 2015. Identification of genes for anatoxin-a biosynthesis in *Cuspidothrix issatschenkoi*. Harmful Algae 46:43–48.

Jorgensen, B. B., Y. Cohen, and D. J. Des Marais. 1987. Photosynthetic action spectra and adaptation to spectral light distribution in a benthic cyanobacterial mat. Applied and Environmental Microbiology 53:879–886.

Joshi, N. A., and J. N. Fass. 2011. Sickle: a sliding-window, adaptive, quality-based trimming tool for FastQ files.

Kaminski, A., B. Bober, Z. Lechowski, and J. Bialczyk. 2013. Determination of anatoxin-a stability under certain abiotic factors. Harmful Algae 28:83–87.

Kanehisa, M., S. Goto, Y. Sato, M. Kawashima, M. Furumichi, and M. Tanabe. 2014. Data, information, knowledge and principle: Back to metabolism in KEGG. Nucleic Acids Research 42:199–205.

Kantor, R. S., K. C. Wrighton, K. M. Handley, I. Sharon, L. A. Hug, C. J. Castelle, B. C. Thomas, and J. F. Banfield. 2013. Small genomes and sparse metabolisms of sediment-associated bacteria from four candidate phyla. mBio 4:1–11.

Karjalainen, M., J. Engstrom-Ost, S. Korpinen, H. Peltonen, J. P. Paakkonen, S. Ronkkonen, S. Suikkanen, and M. Viitasalo. 2007. Ecosystem consequences of cyanobacteria in the northern Baltic Sea. Ambio 36:195–202.

Kearse, M., R. Moir, A. Wilson, S. Stones-Havas, M. Cheung, S. Sturrock, S. Buxton, A. Cooper, S. Markowitz, C. Duran, T. Thierer, B. Ashton, P. Mentjies, and A. Drummond. 2012. Geneious Basic: an integrated and extendable desktop software platform for the organization and analysis of sequence data. Bioinformatics 28:1647–1649.

Kim, M., H. S. Oh, S. C. Park, and J. Chun. 2014. Towards a taxonomic coherence between average nucleotide identity and 16S rRNA gene sequence similarity for species demarcation of prokaryotes. International Journal of Systematic and Evolutionary Microbiology 64:346–351.

Kiviranta, J., K. Sivonen, K. Lahti, R. Luukkainen, and S. I. Niemelae. 1991. Production and biodegradation of cyanobacterial toxins- A laboratory study. Archiv Fur Hydrobiologie 121:281–294.

Koblizek, M. 2015. Ecology of aerobic anoxygenic phototrophs in aquatic environments. FEMS Microbiology Reviews 39:854–870.

Koleff, P., K. J. Gaston, and J. J. Lennon. 2003. Measuring beta diversity for presence–absence data. Journal of Animal Ecology 72:367–382.

Komarek, J. 2013. Süßwasserflora von Mitteleuropa, Bd. 19/3: Cyanoprokaryota Heterocytous Genera. Springer Spektrum, Berlin, Heidelberg.

Komárek, J. 2010. Modern taxonomic revision of planktic Nostocacean cyanobacteria: a short review of genera. Hydrobiologia 639:231–243.

Komárek, J. 2017a. Delimitation of the family Oscillatoriaceae (Cyanobacteria) according to the modern polyphasic approach (introductory review). Brazilian Journal of Botany:1–8.

Komárek, J. 2017b. Several problems of the polyphasic approach in the modern cyanobacterial system. Hydrobiologia.

Kormas, K. A., and D. S. Lymperopoulou. 2013. Cyanobacterial toxin degrading bacteria: who are they? BioMed research international 2013:463894.

Kromkamp, J. C., and L. R. Mur. 1984. Buoyant density changes in the cyanobacterium Microcystis aeruginosa due to changes in the cellular carbohydrate content. FEMS Microbiology Letters 25:105–109.

Kudela, R. M. 2011. Characterization and deployment of Solid Phase Adsorption Toxin Tracking (SPATT) resin for monitoring of microcystins in fresh and saltwater. Harmful Algae 11:117–125.

Kudela, R. M. 2017. Passive Sampling for Freshwater and Marine Algal Toxins. Pages 379–409 *in* J. Diogene and M. Campas, editors. Comprehensive Analytical Chemistry. Elsevier Ltd, Amsterdam.

Kupferberg, S. J., J. C. Marks, and M. E. Power. 1994. Effects of variation in vatural algal and detrital diets on larval anuran (*Hyla regilla*) life-history traits. Copeia 1994:446–457.

Langmead, B., and S. L. Salzberg. 2012. Fast gapped-read alignment with Bowtie 2. Nature methods 9:357–9.

Lennon, J. J., P. Koleff, J. J. D. Greenwood, and K. J. Gaston. 2001. The geographical structure of British bird distributions: Diversity, spatial turnover and scale. Journal of Animal Ecology 70:966–979.

Lezcano, M. A. 2016. Presence or Absence of mlr Genes and Nutrient Concentrations Co-Determine the Microcystin Biodegradation Efficiency of a Natural. Toxins 8:1–17.

Li, H., P. Xing, and Q. L. Wu. 2012. The high resilience of the bacterioplankton community in the face of a catastrophic disturbance by a heavy Microcystis bloom. FEMS Microbiology Ecology 82:192–201.

Li, J., K. Shimizu, H. Akasako, Z. Lu, S. Akiyama, M. Goto, M. Utsumi, and N. Sugiura. 2015. Assessment of the factors contributing to the variations in microcystins biodegradability of the biofilms on a practical biological treatment facility. Bioresource Technology 175:463–472.

Li, X., T. W. Dreher, and R. Li. 2016a. An overview of diversity, occurrence, genetics and toxin production of bloom-forming *Dolichospermum* (*Anabaena*) species. Harmful Algae 54:54–68.

Lisle, T. E. 1990. The Eel River, northwestern California; high sediment yields from a dynamic landscape. Pages 311–314 *in* M. G. Wolman and H. C. Riggs, editors. Surface Water Hydrology. Geological Society of America.

Louati, I., N. Pascault, D. Debroas, C. Bernard, J. F. Humbert, and J. Leloup. 2015. Structural diversity of bacterial communities associated with bloom-forming freshwater cyanobacteria differs according to the cyanobacterial genus. PLoS ONE 10.

Lyra, C., M. Laamanen, J. M. Lehtimäki, A. Surakka, and K. Sivonen. 2005. Benthic cyanobacteria of the genus *Nodularia* are non-toxic, without gas vacuoles, able to glide and genetically more diverse than planktonic *Nodularia*. International Journal of Systematic and Evolutionary Microbiology 55:555–568.

MacKenzie, L. A. 2010. In situ passive solid-phase adsorption of micro-algal biotoxins as a monitoring tool. Current Opinion in Biotechnology 21:326–331.

MacKenzie, L., V. Beuzenberg, P. Holland, P. McNabb, and A. Selwood. 2004. Solid phase adsorption toxin tracking (SPATT): a new monitoring tool that simulates the biotoxin contamination of filter feeding bivalves. Toxicon 44:901–18.

Maier, H. R., M. D. Burch, and M. Bormans. 2001. Flow management strategies to control blooms of the cyanobacterium, *Anabaena circinalis*, in the River Murray at Morgan, South Australia. Regulated Rivers: Research & Management 17:637–650.

McAllister, T. G., S. A. Wood, and I. Hawes. 2016. The rise of toxic benthic *Phormidium* proliferations: A review of their taxonomy, distribution, toxin content and factors regulating prevalence and increased severity. Harmful Algae 55:282–294.

McGregor, G. B., and J. P. Rasmussen. 2008. Cyanobacterial composition of microbial mats from an Australian thermal spring: A polyphasic evaluation. FEMS Microbiology Ecology 63:23–35.

Medrano, E. A., R. E. Uittenbogaard, B. J. H. van de Wiel, L. M. Dionisio Pires, and H. J. H. Clercx. 2016. An alternative explanation for cyanobacterial scum formation and persistence by oxygenic photosynthesis. Harmful Algae 60:27–35.

Méjean, A., K. Dalle, G. Paci, S. Bouchonnet, S. Mann, V. Pichon, and O. Ploux. 2016. Dihydroanatoxin-a is biosynthesized from proline in *Cylindrospermum stagnale* PCC 7417: isotopic incorporation experiments and mass spectrometry analysis. Journal of Natural Products 79:1775–1782.

Méjean, A., R. Mazmouz, S. Mann, A. Calteau, C. Médigue, and O. Ploux. 2010. The genome sequence of the cyanobacterium *Oscillatoria* sp. PCC 6506 reveals several gene clusters responsible for the biosynthesis of toxins and secondary metabolites. Journal of Bacteriology 192:5264–5265.

Méjean, A., G. Paci, V. Gautier, and O. Ploux. 2014. Biosynthesis of anatoxin-a and analogues (anatoxins) in cyanobacteria. Toxicon 91:15–22.

Mekebri, A., G. J. Blondina, and D. B. Crane. 2009. Method validation of microcystins in water and tissue by enhanced liquid chromatography tandem mass spectrometry. Journal of Chromatography A 1216:3147–3255.

Mendoza-Lera, C., L. L. Federlein, M. Knie, and M. Mutz. 2016. The algal lift: Buoyancy-mediated sediment transport. Water Resources Research 52:108–118.

Meybeck M. 1993. C, N, P and S in Rivers: From Sources to Global Inputs. In: Wollast R., Mackenzie F.T., Chou L. (eds) Interactions of C, N, P and S Biogeochemical Cycles and Global Change. NATO ASI Series (Series I: Global Environmental Change), vol 4. Springer, Berlin, Heidelberg

Miller, M. A., R. M. Kudela, A. Mekebri, D. Crane, S. C. Oates, M. T. Tinker, M. Staedler, W. a Miller, S. Toy-Choutka, C. Dominik, D. Hardin, G. Langlois, M. Murray, K. Ward, and D. A. Jessup. 2010. Evidence for a novel marine harmful algal bloom: cyanotoxin (microcystin) transfer from land to sea otters. PloS ONE 5:e125765.

Mohamed, Z. A., H. M. El-Sharouny, and W. S. M. Ali. 2006. Microcystin production in benthic mats of cyanobacteria in the Nile River and irrigation canals, Egypt. Toxicon 47:584–90.

Monteagudo, L., and J. L. Moreno. 2016. Benthic freshwater cyanobacteria as indicators of anthropogenic pressures. Ecological Indicators 67:693–702.

Mou, X., X. Lu, J. Jacob, S. Sun, and R. Heath. 2013. Metagenomic Identification of Bacterioplankton Taxa and Pathways Involved in Microcystin Degradation in Lake Erie. PLoS ONE 8:e61890.

Neilan, B. A., L. A. Pearson, J. Muenchhoff, M. C. Moffitt, and E. Dittmann. 2013. Environmental conditions that influence toxin biosynthesis in cyanobacteria. Environmental Microbiology 15:1239–53.

Nelson, W. C., and J. C. Stegen. 2015. The reduced genomes of Parcubacteria (OD1) contain signatures of a symbiotic lifestyle. Frontiers in Microbiology 6:1–14.

Nicolaus, B., A. Panico, L. Lama, I. Romano, M. C. Manca, A. De Guilio, and A. Gambacorta. 1999. Chemical composition and production of exopolysaccharides from representative members of heterocystous and non-heterocystous cyanobacteria. Phytochemistry 52:639–647.

Niemi, R. M., I. Heiskanen, R. Heine, and J. Rapala. 2009. Previously uncultured β-Proteobacteria dominate in biologically active granular activated carbon (BAC) filters. Water Research 43:5075–5086.

Oksanen, J., F. G. Blanchet, M. Friendly, R. Kindt, P. Legendre, D. McGlinn, P. R. Minchin, R. B. O'Hara, G. L. Simpson, P. Solymos, M. H. Stevens, E. Szoecs, and H. Wagner. 2017. vegan: Community Ecology Package.

Omidi, A., M. Esterhuizen-Londt, and S. Pflugmacher. 2017. Still challenging: the ecological function of the cyanobacterial toxin microcystin– What we know so far. Toxin Reviews:1–19.

Osswald, J., S. Rellán, A. Gago, and V. Vasconcelos. 2007. Toxicology and detection methods of the alkaloid neurotoxin produced by cyanobacteria, anatoxin-a. Environment International 33:1070–1089.

Otten, T. G., J. R. Crosswell, S. Mackey, and T. W. Dreher. 2015. Application of molecular tools for microbial source tracking and public health risk assessment of a *Microcystis* bloom traversing 300km of the Klamath River. Harmful Algae 46:71–81.

Padisak, J., E. Soroczki-Pinter, and Z. Rezner. 2003. Sinking properties of some phytoplankton shapes and the relation of form resistance to morphological diversity of plankton - an experimental study. Hydrobiologia 500:243–257.

Paerl, H. W. 1996. Microscale physiological and ecological studies of aquatic cyanobacteria: Macroscale implications. Microscopy Research and Technique 33:47–72.

Paerl, H. W., N. S. Hall, and E. S. Calandrino. 2011. Controlling harmful cyanobacterial blooms in a world experiencing anthropogenic and climatic-induced change. The Science of the Total Environment 409:1739–45.

Paerl, H. W., and J. Huisman. 2009. Climate change: a catalyst for global expansion of harmful cyanobacterial blooms. Environmental Microbiology Reports 1:27–37.

Paerl, H. W., and T. G. Otten. 2013. Harmful cyanobacterial blooms: causes, consequences, and controls. Microbial Ecology 65:995–1010.

Paerl, H. W., and J. L. Pinckney. 1996. A mini-review of microbial consortia: their roles in aquatic production and biogeochemical cycling. Microbial Ecology 31:225–247.

Pancrace, C., M.-A. Barny, R. Ueoka, A. Calteau, T. Scalvenzi, J. Pédron, V. Barbe, J. Piel, J.-F. Humbert, and M. Gugger. 2017. Insights into the *Planktothrix* genus: Genomic and metabolic comparison of benthic and planktic strains. Scientific Reports 7:41181.

Parks, D. H., M. Imelfort, C. T. Skennerton, P. Hugenholtz, and G. W. Tyson. 2015. CheckM: assessing the quality of microbial genomes recovered from isolates, single cells, and metagenomes. Genome research 25:1043–55.

Parulekar, N. N., P. Kolekar, A. Jenkins, S. Kleiven, H. Utkilen, A. Johansen, S. Sawant, U. Kulkarni-kale, M. Kale, and M. Sæb. 2017. Characterization of bacterial community associated with phytoplankton bloom in a eutrophic lake in South Norway using 16S rRNA

gene amplicon sequence analysis. PloS ONE 12:e0173408.

Parveen, B., V. Ravet, C. Djediat, I. Mary, C. Quiblier, D. Debroas, and J. F. Humbert. 2013. Bacterial communities associated with *Microcystis* colonies differ from free-living communities living in the same ecosystem. Environmental Microbiology Reports 5:716–724.

Peng, Y., H. C. M. Leung, S. M. Yiu, and F. Y. L. Chin. 2012. IDBA-UD: A de novo assembler for single-cell and metagenomic sequencing data with highly uneven depth. Bioinformatics 28:1420–1428.

Pope, P. B., and B. K. C. Patel. 2008. Metagenomic analysis of a freshwater toxic cyanobacteria bloom. FEMS Microbiology Ecology 64:9–27.

Power, M. E. 1990. Benthic turfs vs floating mats of algae in river food webs. Oikos 58:67–79.

Power, M. E., K. Bouma-Gregson, P. Higgins, and S. M. Carlson. 2015. The Thirsty Eel: Summer and winter flow thresholds that tilt the Eel River of Northwestern California from salmon-supporting to cyanobacterially degraded states. Copeia 2015:200–211.

Power, M. E., J. R. Holomuzki, and R. L. Lowe. 2013. Food webs in Mediterranean rivers. Hydrobiologia 719:119–136.

Power, M. E., R. L. Lowe, P. C. Furey, J. R. Welter, M. P. Limm, J. C. Finlay, C. Bode, S. Chang, M. Goodrich, and J. Sculley. 2009. Algal mats and insect emergence in rivers under Mediterranean climates: towards photogrammetric surveillance. Freshwater Biology 54:2101–2115.

Power, M. E., M. S. Parker, and W. E. Dietrich. 2008. Seasonal reassembly of a river food web: floods, droughts, and impacts of fish. Ecological Monographs 78:263–282.

Pritchard, L., R. H. Glover, S. Humphris, J. G. Elphinstone, and I. K. Toth. 2016. Genomics and taxonomy in diagnostics for food security: soft-rotting enterobacterial plant pathogens. Anal. Methods 8:12–24.

Puschner, B., B. Hoff, and E. R. Tor. 2008. Diagnosis of anatoxin-a poisoning in dogs from North America. Journal of Veterinary Diagnostic Investigation 20:89–92.

Quiblier, C., S. Wood, I. Echenique-Subiabre, M. Heath, A. Villeneuve, and J.-F. Humbert. 2013. A review of current knowledge on toxic benthic freshwater cyanobacteria - Ecology, toxin production and risk management. Water Research 47:5464–5479.

R Core Team. 2017. R: a language and environment for statistical computing. R Foundation for Statistical Computing:http://www.r-project.org.

Rantala-Ylinen, A., S. Känä, H. Wang, L. Rouhiainen, M. Wahlsten, E. Rizzi, K. Berg, M. Gugger, and K. Sivonen. 2011. Anatoxin-a synthetase gene cluster of the cyanobacterium Anabaena sp. strain 37 and molecular methods to detect potential producers. Applied and environmental microbiology 77:7271–8.

Rapala, J., K. Lahti, K. Sivonen, and S. I. Niemelä. 1994. Biodegradability and adsorption on lake sediments of cyanobacterial hepatotoxins and anatoxin-a. Letters in Applied Microbiology 19:423–428.

Raveh-Sadka, T., B. C. Thomas, A. Singh, B. Firek, B. Brooks, C. J. Castelle, I. Sharon, R. Baker, M. Good, M. J. Morowitz, and J. F. Banfield. 2015. Gut bacteria are rarely shared by co-hospitalized premature infants, regardless of necrotizing enterocolitis development. eLife 2015:e05477.

Rejmánková, E., and J. Komárková. 2005. Response of cyanobacterial mats to nutrient and salinity changes. Aquatic Botany 83:87–107.

Reynolds, C. S. 1972. Growth, gas vacuolation and buoyancy in a natural population of a planktonic blue-green alga. Freshwater Biology 2:87–106.

Reynolds, C. S., R. L. Oliver, and A. E. Walsby. 1987. Cyanobacterial dominance: The role of buoyancy regulation in dynamic lake environments. New Zealand Journal of Marine and Freshwater Research 21:379–390.

Richter, M., and R. Rossello-Mora. 2009. Shifting the genomic gold standard for the prokaryotic species definition. Proceedings of the National Academy of Sciences 106:19126–19131.

Rigosi, A., C. C. Carey, B. W. Ibelings, and J. D. Brookes. 2014. The interaction between climate warming and eutrophication to promote cyanobacteria is dependent on trophic state and varies among taxa. Limnology and Oceanography 59:99–114.

Sabater, S., E. Vilalta, A. Gaudes, H. Guasch, I. Muñoz, and A. Romaní. 2003. Ecological implications of mass growth of benthic cyanobacteria in rivers. Aquatic Microbial Ecology 32:175–184.

Sciuto, K., C. Andreoli, N. Rascio, N. La Rocca, and I. Moro. 2012. Polyphasic approach and typification of selected *Phormidium* strains (Cyanobacteria). Cladistics 28:357–374.

Scott, J. T., and A. M. Marcarelli. 2012. Cyanobacteria in freshwater benthic environments. Pages 271–289 *in* B. A. Whitton, editor. Ecology of Cyanobacteria II: their diversity in space and time. 2nd edition. Springer Netherlands, Dordrecht.

Shih, P. M., D. Wu, A. Latifi, S. D. Axen, D. P. Fewer, E. Talla, A. Calteau, F. Cai, N. Tandeau de Marsac, R. Rippka, M. Herdman, K. Sivonen, T. Coursin, T. Laurent, L. Goodwin, M. Nolan, K. W. Davenport, C. S. Han, E. M. Rubin, J. A Eisen, T. Woyke, M. Gugger, and C. A Kerfeld. 2013. Improving the coverage of the cyanobacterial phylum using diversity-driven genome sequencing. Proceedings of the National Academy of Sciences of the United States of America 110:1053–8.

Stamatakis, A. 2014. RAxML version 8: a tool for phylogenetic analysis and post-analysis of large phylogenies. Bioinformatics 30:1312–1313.

Stanish, L. F., S. P. O'Neill, A. Gonzalez, T. M. Legg, J. Knelman, D. M. Mcknight, S. Spaulding, and D. R. Nemergut. 2013. Bacteria and diatom co-occurrence patterns in microbial mats from polar desert streams. Environmental Microbiology 15:1115–1131.

Steffen, M. M., Z. Li, T. C. Effler, L. J. Hauser, G. L. Boyer, and S. W. Wilhelm. 2012. Comparative metagenomics of toxic freshwater cyanobacteria bloom communities on two continents. PloS one 7:e44002.

Stevens, D. K., and R. I. Krieger. 1991. Stability studies on the cyanobacterial nicotinic alkaloid anatoxin-a. Toxicon 29:167–179.

Stevenson, R. J., M. L. Bothwell, and R. L. Lowe, editors. 1996. Algal Ecology: Freshwater benthic systems. Academic Press, Inc., San Diego.

Stevenson, R. J., and C. G. Peterson. 1989. Variation in benthic diatom (Bacillariophyceae) immigration with habitat characteristics and cell morphology. Journal of Phycology 25:120–129.

Stevenson, R. J., and C. G. Peterson. 1991. Emigration and immigration can be important determinants of benthic diatom assemblages in streams. Freshwater Biology 26:279–294.

Strunecký, O., J. Komárek, J. Johansen, A. Lukešová, and J. Elster. 2013. Molecular and morphological criteria for revision of the genus *Microcoleus* (Oscillatoriales, Cyanobacteria). Journal of Phycology 49:1167–1180.

Suzek, B. E., H. Huang, P. McGarvey, R. Mazumder, and C. H. Wu. 2007. UniRef: comprehensive and non-redundant UniProt reference clusters. Bioinformatics 23:1282–1288.

Taranu, Z. E., I. Gregory-Eaves, P. R. Leavitt, L. Bunting, T. Buchaca, J. Catalan, I. Domaizon, P. Guilizzzoni, A. Lami, S. McGowan, H. Moorhouse, G. Morabito, F. R. Pick, M. A. Stevenson, P. L. Thompson, and R. D. Vinebrooke. 2015. Acceleration of cyanobacterial dominance in north temperate-subarctic lakes during the Anthropocene. Ecology Letters 18:375–384.

Tromas, N., N. Fortin, L. Bedrani, Y. Terrat, P. Cardoso, D. Bird, C. W. Greer, and B. J. Shapiro. 2017. Characterising and predicting cyanobacterial blooms in an 8-year amplicon sequencing time course. ISME Journal 11:1746–1763.

Vadeboncoeur, Y., and M. E. Power. 2017. Attached Algae: the cryptic base of inverted trophic pyramids in freshwaters. Annual Review of Ecology, Evolution, and Systematics 48:255–279.

Visser, P. M., J. Passarge, and L. R. Mur. 1997. Modelling vertical migration of the cyanobacterium *Microcystis*. Hydro 349:99–109.

Wacklin, P., L. Hoffmann, and J. Komarek. 2009. Nomenclatural validation of the genetically revised cyanobacterial genus *Dolichospermum* (Ralfs ex Bornet et Flahault) comb. nova. Fottea 9:59–64.

Walsby, A. E. 1975. Gas vesicles. Annual review of Plant Physiology 26:427–439.

Walsby, A. E., and D. P. Holland. 2006. Sinking velocities of phytoplankton measured on a stable density gradient by laser scanning. Journal of the Royal Society, Interface 3:429–439.

Walsby, A. E., R. Kinsman, B. W. Ibelings, and C. S. Reynolds. 1991. Highly buoyant colonies of the cyanobacterium *Anabaena-Lemmermannii* form persistent surface waterblooms. Archiv für Hydrobiologie 121:261–280.

Ward, J. H. 1963. Hierarchical Grouping to Optimize an Objective Function. Journal of the American Statistical Association 58:236–244.

Wasmund, K., M. Mußmann, and A. Loy. 2017. The life sulfuric: microbial ecology of sulfur cycling in marine sediments. Environmental Microbiology Reports 9:323–344.

Wilson, A. T. 1965. Escape of algae from frozen lakes and ponds. Ecology 46:376–376.

Wood, R. 2016. Acute animal and human poisonings from cyanotoxin exposure — A review of the literature. Environment International 91:276–282.

Wood, S. A., J. Atalah, A. Wagenhoff, L. Brown, K. Doehring, R. G. Young, and I. Hawes. 2017. Effect of river flow, temperature, and water chemistry on proliferations of the benthic anatoxin-producing cyanobacterium *Phormidium*. Freshwater Science 36:63–76.

Wood, S. A., C. Depree, L. Brown, T. McAllister, and I. Hawes. 2015. Entrapped sediments as a source of phosphorus in epilithic cyanobacterial proliferations in low nutrient rivers. PLoS ONE 10:e0141063.

Wood, S. A., P. T. Holland, and L. MacKenzie. 2011. Development of solid phase adsorption toxin tracking (SPATT) for monitoring anatoxin-a and homoanatoxin-a in river water. Chemosphere 82:888–94.

Wood, S. A., and J. Puddick. 2017. The Abundance of Toxic Genotypes Is a Key Contributor to Anatoxin Variability in *Phormidium*-Dominated Benthic Mats. Marine Drugs 15:307.

Wood, S. A., F. M. J. Smith, M. W. Heath, T. Palfroy, S. Gaw, R. G. Young, and K. G. Ryan. 2012. Within-mat variability in anatoxin-a and homoanatoxin-a production among benthic *Phormidium* (cyanobacteria) strains. Toxins 4:900–12.

Woodhouse, J. N., A. S. Kinsela, R. N. Collins, L. C. Bowling, G. L. Honeyman, J. K. Holliday, and B. A. Neilan. 2016. Microbial communities reflect temporal changes in cyanobacterial composition in a shallow ephemeral freshwater lake. ISME Journal 10:1337–1351.

Wrighton, K. C., B. C. Thomas, I. Sharon, C. S. Miller, C. J. Castelle, N. C. VerBerkmoes, M. J. Wilkins, R. L. Hettich, M. S. Lipton, K. H. Williams, P. E. Long, and J. F. Banfield. 2012. Fermentation, hydrogen, and sulfur metabolism in multiple uncultivated bacterial phyla. Science 337:1661–5.

Xie, M., M. Ren, C. Yang, H. Yi, Z. Li, T. Li, and J. Zhao. 2016. Metagenomic analysis reveals symbiotic relationship among bacteria in microcystis-dominated community. Frontiers in Microbiology 7:1–10.

Yang, X. 2007. Occurrence of the Cyanobacterial Neurotoxin, Anatoxin-a, in New York State Waters. State University of New York, Syracuse.

Yurkov, V. V, and J. T. Beatty. 1998. Aerobic Anoxygenic Phototrophic Bacteria. Microbiology and Molecular Biology Reviews 62:695–724.